AN ASSESSMENT OF GROUND PENETRATING RADAR AS A TECHNIQUE IN QUANTIFYING SEDIMENT ACCUMULATION ON THE TRINITY RIVER DELTA, TX

By

LEE MICHAEL TODD

Bachelor of Science, 2003
University of Nebraska at Omaha
Omaha, NE

Submitted to the Graduate Faculty of the
College of Science and Engineering
Texas Christian University
In partial fulfillment of the requirements
for the degree of

Master of Science

May 2008

ACKNOWLEDGEMENTS

This work was partially funded by the Texas Water Development Board. Field support was provided by Brian Atwell, Rick Garnett, Lauren Geffert, and Michael Steed. All of whom, I am forever in their debt. Thank you to Dr. Arthur Busbey, Dr. Tony Burgess, Dr. Ranjan Muttiah, Dr. Stephen Weis, and Greg Johnston for all their technical support. I would like to thank Dr. John Breyer for sharing his time, kindness, and wealth of knowledge with me during my time at Texas Christian University. Last but not least, I would like to thank Dr. Michael Slattery, without whom, this thesis would not have been possible.

TABLE OF CONTENTS

ACKNOWLEDGEMENTS ii

LIST OF FIGURES v

LIST OF TABLES vii

CHAPTER 1 INTRODUCTION AND BACKGROUND 1

1.1 Introduction and Objectives 1

1.2 Background 5

1.2.1 Sediment Accretion on the Trinity River Delta 5

1.2.2 Ground Penetrating Radar 9

CHAPTER 2 STUDY AREA 17

2.1 Trinity River Basin 17

2.2 Trinity River Delta 18

2.3 GPR Survey and Sediment Sampling Locations 20

CHAPTER 3 GROUND PENETRATING RADAR ANALYSIS 27

3.1 GPR Methodology 27

3.2 GPR Results and Interpretation 32

CHAPTER 4 SEDIMENT CORING ANALYSIS 42

4.1 Coring Methodology 42

4.2 Sediment Description Methodology 44

4.3 Grain-size Methodology 45

4.4 Bulk Density Methodology 45

4.5 Sediment Results 46

4.6 Radiocarbon Dating Methodology 54

TABLE OF CONTENTS

4.7 Radiocarbon Dating Results 55

CHAPTER 5 DISCUSSION AND CONCLUSIONS 57

5.1 Ground Penetrating Radar Usefulness 57

5.2 Trinity River Delta Sediment Accumulation 58

APPENDICES 64

APPENDIX A GROUND PENETRATING RADAR PROFILE 64

APPENDIX B GRAIN-SIZE ANALYSIS 86

APPENDIX C BULK DENSITY ANALYSIS 104

APPENDIX D RADIOCARBON DATING ANALYSIS 105

REFERENCES 106

VITA

ABSTRACT

LIST OF FIGURES

1. Trinity River Basin 2

2. Sediment sampling locations within Trinity River delta 6

3. Electromagnetic wave transmittal and response 10

4. Ground penetrating radar survey locations 21

5. Site 08 lines 01-05 and site 01 line 01-02 22

6. Site 09 lines 01-04 and site 01 line 04 23

7. Site 05 line 01 and site 01 lines 05-08 24

8. Site 03 25

9. Site 07 26

10. Site 08 line 05 GPR profile 33

11. Site 01 line 08 GPR profile 34

12. GPR survey lines 05 and 06 merged 35

13. GPR survey site 06 line 01 36

14. GPR survey site 03 line 01 and 02 merged 37

15. GPR survey site 05 line 01 38

16. GPR survey site 07 line 04 39

17. GPR survey site 07 line 01 40

18. GPR survey site 09 line 02 and 03 merged 41

19. GPR survey site 09 line 04 41

20. Stratigraphic column S7B1 48

21. *Mactra* shells recovered in S7B1 and S8B1 50

LIST OF FIGURES

22. Stratigraphic column S8B1 52

23. Sediment required to cover 25-100% of the delta surface 61

LIST OF TABLES

1. Accretion rates at sites 07 and 08 56

2. Delta accretion rates in southeast Texas 59

CHAPTER 1

INTRODUCTION AND BACKGROUND

1.1 Introduction

The disappearance of wetlands, erosion of shorelines, and subsidence of deltas is a major concern along the Texas coast. In fact, the Texas coast has been eroding in most places since the 1950s and in some locations since before 1930 (Morton, 1977; Phillips et al., 2004). The loss of wetlands and shoreline can be attributed to a number of factors, such as climate change, relative sea level rise, and anthropogenic influence. Phillips et al. (2004) examined historical aerial photos of the coastal zone near the mouth of the Trinity River and noted subsidence, wetland loss, and erosion of barrier beaches. The rate of wetland marsh loss has been estimated at *c.* 46 ha yr^{-1}, and shoreline retreat of 1.5 to 3 m yr^{-1} has been observed in the Trinity River delta (White et al., 2002; White and Calnan, 1991; Morton and Payne, 1990). This erosion and loss of land has increased in recent years, even though the Trinity River delta has been prograding. The shift to degradation of these systems started somewhere between 1956 and 1974 coinciding with the closure of several dams along Texas rivers, including the Trinity (Phillips et al., 2004; Dollar, 2005). This acceleration of erosion and land loss suggests that anthropogenic factors could be modifying the Texas coastal system.

One such man-made factor potentially affecting land loss and erosion in the Trinity River delta is Livingston Dam, a flow-through reservoir completed in 1968 to form Lake Livingston (see Figure 1). The primary purpose of the dam is as a water supply reservoir for Houston, TX, and it has a conservation pool capacity of >2.2 billion m^3 (Phillips et al., 2004; Wellmeyer et al., 2005). Dams have been known to significantly affect the geomorphology

of a river downstream. In some cases, the effects extend significantly downstream. In other cases, the effects are localized to the area immediately below the dam. Dams act as large-scale sediment traps, with water passing through the dam having a higher carrying capacity than its actual sediment load (Brandt, 2000; Phillips, 2001). This so-called "hungry water" causes channel scour, bank erosion, and increased sediment transport. Such dam related effects are evident up to 60 km downstream of Livingston Dam (Phillips et al., 2004; Phillips et al., 2005).

Figure 1. Trinity River Basin.

Rivers provide the major source of sediment to the coastal zone. However, the movement of sediment through a drainage basin is not as simple as upland erosion, transport through the basin, and deposition at the coast. Erosion, transport, deposition, and storage of sediment can (and generally does) occur throughout the sediment delivery system.

Quantifying this erosion and deposition in the fluvial system is frequently accomplished through construction of a sediment budget.

Changes in erosion and sediment transport within a drainage basin are not always reflected in changes in sediment delivery to the coast. This is especially true when considering large, low-gradient coastal plain river systems which are generally viewed as inefficient conveyors of sediment. It has been shown that coastal plain rivers have sediment delivery ratios of less than 10% (Phillips and Slattery, 2006). In these systems, accommodation space is high and stream power is low, often causing upper and lower-basin decoupling to occur (Phillips et al., 2004; Phillips and Slattery, 2006). This means eroded upper basin sediments are stored as alluvium in channels or flood plains, instead of being transported to the mouth of the river. The decoupling effect has been noted in many environments, including coastal river systems in North Carolina, New Zealand, Australia, and Texas (Fryirs and Brierly, 1999; Phillips, 1991; Phillips et al., 2004; Phillips and Gomez, 2007). When there is a limited amount of upper basin sediment compared to lower basin sediment sources, changes along the coast are affected by lower basin and not upper basin controls. This means that reduced sediment from lower erosion or reservoirs upstream will not affect sediment output to the coast.

The "hungry water" effects produced by dam closures upstream are known to be greatest near the dam and diminish downstream where drainage area increases and stream gradient decreases, causing sediment delivery ratios to decrease and sediment to deposit (Blum and Tornqvist, 2000; Brandt, 2000). When sediment supply exceeds the stream transport capacity there will be a net increase in storage, and only a small amount of sediment will leave the basin (Phillips, 1987, 1991). The lowermost reaches of the Trinity

River have high alluvial storage in floodplains and act as a "sediment bottleneck" effectively withholding sediment from the bay. This extensive alluvial storage buffers the Trinity delta from any reduction of sediment upstream. If capacity is not achieved with sediment from upland sources, flood plain deposits will replace it via lateral erosion of the channel. Farther downstream at Liberty, TX, the Trinity River shows no decline in sediment load. Recent work has shown that most of the sediment reaching the Trinity River delta comes from the banks and flood plain of the lower Trinity River (Dollar, 2005). Therefore, the upper and lower Trinity have been decoupled and have been throughout the Holocene (Phillips et al., 2004).

Much work has been done to characterize sediment delivery in the lower Trinity River basin (Phillips et al., 2004; Phillips and Slattery, 2006; Dollar, 2005; Wellmeyer et al., 2005). This work has shown that there is a disconnect between sediment delivery to the coastal zone and the amount of sediment eroded within the basin. Nevertheless, little work has been done to determine rates of sediment accumulation in the Trinity River delta. This thesis attempts to quantify sediment accretion in the Trinity delta using both rapid, non-invasive ground penetrating radar (GPR) technology, as well as traditional coring methods. A second objective of this thesis was to test the usefulness of GPR in the interdistributary marshes of a fine-grained delta and a sand bar along the lower Trinity River to determine subsurface stratigraphy.

1.2 Background

1.2.1 Sediment Accretion on the Trinity River Delta

The bird foot-shaped, subaerial Trinity River delta plain is composed of an intricate system of anastomosing/bifurcating channels, levees, lakes, and interdistributary marshes. The present day long axis of the Trinity River delta is 23 km from apex of the delta, where the distributaries begin to diverge from the main channel, to the mouth in Trinity Bay. The maximum width of the delta is 16 km at the base, and the modern surface area of the delta, excluding open water, is 126.1 km^2 (Phillips, 2006, see Figure 2).

Sediment accretion rates for a region are often difficult to measure in the short term because sedimentation events are neither temporally nor spatially uniform. Sediment accumulation occurs either very slowly or is discontinuous and rapid. Therefore, the most widely used method of determining an accumulation rate at a sight is to measure the thickness of sediment and then divide by the amount of time over which deposition occurred. This produces an average sedimentation rate for a given time period, and represents the net accumulation minus removal of sediment (Phillips, 2006). Such average sedimentation rates cannot resolve episodes of rapid or slow accumulation. Sedimentation events are also spatially heterogeneous; meaning a portion of the study area could be experiencing high rates of accumulation, while another portion may be eroding. The lack of spatial uniformity is a problem in the Trinity River delta, as the size of the delta has changed and the location has moved during the Holocene (Rodriguez et al., 2005; Phillips, 2006).

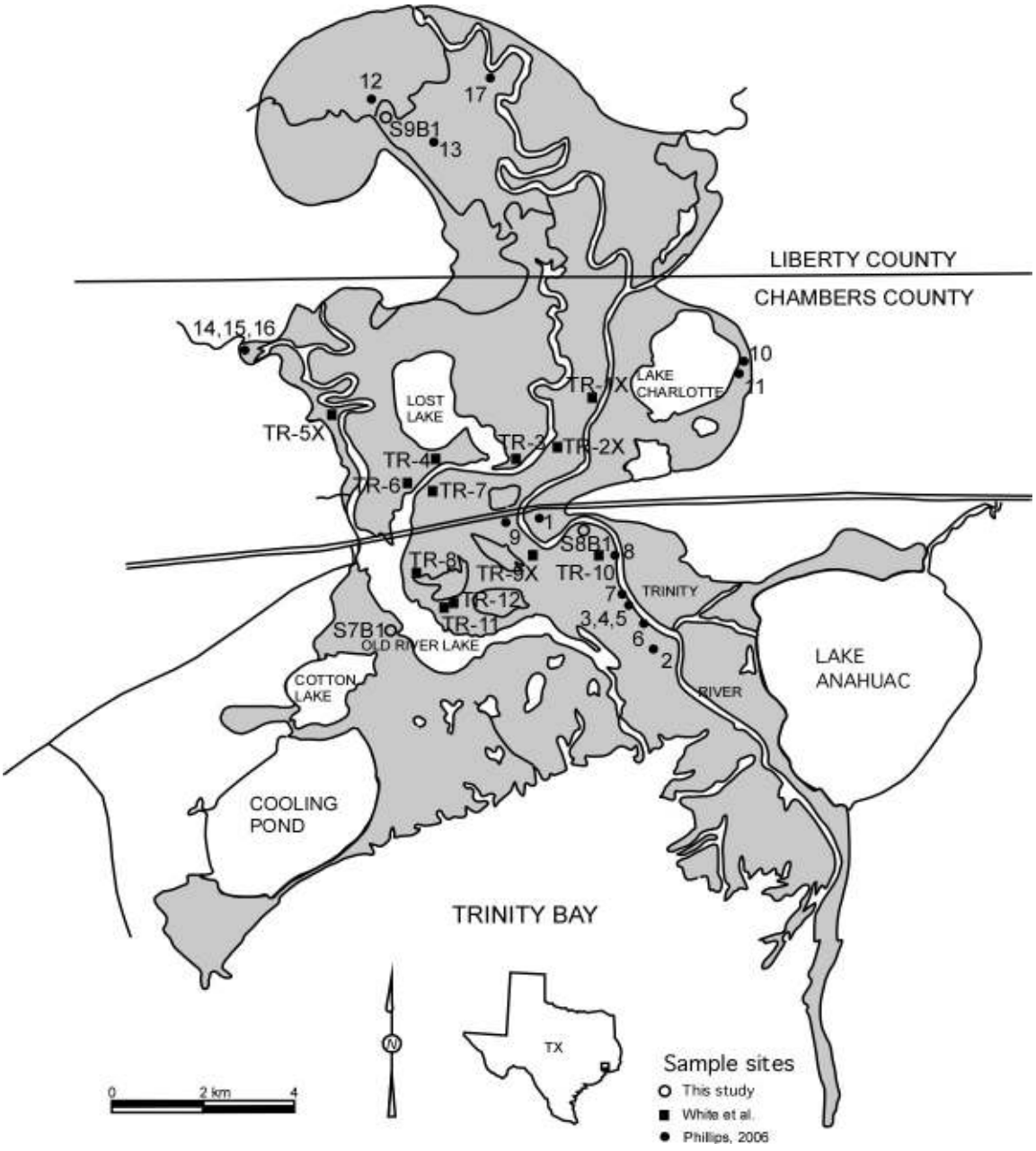

Figure 2. Sediment sampling locations within Trinity River delta (redrawn from White et al., 2002; Phillips, 2006).

Several previous studies undertaken in the Trinity River delta have produced data describing Holocene sediment thicknesses. Soil survey descriptions from Chambers and Liberty Counties extend to depths of 1.5 to 2.0 m, and show Holocene sediment to extend deeper than the extent of their descriptions (Crout, 1976; Griffith, 1996). A series of short

cores were taken in the Trinity River delta by McEwan (1963), who found Holocene delta sediments to be generally thicker than 3 m. Morton et al. (1996) showed Holocene sediment thicknesses ranging from approximately 2 to 11 m within the delta from soil cores collected by the Texas Department of Transportation during deep foundation borings for bridges over the Trinity River. A mean thickness of 8.7 m for Holocene mud in the Trinity River delta was reported by White et al. (2002). The thickest Holocene sediment deposit recorded came from a core on the distal edge of the Trinity River delta, in the pro-delta, not the delta plain. This core extended to a depth of 13.8 m in Holocene deposits (Rodriguez et al., 2005).

Once the thickness of sediment is known, only the time of deposition is needed to determine the accretion rate. Holocene deposition in the Trinity River delta is believed to have started during a terrace inundation event 7.7 to 8.5 Ka. This date comes from the same study by Rodriguez et al. (2005) which produced the 13.8 m core of Holocene sediment. Wood fragments in the basal portion of the core (13.4 m) were radiocarbon dated at 7.738 ± 60 Ka conventional and 8.495 ± 50 Ka calibrated. The timing of Holocene deposition is also supported by the retreat of barrier shorelines with increased rates of sea level rise (Rodriguez et al., 2004).

Using an average thickness of Holocene muds of 8.7 m presented by White et al. (2002) and the initiation of Holocene deposition at 8 Ka presented by Rodriguez et al. (2004, 2005), mean accretion is computed at 1.1 mm yr^{-1}. The thickness of reported Holocene delta deposits ranged from ~2 to ~14 m. With this spatial variation in sediment thicknesses, localized accretion rates range from ~0.25 to ~1.75 mm yr^{-1}.

Trinity River delta Holocene accretion rates have been studied in three previous studies using three different methods. White et al. (2002) collected sediment cores up to 80

cm long at twelve marsh sites within the Trinity River Delta (Figure 2). The cores were then dated using ^{210}Pb methods which apply to the previous 100 years. Accretion rates from this study ranged from 1.6 to 13.05 mm yr^{-1}, with a mean of 5.1 mm yr^{-1}. White et al. (2002) also noted that a similar mean accretion rate (5.4 mm yr^{-1}) was calculated for Trinity River delta marshes by White and Calnan (1990).

As noted previously, a core was sampled to a depth of 13.8 m in Holocene deposits along the distal edge of the Trinity River delta by Rodriguez et al. (2005). Nine samples of shell or wood fragments ranging in depth from 178 to 1,342 cm were then radiocarbon dated. Wood fragments in the basal portion of the core were dated at 7.738 ± 60 Ka conventional and 8.495 ± 50 Ka calibrated. Using the calibrated age of the oldest and deepest sample from the core, an average accretion rate of 1.58 mm yr^{-1} was calculated for a time span of ~8,500 years. Individual accretion rates from all nine samples dated ranged from 0.52 to 5.68 mm yr^{-1}.

Phillips (2006) used dendrochronological methods at 17 swamp forest sites within the Trinity River delta to determine Holocene sediment accumulation rates (Figure 2). This method involves measuring the burial of tree roots and basal flares by sediment, and determining the maximum date of burial by counting tree rings. Dendrochronological methods depend on significant burial and only reflect short periods of time. Therefore low sediment accumulation rates are difficult to detect (Phillips, 2006). Phillips (2006) produced a mean sediment accretion rate of 3.3 mm yr^{-1}for Trinity River delta swamp forest sites. Accumulation rates in the 17 sites ranged from negligible (~0) to 16.7 mm yr^{-1}.

1.2.2 Ground Penetrating Radar

Ground penetrating radar (GPR) is a rapid and noninvasive technique used for detection and characterization of the shallow subsurface. GPR is similar to seismic reflection surveying except that it uses electromagnetic energy instead of sound waves and therefore can produce higher resolution images of the subsurface. GPR systems are comprised of five basic elements: the transmitter, receiver, antennae, control unit, and display unit. The transmitter produces a short, high voltage pulse, which is sent through the antenna as high frequency (10-1000 MHz) electromagnetic energy into the ground (Davis and Annan, 1989; Butnor et al., 2001; Neal, 2004). Each pulse consists of a frequency spectrum, which is distributed around the central frequency of the transmitting antenna. A portion of the electromagnetic energy transmitted into the ground travels directly to the receiving antenna as air wave and ground wave, producing the signal at the top of the GPR profile (Figure 3). The remainder of the electromagnetic wave travels through the subsurface, where it comes in contact with geologic materials of different electrical properties. The interface separating these layers of differing electrical properties alters the velocity of the wave. If the velocity changes are large or abrupt, a fraction of the electromagnetic wave energy will be reflected back to the surface where it is received by the receiving antenna (Davis and Annan, 1989; Augustinus and Nichol, 1999; Neal, 2004). The receiver then amplifies the signal and transfers it to the control unit. The control unit stores and formats the quantity of energy received and its associated arrival time so it can be presented by the display unit.

The two factors that describe the propagation of high frequency electromagnetic waves through the earth are velocity and attenuation. Velocity is the rate at which the electromagnetic wave travels through the ground, and attenuation is the reduction in

amplitude and intensity of the wave due to absorption in the ground (Olhoeft, 2006). Therefore, velocity and attenuation are dependent on the electrical properties of the subsurface geology and its water content. Dielectric constant is the term used to represent the material properties that control electromagnetic energy in a medium. The dielectric constant is composed of electrical conductivity, dielectric permittivity, and magnetic permeability. Electrical conductivity is a measure of a material's ability to transport an electrical charge. The conductive material will absorb a portion of the electromagnetic wave and dissipate that energy as heat (Davis and Annan, 1989; Neal, 2004; Olhoeft, 2006). Dielectric permittivity is a material's ability to store an electrical charge, and results from a charge separation over a distance (Neal, 2004; Olhoeft, 2006). Magnetic permeability measures a material's ability to store magnetic energy, and is the result of motion in atomic orbits. All the dielectric properties which make up the dielectric constant of a geologic material are controlled primarily by water content (Davis and Annan, 1989; Neal, 2004).

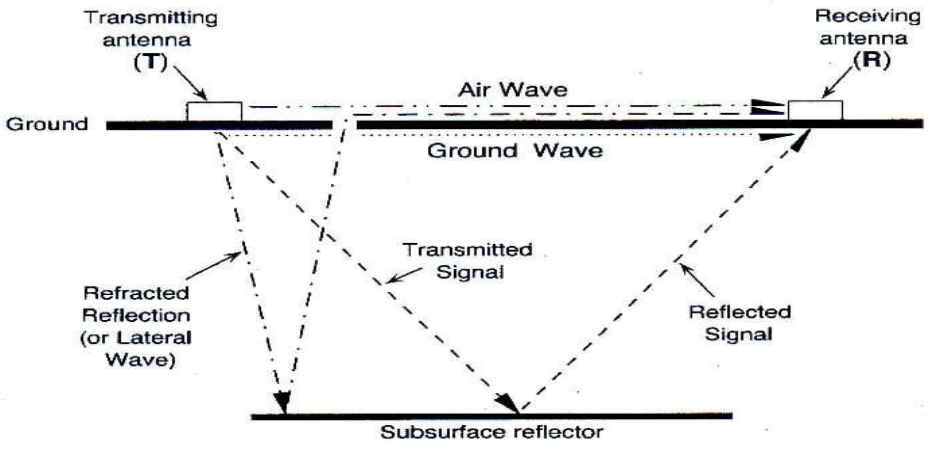

Figure 3. Electromagnetic wave transmittal and response (Neal, 2004).

There is a negative correlation between a materials dielectric constant and the velocity at which an electromagnetic wave will pass through it. Materials such as water and

clays with large dielectric constants will cause an electromagnetic wave to slow as it passes through the media. Although there is a negative correlation between the dielectric constant and velocity, the dielectric constant is positively correlated to attenuation. As an electromagnetic wave passes through a material with a large dielectric constant, there is greater reduction in amplitude and intensity of the wave. Therefore, the electromagnetic energy will not be able to pass through the media.

Not only are energy losses due to electrical conductivity, dielectric permittivity, and magnetic permeability, attenuation of an electromagnetic wave through the earth can result from scattering and spherical spreading. Energy loss from scattering occurs when an electromagnetic wave encounters a point source, and wave energy is sent in many different directions. Scattering is a problem in heterogeneous materials such as glacial till, where there are numerous point sources to split the wave energy. Spherical spreading occurs as the electromagnetic wave travels away from the transmitting antenna. The electromagnetic wave spreads causing a decrease in power (Davis and Annan, 1989; Olhoeft, 2006).

In addition to velocity and attenuation, depth of penetration and resolution of electromagnetic energy are affected by electrical conductivity, dielectric permittivity, and magnetic permeability. Depth of penetration of an electromagnetic wave can vary anywhere from 5,400 m in glacial ice to less then a meter in saturated clays (Olhoeft, 2002). Maximum depth of electromagnetic energy is dependant on the wave frequency and the electromagnetic properties of the surrounding media. A low frequency (longer wavelength) electromagnetic wave will travel deeper into the ground than a high frequency (short wavelength) wave. As stated previously, materials with large dielectric constants increase attenuation as

electromagnetic waves pass through them. Therefore, large dielectric constants limit depth of penetration.

Resolution can be defined as the ability to distinguish between two closely spaced features (Butnor et al., 2001; Neal, 2004). GPR data has the ability to attain excellent resolution. For example, tree roots 0.5 cm in diameter have been detected through the use of GPR (Butnor et. al., 2001). Resolution of GPR data is dependent on the electromagnetic wave frequency, the electromagnetic properties of the surrounding media, and the size, shape and orientation of reflectors. Due to the high dielectric constants of some materials, wave energy can be attenuated causing poor resolution of GPR data. Whereas depth of penetration decreases with high frequency electromagnetic waves, resolution increases with high frequency waves. This contrast forces a compromise to be made between the importance of resolution and depth of penetration.

There are many advantages in using ground penetrating radar to interpret subsurface geology rather than using the standard methods of soil or rock coring. The process of collecting a GPR survey requires a limited amount of equipment, is non-intrusive, and can cover a large geographic area in a short time period. Horizontal resolution is another benefit that GPR holds over coring. Soil and rock cores are often spaced large distances apart. Therefore, subsurface stratigraphy between boreholes must be interpreted by correlation using only the limited amount of core data available. A GPR survey collects subsurface data spaced only a short distance (0.02-2 m) apart (Sensors and Software, 2005). GPR has been proven to work well in coarse grained sediments with limited water content by studies which compared GPR and core data (Roberts et al., 2003; Fisher et al. 1992).

Although there are many advantages to using GPR for subsurface investigations, there are limitations as well. Lithology and water content can limit the usefulness of GPR. It has been shown in several studies that electromagnetic waves get attenuated very quickly in conductive fine-grained sediments with high pore water content (Bristow and Jol, 2003; Pelpola and Hickin, 2004; Van Dam and Schlager, 2000). This rapid attenuation can result in a lack of subsurface reflections below the conductive material or can produce a high frequency ringing. This high frequency ringing can produce multiple reflections which can obscure primary reflections (Neal, 2004). GPR surveys are also limited in heterogeneous geologic units such as glacial till by the scattering effect due to the numerous point sources. Not only is GPR affected by the subsurface geology being studied, it is also affected by technology. Interference from power lines, walkie talkies, and television, radio, and cellular phone transmitters can disrupt the signal returning to the GPR receiving antenna (Olhoeft, 2002; Neal, 2004).

Ground Penetrating Radar has been used for many purposes and in several different sedimentary environments. GPR has been a geophysical tool used in archaeology to locate buried artifacts and structures (Conyers and Goodman, 1997); geotechnical investigations to locate pipes and other utilities, depth to bedrock, and karst topography (Davis and Annan, 1989); groundwater flow modeling, environmental site characterization, and monitoring (Davis and Annan, 1989; Ezzy et al., 2006), and agriculture to study root systems (Butnor et al., 2001). Since one of the purposes of this study is to determine the effectiveness of GPR on fine-grained delta sediments, it is prudent to highlight several cases by different authors involving a variety of sedimentary environments.

As mentioned above, GPR has been used to study root systems. One such study tested the usefulness of GPR to locate tree roots in a variety of different soil conditions (Butnor et al., 2001). Soils in the study areas ranged from well-drained sandy soils to saturated clay-rich sediments. Ground penetrating radar was successful locating tree roots in most soils, with the best resolution occurring in sandy, drained soils. The GPR was able to locate a 0.5 cm diameter tree root in that soil. The soil that hindered the GPR most was water saturated clays. The GPR was rendered ineffective due to the high electromagnetic attenuation. This study also brought to light another limitation of the technique: GPR resolution decreases if the GPR antennae do not maintain contact with the ground (Butnor et al., 2001). Maintaining ground contact is a common obstacle in the field due to uneven ground, vegetation, and debris.

Bristow et al. (1999) used GPR to analyze the internal structure of recent floodplain deposits along the Niobrara River, Nebraska. GPR data were compared to sediment cores which were taken by a vibracore sampler on two crevasse splays. GPR analysis was able to locate gently dipping discontinuous reflectors which were interpreted as medium-scale trough cross-bedded dunes. Planar cross-stratification with a vertical thickness of 0.5 m was also noted. Some survey lines covering the splays lacked internal reflectors. The authors attributed the lack of reflectors to either attenuation by mud drapes, or the size of the structures being smaller than the resolution of the GPR (Bristow et al., 1999).

GPR was used to interpret the internal stratigraphy of four coarse-grained deltas and two different barrier spits in a study conducted by Tercier et al. (2000). The GPR surveys resulted in a resolution of 0.5 m and had a depth of penetration from 7-16 m into the ground. Based on the correlation structures and character of GPR reflections, the authors were able to

break the deltas and barrier spits into different depositional settings such as beach foreshore and middle, lower shore face (Tercier et al., 2000).

Aeolian and tidal deposits next to an open pit quarry in the Netherlands were surveyed with GPR and compared to the exposed section in the quarry (Van Dam and Schager, 2000). The GPR was able to locate gently dipping planar beds of sand and medium-scale cross-bedded sands in the aeolian dunes with a vertical thickness of 0.5 m. The fine grained tidal sediments produced a very high amplitude reflector, but the GPR was unable to penetrate the unit due to rapid attenuation (Van Dam and Schager, 2000).

A study to characterize the internal structure of channel bars in the Calamus River, Nebraska, utilized GPR and vibracores for correlation (Bridge et al., 1998). The Calamus River is a braided stream which transports primarily fine sand to gravel. GPR of the channel bars identified low amplitude discontinuous reflectors which were interpreted as small-scale ripple-laminated sands less than 3 cm thick. 3-25 cm trough cross-bedding was also noted in the survey, along with low angle reflectors dipping in the direction of stream flow. The low angle reflectors represent growth of the channel bar (Bridge et al., 1998).

There have been numerous studies using GPR to characterize the internal structure of delta deposits (Jol and Smith, 1991; Smith and Jol, 1997; Bristow and Jol, 2003; Pelpola and Hickin, 2004; Barnhardt and Sherrod, 2006). However, these studies have focused primarily on coarse-grained deltas, only mentioning the finer sediments as the lower bounding surface to the GPR profile (Jol and Smith, 1991; Pelpola and Hickin, 2004). In such studies, GPR depth of penetration ranged from 10-32 m in coarse-grained sediments (Smith and Jol, 1997; Pelpola and Hickin, 2004). Several studies were also able to identify type and orientation of sedimentary structures, bedding planes, and facies assemblages. Barnhardt and Sherrod

(2006) were able to identify planar sheet-like sand bodies ranging in thickness from 1-4 m, and 1 m thick seaward dipping clinoforms to determine episodic sedimentation history of the Nisqually River delta. Another study used GPR reflection textures to evaluate facies assemblages in the William River delta (Moysey et al., 2006). Jol and Smith (1991) conducted GPR surveys on six coarse-grained deltaic sedimentary environments. The survey was able to identify subsurface stratigraphy, different sedimentary facies, and reconstruct ancient depositional environments.

CHAPTER 2

STUDY AREA

2.1 Trinity River Basin

The Trinity River basin trends northwest to southeast from the rivers headwaters which begin west of Fort Worth, TX, and flow 885 km to the mouth of the river which is in Trinity Bay, part of the Galveston Bay estuarine system (see Figure 1). The Trinity River drains an area of 46,100 km^2 and has an average discharge of 7.1 X 10^9 m^3 per year (Rodriguez et al., 2005). The majority of the Trinity basin has a humid subtropical climate, and rainfall averages 69 to 127 cm yr^{-1} (Lankford and Rehkemper, 1969). The basin is covered by thick, continuous soil and regolith. The soils in the drainage basin can be characterized as Alfisols and Ultisols, which are dominated by clays and have been extensively leached (Phillips et al., 2004; Dollar, 2005). The Trinity River is typical of many large coastal plain rivers in that the channel gradient is very low. In fact, the channel bed is at or below sea level 60 km upstream from the mouth of the river (Phillips, 2003, Phillips et al., 2004). This translates to low stream power and a reduction in competence and capacity. This in combination with the high accommodation space of the Trinity River flood plain, results in extensive alluvial storage in the lower reaches.

Flow of the lower Trinity River is partially regulated by Lake Livingston Dam which was closed in 1968. The dam was constructed to provide drinking water for the city of Houston. Although Lake Livingston is a flow through reservoir, it does reduce sediment supply immediately downstream, as can be seen in sediment records from the Trinity River gaging station 51 km below the dam (White and Calnan, 1991; Solis et al., 1994). This reduction in sediment supply has led to vertical and lateral channel erosion below the dam.

Downstream of Livingston Dam, the Trinity River meanders 95 km to its mouth in Trinity Bay. Within that 95 km distance, the river has a well developed flood plain with a mean width of 5 km and an average bank height of 7 m (Phillips, 2003; Phillips et al., 2004). The main channel of the lower Trinity River has been actively migrating throughout the Quaternary. Evidence of this comes from bank erosion, abandoned channels, point bar accretion, meander scars, and oxbow lakes (Lankford and Rehkemper, 1969; Phillips et al., 2004). Numerous Pleistocene alluvial terraces have been preserved in the lower Trinity and are evidence of down cutting due to past sea level, climate, and sediment delivery changes (Phillips et al. 2004, Morton et al., 1996). During the Wisconsin glaciation, sea level fell forcing the Trinity River to incise into underlying Pleistocene deposits forming terraces. As the glaciers retreated, there was a rapid rise in sea level. And with this rise in sea level, valleys were filled with Holocene fluvial and marine deposits (Morton et al., 1996).

2.2 Trinity River Delta

The Trinity River delta is a tide and mixed-load river-dominated delta, with minimal wave forces acting upon it (Figure 2). The majority of the delta is at or below sea level and thus is affected greatly by lunar and wind tides (Phillips and Slattery, 2006). The mean lunar tidal range is 0.3 m, and wind tides can raise the bay quickly 0.61 to 0.91 meters causing high velocity currents to transport large quantities of sediment (Lankford and Rehkemper, 1969). The bird foot-shaped subaerial Trinity River delta plain is composed of an intricate system of anastomosing/bifurcating channels, levees, lakes, and interdistributary marshes. The present day long axis of the Trinity River delta is 23 km from apex of the delta, where the distributaries begin to diverge from the main channel, to the mouth in Trinity Bay. The

maximum width of the delta is 16 km at the base, and the modern surface area of the delta, excluding open water, is 126.1 km^2 (Phillips, 2006). Vegetation in the delta is dominated by fresh-water to brackish-water vegetation such as; Cattail (*Typha* sp.), Bulrush (*Schoenoplectus* sp.), Barnyard Grass (*Echinochloa* sp.), and Common Reed (*Phragmites australis*).

Size and location of the Trinity River delta has changed many times due to channel avulsion during its Holocene evolution (Rodriguez et al., 2005; Phillips, 2006). The present day delta is on the eastern side of the Trinity River floodplain, and remnants of ancient delta positions mark the western portion. The Trinity River delta was prograding throughout most of the Holocene. During this progression, delta sediments isolated a portion of Trinity Bay forming Lake Anahuac. Although the delta was prograding in recent times, a shift to degradation started somewhere between 1956 and 1974 (Phillips et al., 2004). The loss of wetlands and coastal shoreline has been noted in several studies (Blum et al., 2001; White et al., 2002; Phillips et al., 2004). This loss of land can be attributed to a number of factors including subsidence, sea level rise, and a reduction in sediment delivery to the coast.

The sediments in the Trinity River delta can be grouped and described as different sedimentary facies displaying a coarsening upward sequence (McEwan, 1963). The subaerial delta plain contains facies assemblages from distributary channels, natural levees, and interdistributary marshes. Distributary channel facies range from cross-bedded well sorted sands to structureless, poorly sorted silty clays. Natural levee facies consist of structureless to horizontally laminated poorly sorted silty clays to clayey sands. Marsh facies range from structureless organic-rich clays to sandy clays. Delta front facies are well-sorted

structureless to clay-laminated fine sands, and prodelta deposits can be described as structureless clays (McEwan, 1963; Rodriguez et al., 2005).

2.3 GPR Survey and Sediment Sampling Locations

This study focused on the sediment accretion in three interdistributary marshes within the Trinity River delta (sites 07-09), but also utilized five other locations (sites 01-03 and sites 05-06 for GPR testing and training purposes (see figures 2 and 4). The first area studied was an interdistributary marsh to the southwest of a meander in the main channel of the lower Trinity River (site 08, Figure 4 and Figure 5). The marsh was bounded to the north and east by a man-made levee and contained numerous small distributary channels, and small bodies of standing water. The thick vegetation in this marsh consisted of Cattail (*Typha* sp.), Bulrush (*Schoenoplectus* sp.), and Barnyard Grass (*Echinochloa* sp.).

The second area studied was approximately 300 m northeast of site 08. This is a natural levee adjacent to the same meander in the main channel of the Trinity River described in site 08 (site 01 line 03, Figure 4). The natural levee is positioned on the west side of the river, and is bordered to its west by an interdistributary marsh. Vegetation on the levee consisted of small brush and Water Elm (*Planera aquatica*).

The third area studied was a heavily wooded interdistributary swamp/marsh 300 m northeast of the Trinity River National Wildlife Refuge, Champion Pier (site 09, Figure 4 and Figure 6). This site is located at the apex of a bifurcated distributary channel of the Trinity River. The site was bounded to the west and north by a man-made levee, and was transected by a clear cut dirt road and an oil and gas pipeline. This area was later renamed site 09 and was used for further study. During the time of this study, site 09 was flooded to the top of

the man-made levee for the entire summer. The wetland vegetation at this site include Cypress (*Taxodium*), Water Tupelo (*Nyssa aquatica*), and Water Elm (*Planera aquatica*).

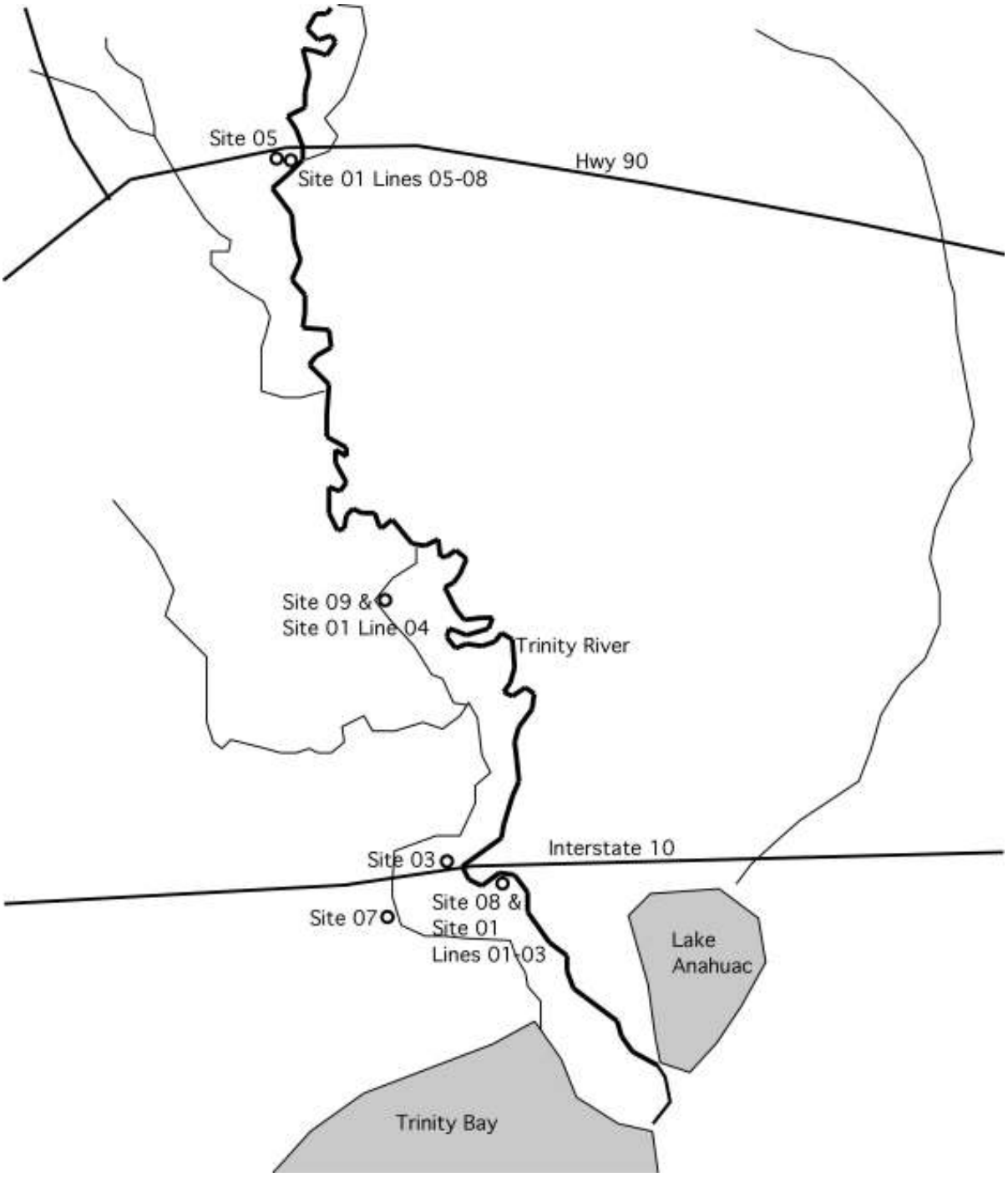

Figure 4. Ground penetrating radar survey locations.

Figure 5. Site 08 lines 01-05 and site 01 lines 01-02.

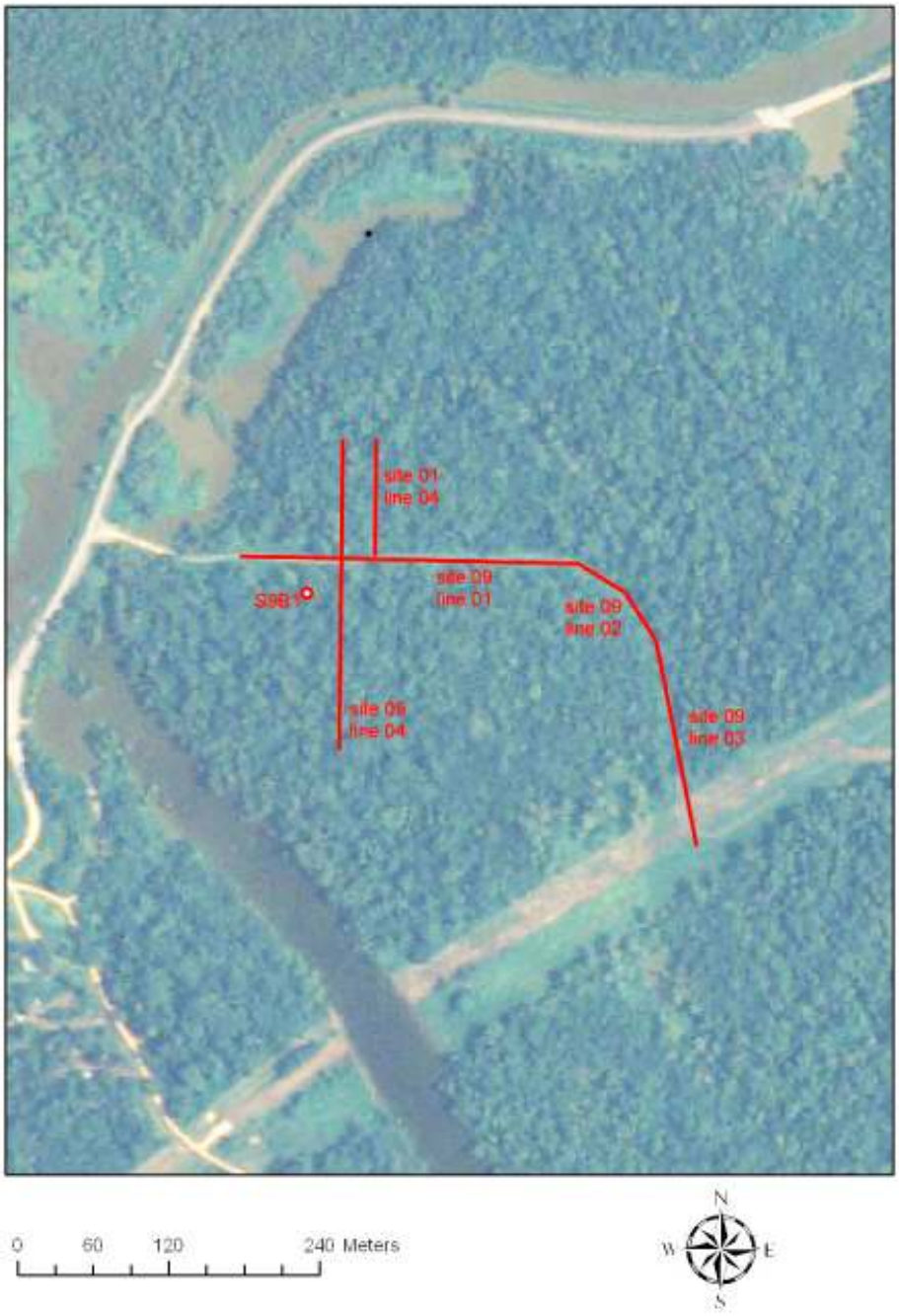

Figure 6. Site 09 lines 01-04 and site 01 line 04.

The next area studied was a sand bar adjacent to the main channel of the Trinity River approximately 13 km north of the Trinity River delta study area and directly south of Texas Hwy 90 (site 01, Figure 4 and Figure 7). At the time of sampling, the sand bar had a total length of 255.5 m and a horizontal width of 70 m.

Figure 7. Site 05 line 01 and site 01 lines 05-08.

Two of the test sites outside the Trinity River delta study area (site 02 and site 06) were located on the lawns of Texas Christian University campus. Both sites at TCU were used solely to train field assistants on the use of the GPR system.

Survey site 03 was located in a constructed wetland just north of a construction road adjacent to Interstate 10 within the Trinity River delta (site 03, Figure 4 and Figure 8). Survey site 05 was just south of Texas Hwy 90, which is approximately 13 km north of the Trinity River delta study area (site 05, Figure 4 and Figure 7). Both locations are directly west of the main channel of the Trinity River.

Figure 8. Site 03.

Site 07 is a highly vegetated interdistributary marsh on the southwestern edge of the Trinity River delta known as Cotton Bayou (site 07 Figure 4 and Figure 9). This interdistributary marsh is positioned between Cotton Lake on the west and Old River Lake on the east. A man-made levee borders the marsh to the east, and a natural terrace confines the marsh to the north. The robust vegetation consisted of Cattail (*Typha* sp.), Bulrush (*Schoenoplectus* sp.), and Common Reed (*Phragmites australis*).

Figure 9. Site 07.

CHAPTER 3

GROUND PENETRATING RADAR ANALYSIS

3.1 GPR Methodology

Ground-penetrating radar (GPR) surveys were conducted using a Sensors and Software Inc., Canada Pulse Ekko 100 radar system. The system is backpack portable and is comprised of a control console, a digital video logger (DVL), a 1000 V transmitter, a receiver, two 50 MHz center frequency antennae, and the fiber optic transmitter and receiver cables. The control console and DVL are powered by two separate 12 V batteries.

The GPR system was first employed at five field sites for testing and training purposes. These field sites included three sites outside the Trinity River Delta study area (site 02 and site 06 at TCU and site 05, Figure 4), one site inside the study area (site 03, Figure 4), and one site with locations inside and outside of the delta (site 01, Figure 4). The test sites inside and outside of the Trinity River delta study area were chosen for their accessibility, and to test the GPR in different sedimentary environments. Two of the test sites outside the study area (site 02 and site 06) were located on the lawns of Texas Christian University campus. One GPR survey line was collected at each site, and both survey lines were less than 25 m long. Both sites at TCU were used to train field assistants on the use of the GPR system.

Site 01 consisted of eight GPR survey lines at three different locations inside and outside the Trinity River delta. Survey lines 01 and 02 were chosen for their position in an interdistributary portion of the delta (Figure 4 and Figure 5). Survey line 01 extended 57 m to the southwest and ran perpendicular to a man-made levee. Survey line 02 began at the end of line 01 to form a tie point for correlation, and it sampled to the northwest running parallel

to the man-made levee. Survey line 03 is 23 m in length and is approximately 300 m northeast of survey lines 01 and 02. The survey line sampled a natural levee adjacent to the main channel of the Trinity River. Survey line 04 sampled a wooded interdistributary area in the northern portion of the delta (Figure 4 and Figure 6). The survey line was 55 m in length and sampled the area from south to north.

A sand bar along the main channel of the Trinity River was sampled in survey lines 05 through 08 at site 01 (Figure 4 and Figure 7). This sand bar is approximately 13 km north of the Trinity River delta study area. It was selected for its accessibility and to test the GPR system in a different sedimentary environment. Survey lines 05 and 06 transversed the length of the sand bar sampling a total of 255.5 m. Survey line 07 started at the apex of the sand bar and sampled perpendicular to survey lines 05 and 06. Line 07 was 39 m in length and transected line 05 creating a tie point for correlation. All survey lines at site 01 were sampled with 50 MHz antennae, with the exception of survey line 08. Survey line 08 followed the same path as line 05 for 81 m until the GPR transmitter batteries died. 100 MHz antennae were used with the ground penetrating radar system for survey line 08 for comparison purposes, and to determine their depth of penetration and vertical resolution.

Survey site 03 involved the collection of two GPR survey lines adjacent to Interstate 10 within the Trinity River delta (Figure 4 and Figure 8). The two survey lines were located in a constructed wetland just north of a construction road. Survey line 01 and 02 at site 03 ran from east to west and sampled a total of 133.5 m. Survey site 05 collected one survey line adjacent to Texas Hwy 90, which is approximately 13 km north of the Trinity River delta study area (Figure 4 and Figure 7). Survey line 01 sampled a dirt path which ran from west to east perpendicular to the Trinity River, and was 145.5 m in length. Both locations are

directly west of the main channel of the Trinity River. Sites 03 and 05 were selected for study based on the prior knowledge of their underlying geology. Morton et al. (1996) described the stratigraphy of the two sites known from soil cores collected by the Texas Department of Transportation during deep foundation borings for bridges over the Trinity River. Morton et al. (1996) showed Holocene sediment thicknesses ranging from approximately 2 to 11 m in the area overlying the Pleistocene aged Deweyville terrace.

After data from the five test sites were evaluated, sampling methods and three study sites within the Trinity River delta (sites 07-09) were chosen. These sites were chosen for their accessibility, and to test the variation in sediment accumulation rates within the Trinity River delta. Vegetation was cut or flattened in order to collect the GPR surveys. At the time of sampling the ground was saturated at all three sites, and there was surface water standing in numerous places at survey site 08. The wet conditions and the high vegetation encumbered field work with the GPR. The GPR surveys were constrained to areas with the least amount of vegetation and dry soils. Access to the study sites was limited due to the fragile nature of the ecosystem.

Each survey line was collected in perpendicular broadside reflection mode in which the transmitting and receiving antennae were oriented in the same direction perpendicular to the survey line and were kept at a constant separation of 2 m. Step mode movement of the antennae by 0.5 m between data collection points was used to transport the antennae by hand along the survey lines. Having both antennae stationary during collection of the data points, allows reflections to be higher amplitude and more coherent (Neal, 2004). A time zero calibration was made at the start of sampling at each study site. This calibration ensures that the first arrival of the radar wave is the start of the trace and corrects for electronic drift. A

sampling interval of 1600 ps was utilized along with a 433 ns time window. Each measurement stacked 32 shots at each point to optimize reflection depth, image quality, and improve signal to noise ratio (Davis and Annan, 1989; Sensors and Software, 2005). Gain functions were not applied during data collection, allowing the later processing of undistorted data. Latitude and longitude was collected at the start and end of every profile and at significant landmarks in between by using a Meridian GPS unit by Magellan.

Four survey lines were sampled at site 07 (Figure 4 and Figure 9). The survey lines totaled 378.5 m in length. Survey line 01 ran from the northeast to the southwest along a natural terrace. The survey line was taken just to the north of a highly vegetated interdistributary marsh on the southwestern edge of the Trinity River delta known as Cotton Bayou. Access to the northern portion of the interdistributary area itself was impossible given the robust vegetation. Further sampling locations at site 07 were limited to areas where the thick vegetation could be cleared or pushed down. Survey lines 02 and 04 were taken perpendicularly to a man-made levee. Both survey lines run from the northeast to the southwest and total 129 m in length. Survey line 03 samples from the end of survey line 02 and runs parallel to the man-made levee transecting line 04 creating tie points for correlation.

Site 08 is an interdistributary area to the southwest of a meander in the main channel of the lower Trinity River (Figure 4 and Figure 5). This site was scouted and tested as site 01, lines 01 and 02. Thick vegetation, saturated soils, and standing water limited the potential sampling locations. Therefore, GPR sampling locations at site 08 were chosen in an opportunistic manner. Five GPR survey lines were sampled at site 08 totaling 762.5 m. Three of the survey lines ran parallel to the levee, and the other two survey lines ran perpendicular to the levee. The survey lines were set up to intersect one another to form tie

points for better correlation. While sampling line 03, the transmitter cable became separated from the transmitter. The equipment error was not noticeable with the Digital Video Logger for 8 traces (4 m). Survey line 03 was stopped, a GPS reading was taken, and then the survey line was continued as survey line 04.

Site 09 was scouted and tested as site 01 line 04 (Figure 4 and Figure 6). Site 09 is an interdistributary marsh 300 m northeast of the Trinity River National Wildlife Refuge, Champion Pier. Site 09 consisted of four GPR survey lines. Survey lines 01-03 sampled along the tree line of a clear cut dirt access road. Line 01 was 178.5 m in length and ran in an east-southeast direction. Survey line 02 sampled to the southeast from the end of line 01 and was 55.5 m. Survey line 03 ran north to south for 114 m from the end of line 02 and transected a pipeline. The final survey line at site 09, line 04, ran north to south and sampled 163 m. This survey line not only intersected line 01 to create a tie point for correlation, it also transected the clear cut dirt access road.

After the GPR surveys were collected, they were processed and plotted with Sensors and Software Inc. EKKO_View Deluxe software. The initial processing step employed a temporal high pass filter referred to as DEWOW. This filter removes low frequency components of the data, known as WOW, which are superimposed on high frequency reflections. This WOW is produced by electrical properties in the ground as well as instrumentation range limitations (Annan, 1999; Sensors and Software, 2003).

Next, the data was processed with the Spreading and Exponential Compensation (SEC) gain. The SEC gain function increases signal strength exponentially down each data trace in an attempt to compensate for geometric spreading and the exponential dissipation of energy with depth (Olhoeft, 2002; Sensors and Software, 2003). Input values used for the

SEC gain function were a starting value of 0.01, an attenuation value of 10, and a maximum value of 500 (Johnston, 2007, personal comm.).

The aforementioned processing steps were all that were needed to process the GPR data, with the exception of site 03 lines 01 and 02, site 08 lines 03 and 04, and site 09 lines 02 and 03. Due to the separation of the transmitter cable from the transmitter during the sampling of site 08 line 03, the last 8 traces collected during survey line 03 were unusable. Therefore the unusable traces were deleted, and lines 03 and 04 were merged together for continuity. Site 03 lines 01 and 02 and site 09 lines 02 and 03 were merged for display purposes only.

No elevation corrections were made to the data because topographic relief in these areas of the delta is negligible. No time zero corrections were needed due to prior calibration in the field. GPR surveys were then plotted in both wiggle-trace and color-trace formats prior to interpretation. A uniform velocity of 0.06 m/ns was applied to all profiles based on average signal velocity in wet clays (Neal, 2004). Principles of GPR operation and processing were utilized based off descriptions by (Annan, 1999; Sensors and Software, 2003, 2005).

3.2 GPR Results and Interpretation

As previously described in the study site and methodology sections, site 01 lines 01-03 and site 08 lines 01-05 surveyed the same interdistributary marsh in the Trinity River delta (Figure 5). All GPR survey lines at this location displayed similar profiles (see Appendix A). Site 08 line 05 will serve here as the type section for this interdistributary marsh and will be used for interpretation and explanation purposes (Figure 10). The first

return on the site 08 line 05 radar profile is positioned just below 0 ns on the time axis and is a trough shaded in black. This low amplitude, continuous reflector is interpreted to be the GPR air wave. The air wave is that portion of the electromagnetic wave transmitted to the receiving antenna through the air (Augustinus and Nichol, 1999). The next return is a high amplitude, continuous reflector at a depth of 0 m. This reflector is the ground wave, and is that portion of the electromagnetic wave transmitted directly to the receiving antenna through the ground surface. Due to the high dielectric constant in the subsurface at this survey location, rapid attenuation of the electromagnetic wave resulted in a lack of subsurface reflections below the conductive material and produced a high frequency ringing (Johnston, 2007, personal comm.; Neal, 2004). This high frequency ringing generated multiple reflections which can be observed as low amplitude discontinuous responses spaced every 40 ns apart, and show a decrease in amplitude with depth.

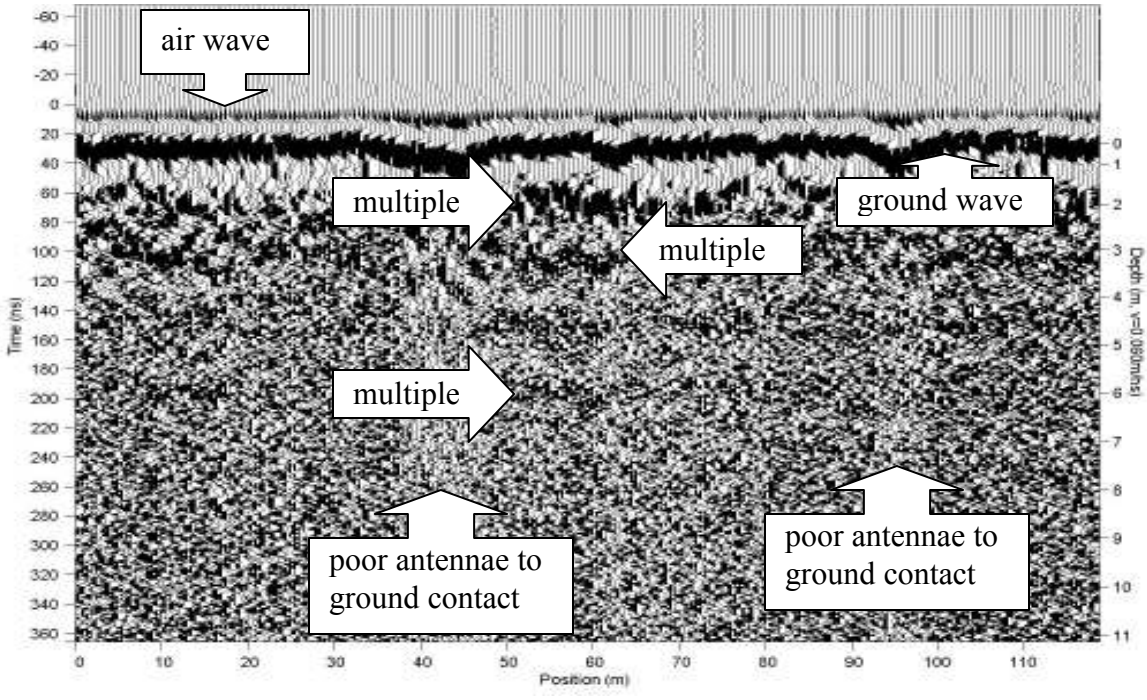

Figure 10. Site 08 line 05 GPR profile.

A sand bar along the main channel of the Trinity River was sampled in survey lines 05 through 08 at site 01 (Figure 7). This sand bar is approximately 13 km north of the Trinity River delta study area. 100 MHz antennas were used to survey line 08, while 50 MHz antennas were used to sample survey lines 05-07. Due to the topography of the point bar, all survey lines were topography-shifted. The first two returns on the site 01 line 08 profile were the air and ground waves (Figure 11). The air wave is the low amplitude continuous return shaded in black and positioned just below 20 ns on the time axis. The ground wave is the high amplitude continuous reflector at 30 ns. Beneath the ground wave at 35 ns is a high amplitude continuous reflector that moves horizontally from left to right across the image. This reflector is interpreted to be the water table, and no reflections can be seen below it. Between the ground wave and the water table, a number of downlapping sigmoidal reflections can be observed. These sigmoidal reflections are bedding planes which are characteristic of lateral accretion surfaces. The 100 MHz antennas used for line 08 reached a maximum depth of 1 m and had a vertical resolution of 0.25 m.

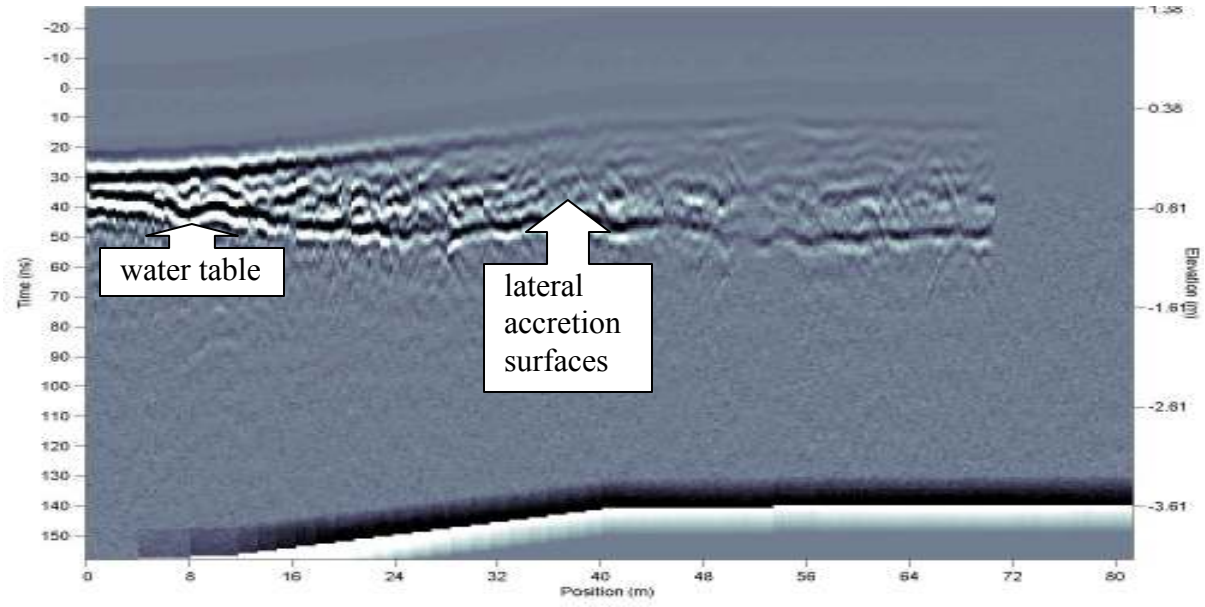

Figure 11. Site 01 line 08 GPR profile.

The 50 MHz antennas were used for survey lines 05-07 at site 01 (Figure 7). The 50 MHz antennas had a greater depth of penetration (5 m, see Figure 12), but worse resolution (0.5 m) than the 100 MHz antennas at the point bar (Figure 12). The 50 MHz antennas were able to discern the same downlapping sigmoidal reflections interpreted to be lateral accretion surfaces and below the water table, but the low resolution was not able to display the water table itself effectively.

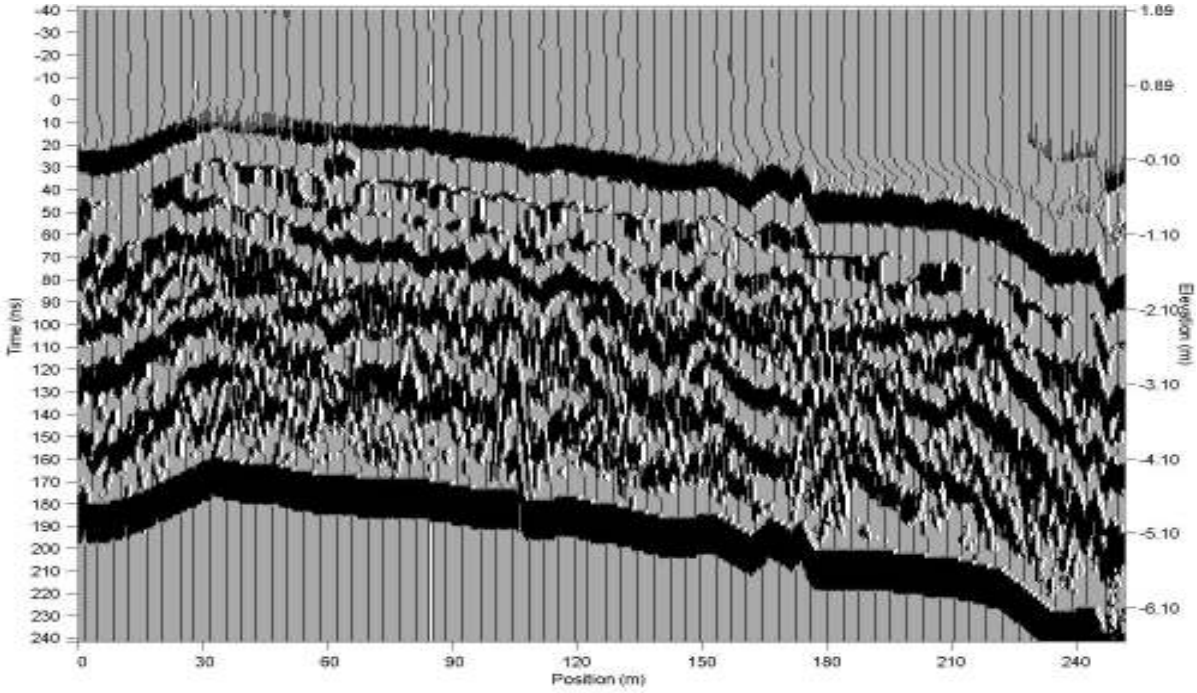

Figure 12. GPR survey lines 05 and 06 merged.

Site 02 line 01 and site 06 line 01 were GPR surveys conducted on the grassy lawns of Texas Christian University in Fort Worth, TX. Both surveys were used primarily to train field assistants on the use of the GPR system. The first two returns on both GPR profiles were the air and ground waves (Figure 13). The air wave is the low amplitude continuous return shaded in black and positioned just below 0 ns on the time axis. The ground wave is the high amplitude continuous reflector at a depth of 0 m. The GPR surveys at these sites had a maximum depth of penetration of 11.25 m, and 1.0 m vertical resolution. Numerous

discontinuous high amplitude reflectors can be seen in the survey lines, but due to the short distance of the survey lines and the 0.5 m step size subsurface stratigraphy could not be interpreted. The GPR survey lines at site 02 and site 06 display one of the fundamental problems with GPR systems; they are affected by technology. Interference from power lines, walkie talkies, and television, radio, and cellular phone transmitters can disrupt the signal returning to the GPR receiving antenna (Olhoeft, 2002; Neal, 2004). This interference can be seen at the top of the radar profiles by the low amplitude excursions in each trace above the air wave.

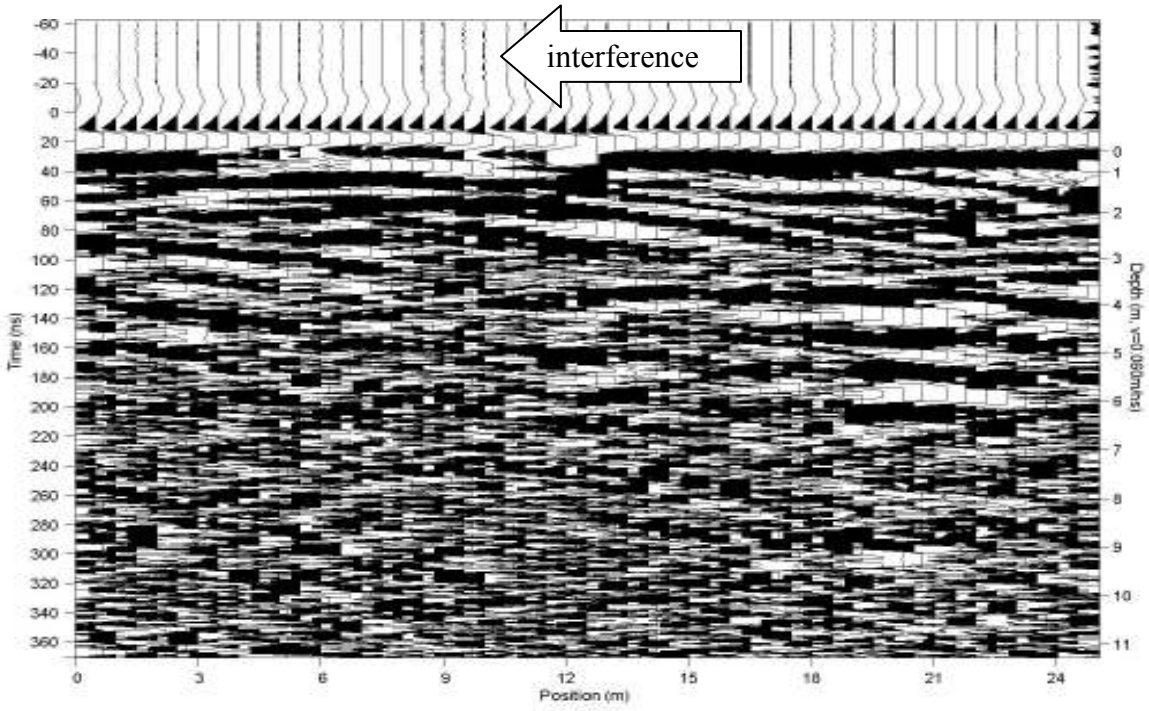

Figure 13. GPR survey site 06 line 01.

Survey site 03 involved the collection of two GPR survey lines adjacent to Interstate 10 within the Trinity River delta (Figure 8). The two survey lines were located in a constructed wetland just north of a construction road. The survey lines 01 and 02 were merged together (Figure 14). The first two returns on the GPR profile were the air and ground waves. The air wave is the low amplitude continuous return shaded in black and

positioned just below 0 ns on the time axis. The ground wave is the high amplitude continuous reflector at a depth of 0 m. Due to the high dielectric constant in the subsurface at this survey location, rapid attenuation of the electromagnetic wave resulted in a lack of subsurface reflections below the conductive material. There are many hyperbolic-shaped responses in the profile and they are interpreted to be air wave events from above-ground objects, most likely nearby trees. As noted previously, a portion of the GPR systems electromagnetic energy travels through the air. When this air wave strikes an object, the energy can be returned to the receiver and displayed as a reflector (Neal, 2004; Johnston, 2007, personal comm.). There is also a deeper low amplitude linear reflector dipping from the 0 m mark on the depth scale to the 65 ns mark on the time scale. This dipping reflector is also an air wave event from a plastic construction fence which ran roughly parallel (7º angle) to the survey line.

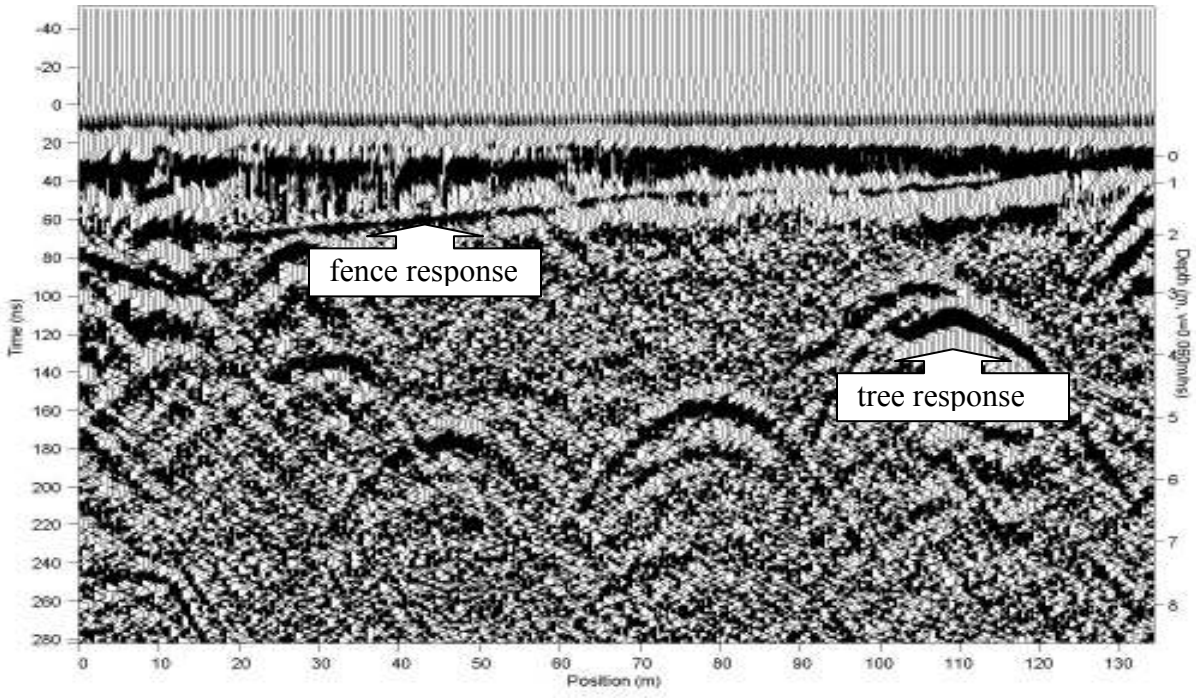

Figure 14. GPR survey site 03 line 01 and 02 merged.

At survey site 05, one survey line adjacent to Texas Hwy 90 was collected, which is approximately 13 km north of the Trinity River delta study area (Figure 7). Survey line 01 sampled from west to east perpendicular to the Trinity River. The first two returns on the GPR profile were the air and ground waves (Figure 15). The air wave is the low amplitude continuous return shaded in black and positioned just below 0 ns on the time axis. The ground wave is the high amplitude continuous reflector at a depth of 0 m. As with all other GPR surveys, rapid attenuation of the electromagnetic wave resulted in a lack of subsurface reflections below the conductive material and produced a high frequency ringing. This high frequency ringing generated multiple reflections which can be observed as high amplitude, continuous responses spaced every 0.75 m apart. The multiples extend to a depth of 10.5 m and show a decrease in amplitude with depth. There are many hyperbolic-shaped responses in the profile and they are interpreted to be air wave events from above-ground objects, most likely nearby trees.

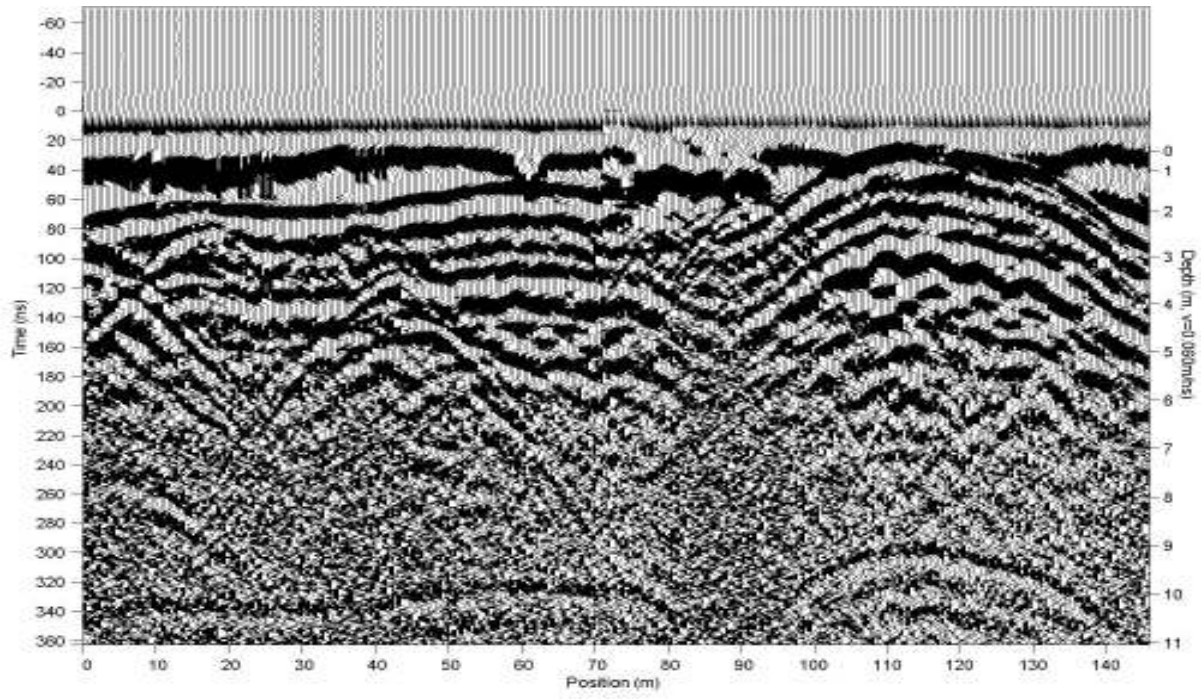

Figure 15. GPR survey site 05 line 01.

Four GPR survey lines were collected at site 07, which is a highly vegetated interdistributary marsh on the southwestern edge of the Trinity River delta known as Cotton Bayou (Figure 9). All GPR survey lines at this location displayed similar profiles in that the first two returns on the GPR profile were the air and ground waves (Figure 16). The air wave is the low amplitude continuous return shaded in black and positioned just below 0 ns on the time axis. The ground wave is the high amplitude continuous reflector at a depth of 0 m. The high dielectric constant of the surface sediments prevents subsurface reflections below this point, and generated multiple reflections which can be observed as low amplitude discontinuous responses spaced every 1 m apart. Along line 01, however, nearby trees caused hyperbolic-shaped air wave responses which masked the multiples (Figure 17).

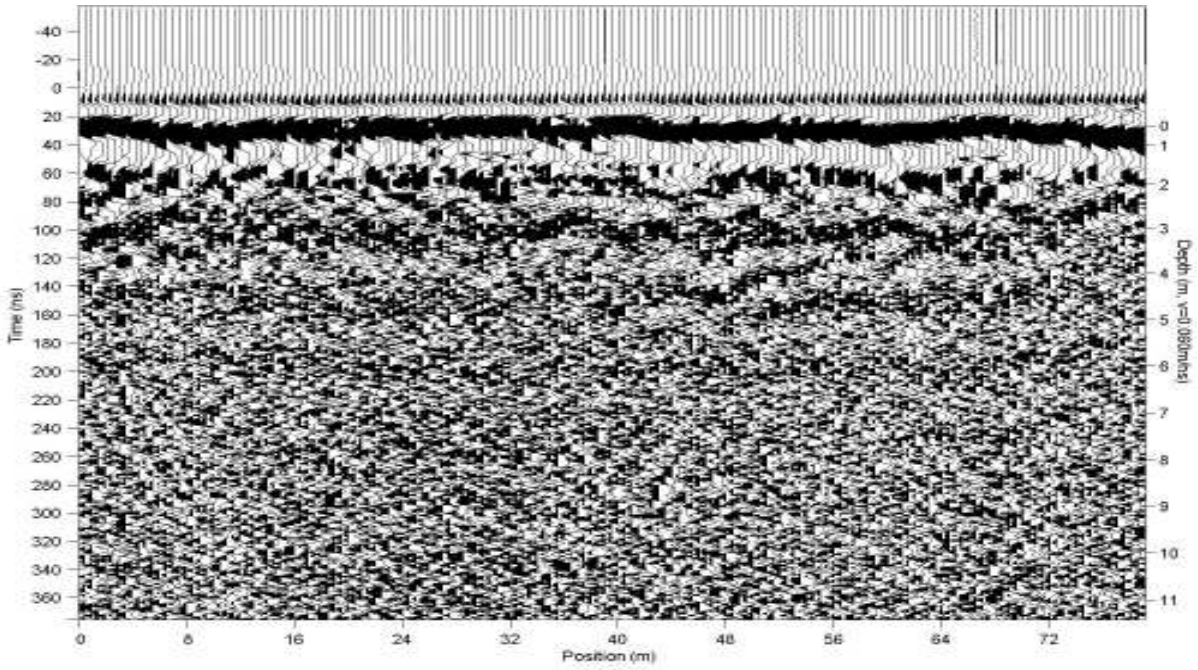

Figure 16. GPR survey site 07 line 04.

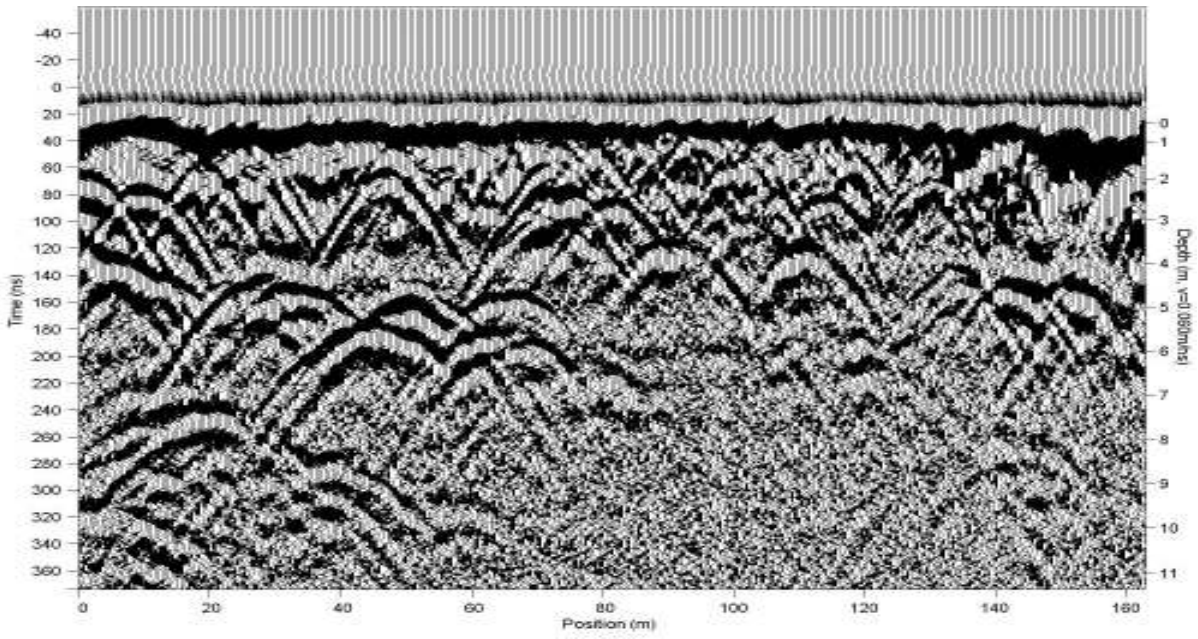

Figure 17. GPR survey site 07 line 01.

As previously noted in the study site and methodology sections, site 01 line 04 and site 09 lines 01-04 surveyed the same interdistributary marsh 300 m northeast of the Trinity River National Wildlife Refuge, Champion Pier (Figure 6). Survey lines 02 and 03 followed the tree line of a clear cut dirt access road intersecting a pipeline. The two lines are merged here for display purposes (Figure 18). As before, the rapid attenuation of the electromagnetic wave by the conductive sediments resulted in no subsurface reflectors being observed. Even the pipeline that crossed at 160 m was masked by the surface sediments. Survey lines 03 and 04 display the effect nearby trees have on a GPR survey. Hyperbola-shaped air wave responses dominate the profiles until the GPR system enters the clearings made for the pipeline at 160 m in (Figure 18) and the access road from 55-79 m in (Figure 19). In the clearings, there were no trees contacting the air wave to cause a reflection.

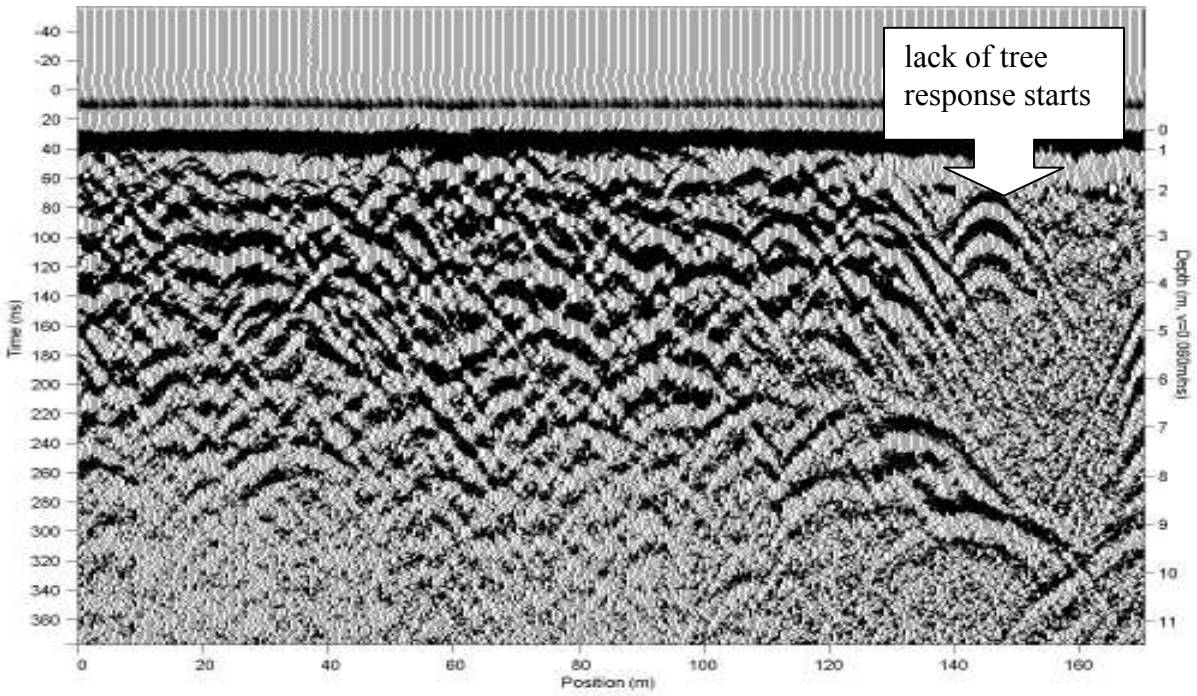

Figure 18. GPR survey site 09 line 02 and 03 merged.

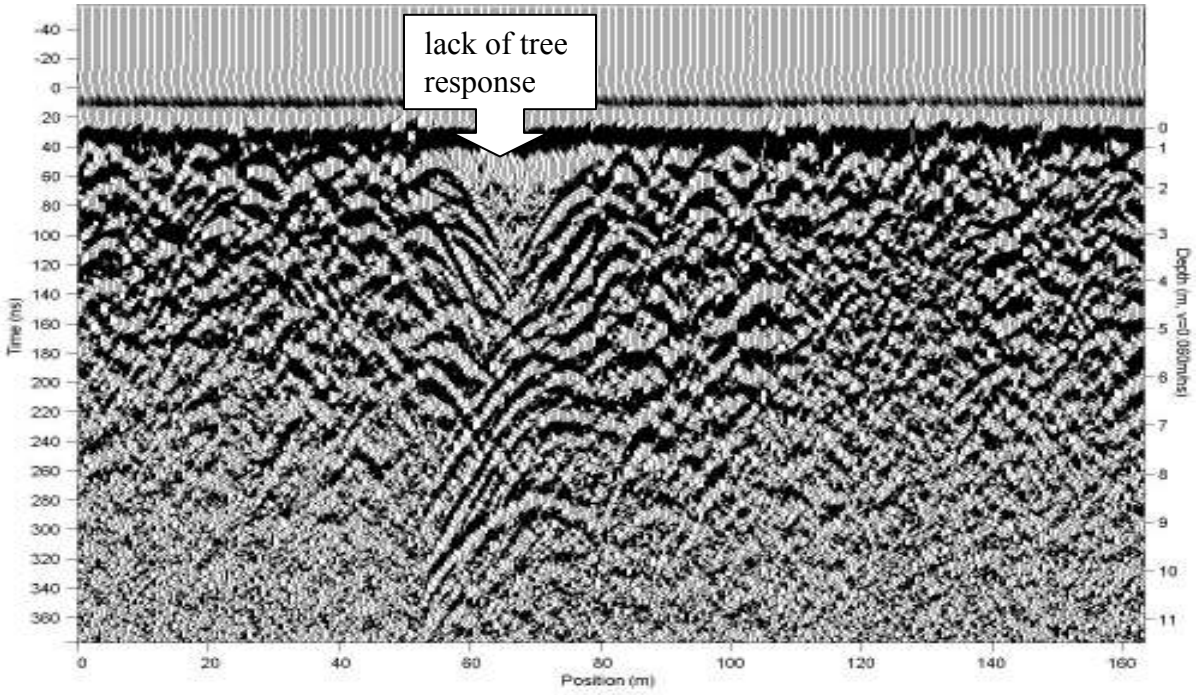

Figure 19. GPR survey site 09 line 04.

CHAPTER 4

SEDIMENT CORING ANALYSIS

4.1 Coring Methodology

Sediment coring was attempted at each of the three GPR sites (site 07-09) within the Trinity River delta study area (Figure 2). When possible, coring sites were located on or near one of the GPR survey lines. A Russian core sampler with 1.2 m extension rods from Rickly Hydrological Company was used in an attempt to sample a depth of 10 m. The Russian core sampler is composed of a 0.5 m long half cylinder with sharpened edge and a rotating fin system. The sampler was hammered into the ground using either a slide hammer or post-hole driver, until the appropriate sampling depth was reached. The sampler or extension rods were then turned clockwise causing the sharpened sampler edge to cut through the soil. The sampler or extension rods were turned until the sampler rotated 180 degrees around the fin, trapping a half core of sediment in the sampler. Every sample was taken in 0.5 m intervals in an attempt to provide one continuous core. The sampler was then removed from the ground by hand or with the assistance of a toe jack. Sediment samples were extracted from the sampler, measured, labeled, and wrapped in foil for transport to the lab for further analysis.

The first attempt at sediment coring in the Trinity River delta was in August of 2007 at site 08 (Figure 5). S8B1 was offset approximately 6 m to the north of site 08 survey line 02 due to standing water at the time of sampling. All samples were collected continuously at 0.5 m intervals with the exception of samples S8B1-5 and S8B1-6. The sampler hit refusal at 0.4 m and 0.23 m when sampling the 0.5 m progression in these two samples. After collecting samples S8B1-5 and S8B1-6, the sampler was then reinserted to the appropriate depth and sampling continued at 0.5 m intervals. S8B1 was unable to reach the intended

depth of 10 m due to equipment failure. Many of the Russian sampler's extension rods broke due to the stress placed on them by the compacted sediments, and sampling was terminated at a maximum depth of 5.6 m.

An attempt at sediment coring was undertaken the following morning at site 07 with the undamaged sampling equipment. The location for the proposed sediment core was 2 m to the south of the starting point for site 07 survey line 01 (Figure 9). Once again, equipment failures caused the boring to be terminated. An extension rod buckled, and the Russian sampler itself split apart when rotated in the soil. The decision was made to not attempt a sample until the equipment was replaced or repaired.

After repairs were made to the Russian sampler and extension rods were replaced, another attempt was made to acquire a sediment core at site 07. S7B1 was located at the starting point of site 07 survey line 02. This location is in an interdistributary marsh of the Trinity River delta and was approximately 10 m southwest of a man-made levee at site 07. Samples S7B1-1 through S7B1-5 were sampled without problems. At this point the extension rods began to wear down and break. Sample S7B1-6 was collected at a depth of 3 to 3.5 m after changing out multiple broken extension rods. The boring was unable to reach the intended depth of 4 m for sample S7B1-7, and sampling was suspended.

S7B1 was continued later that afternoon when replacement parts were found. The remaining samples were taken with the same Russian sampler, but the extension rods were replaced with 4' long ¾" plumbing pipe from a local hardware store. S7B1-7 through S7B1-10 were each taken at the standard 0.5 m interval to a maximum depth of 5 m. Sediment coring at S7B1 was stopped at this point due to lack of additional extension rods, darkness, and the presence of radiocarbon datable material in the samples collected.

The next sediment boring attempted was S9B1 at survey site 09 Trinity River National Wildlife Refuge, Champion Pier in the northern portion of the Trinity River delta (Figure 6). S9B1 was intended to sample an interdistributary marsh 25 m to the east of GPR survey line 04 at site 09. Sampling was to continue using the makeshift equipment used from the previous days work at site 07. This portion of the delta was flooded months earlier by an unusually wet summer, and was still saturated at the time of the GPR survey. However, at the time of sediment sampling, site 09 had not received rainfall in over a month and the soil had dried. The hard soil made it very difficult to drive the Russian sampler the 0.5 m into the ground to take the first sample. While attempting to take the first sample, the Russian sampler began to split apart. Due to the location in a National Wildlife Refuge, the hardness of the soil, and equipment failure, S9B1 was aborted.

4.2 Sediment Description Methodology

Once back in the laboratory, the sediment samples were unwrapped, measured for length, and photographed. A detailed description of sample characteristics was recorded in an attempt to correlate the soil core to the GPR survey lines. The description of each sample included wet and dried color, texture, moisture content, plasticity, and anything noteworthy about the sample, such as content of shells. Color of each sample was determined with the use of a Munsell soil color chart, and the textural classification was determined using techniques described in Levine (2001). Moisture content and plasticity were estimated by hand. After detailed descriptions of the soil core were made, the soil core was separated into different textural units. Representative samples of each textural unit were collected and subjected to bulk density and grain-size analysis.

4.3 Grain-size Methodology

Grain-size analysis was performed on the coarser than 4 Φ fraction of each representative sample. To perform grain-size analysis, the soil cores were air dried and 40-60 g of sediment were collected from each textural unit. The samples were weighed and then disaggregated by working the dried sample in a large mortar with a pestle. After the proper degree of disaggregation was achieved, the samples were immersed in a 150 ml beaker containing a warm sodium sulfate saturated solution and stirred for 15 minutes. The solution was then allowed to cool, causing the formation of crystals in the interstitial pores, forcing the grains apart (Royse, 1970).

The sample and solution was then passed through a # 4 Φ wet sieve. The water, saturated salt solution, and the associated silt and clay particles were removed from the coarse fraction of the sample. The material remaining in the sieve was dried in an oven overnight at 90 °C. Once dry, the samples were passed through the # -2, -1, 0, 1, 2, 3, and 4 Φ dry sieves by agitation for ten minutes in a sieve shaker. The portion remaining in each sieve was then weighed, and the data were graphed. A visual estimation of sorting and particle roundness or angularity was noted. Grain-size analysis followed procedures outlined in Royse (1970).

4.4 Bulk Density Methodology

Bulk density analysis was performed on the representative samples from each textural unit. The samples were collected from soil core S8B1 by pushing a clear plastic cylinder with a known diameter of 2.1 cm into the soil core and extracting the sample. The height of each sample was then measured on four sides of the cylinder to calculate an average height

for each sample. Volume of bulk density samples from S8B1 ranged from 2.2-5.4 cm^3. The samples from soil core S7B1 were collected with a slightly more accurate method. The same clear plastic cylinder with a known diameter of 2.1 cm was cut down to a height of 1.8 cm, creating a 6.23 cm^3 cylinder. The cylinder was pressed into the soil core and the excess sediment was shaved from the top of the cylinder. All samples were then extracted from the cylinder placed in 50 ml beakers of known weight and weighed. The samples were then placed in an oven and dried overnight at a temperature of 110 °C. The next day, samples were extracted from the oven and weighed. Bulk density was calculated by dividing the dry sample weight by the initial volume. Bulk density analysis followed procedures outlined by Tisdal (1951).

4.5 Sediment Results

S7B1 was located at the starting point of site 07 survey line 02. This location is in a highly vegetated interdistributary marsh on the southwestern edge of the Trinity River delta known as Cotton Bayou and was approximately 10 m southwest of a man-made levee at site 07 (Figure 9). A total of 500 cm of sediment was collected in boring S7B1 and seven different stratigraphic units were noted (Figure 20). The upper 20 cm of sediment was a moist, dark gray (2.5Y 4/1), high plastic silty clay with 5 percent sub-rounded fine-grained sand and high organic root content. Analysis of the unit produced a bulk density of 0.84 g cm^{-3}. Below a depth of 20 cm is a 171 cm thick high plastic clay. The clay becomes wet and changes color from dark gray (2.5Y 4/1) at 20 cm to very dark gray (GLEY 1 3/N) with depth. Iron staining can be noticed at a depth of 140 cm and the unit has a bulk density of 1.11 g cm^{-3}. The next stratigraphic unit is a wet, dark gray (GLEY 1 4/N), high plastic sandy

clay with 45 percent fine to medium-grained rounded to sub-rounded sand. The unit ranges from 191 cm to 200 cm and has a bulk density of 1.54 g cm^{-3}. From 200 cm to 266 cm is a wet, dark gray (GLEY 1 4/N), high plastic clay with a bulk density of 1.48 g cm^{-3}. Fine to medium-grained sub-rounded to sub-angular sand increases with depth within the unit. At a depth of 266 cm, there is a unit of wet, dark gray (GLEY 1 4/N), high plastic sandy clay. The sandy clay consists of 40 percent fine to medium-grained sub-rounded sand with *Mactra* shell fragments throughout and a bulk density of 1.71 g cm^{-3} (Figure 21). Below 300 cm in depth is a layer of wet, dark gray (GLEY 1 4/N), low plastic sandy clay loam with 35-45 percent fine to medium-grained sub-rounded to sub-angular sand. The unit has an average bulk density of 1.51 g cm^{-3} and becomes high plastic at a depth of 350 cm. *Mactra* shell fragments become abundant at a depth of 372 cm and continue to the bottom of the boring. The final stratigraphic unit in S7B1 is a wet, dark gray (GLEY 1 4/N), high plastic sandy clay with 40 percent fine to medium-grained sub-rounded to sub-angular sand. This unit had trace coarse-grained sand and wood fragments with a bulk density of 1.58 g cm^{-3}. The sandy clay unit ranges from 412 cm to a depth of 500 cm which was the maximum depth of S7B1.

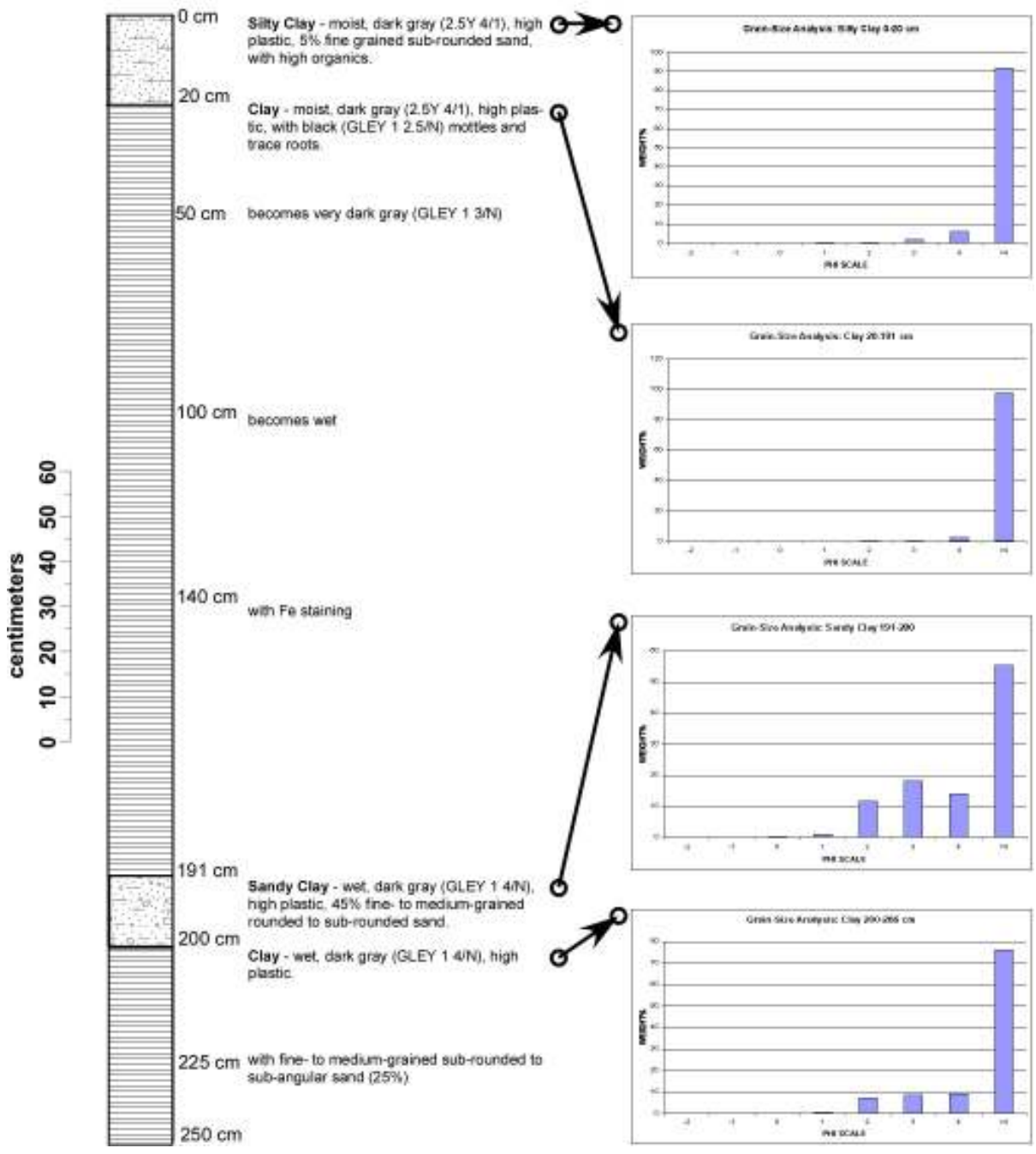

Figure 20. Stratigraphic column S7B1.

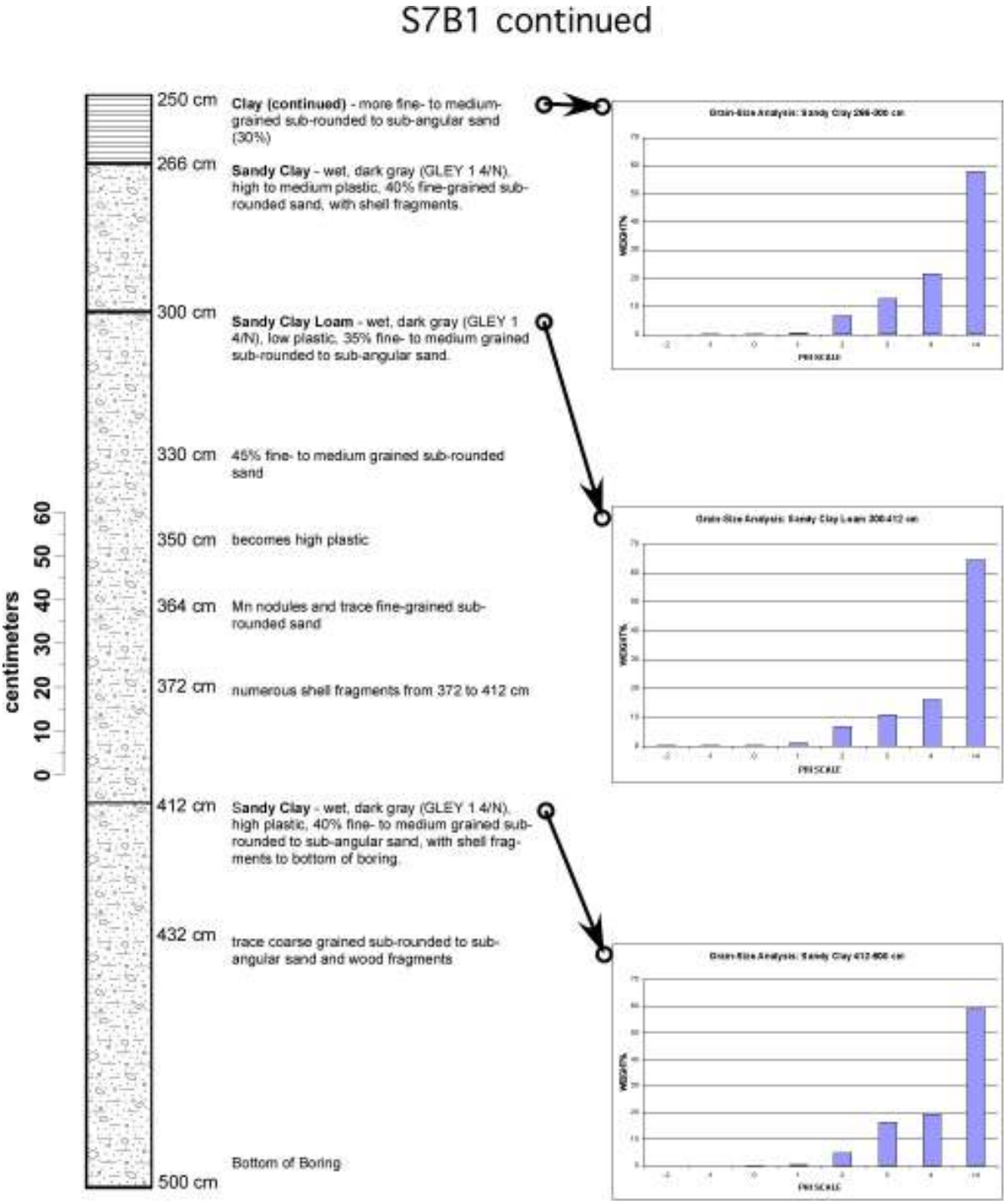

Figure 20 continued. Stratigraphic column S7B1 continued.

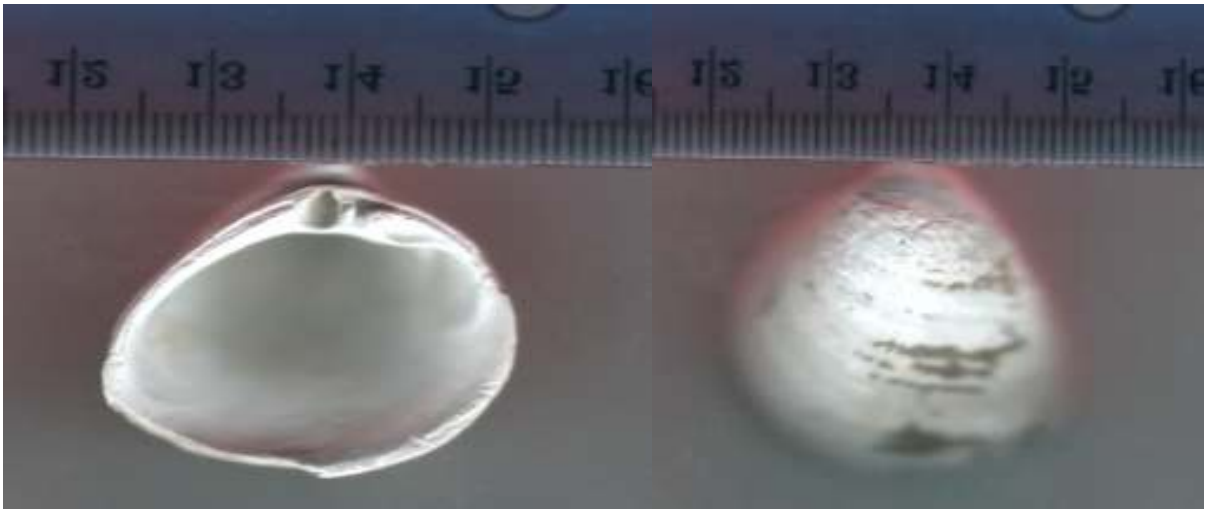

Figure 21. *Mactra* shells recovered in S7B1 and S8B1.

Site 08 is an interdistributary marsh to the southwest of a meander in the main channel of the lower Trinity River (Figure 5). S8B1 was offset approximately 6 m to the north of site 08 survey line 02 due to standing water at the time of sampling. A total of 563 cm of sediment was collected in boring S8B1 and eight different stratigraphic units were noted (Figure 22). The upper 33 cm of sediment was a wet, very dark gray (2.5Y 3/1), high plastic silty clay loam with 10 percent sub-rounded to rounded fine-grained sand with organics and iron staining. Analysis of the unit produced a bulk density of 1.9 g cm^{-3}. Below a depth of 33 cm is a 153 cm thick wet, dark greenish gray (GLEY 2 4/1), high plastic clay with five percent fine to medium-grained rounded to sub-rounded sand. Mottling and organic materials are present at the top of the unit and decrease with depth. The unit has a bulk density of 1.9 g cm^{-3}. The next stratigraphic unit is a wet, gray (GLEY 1 6/N) sandy loam composed of 55 percent fine to medium-grained rounded sand. The unit ranges from 186 cm to 210 cm and has a bulk density of 2.0 g cm^{-3}. From 210 cm to 313 cm is a wet, gray (GLEY 1 5/N), sandy loam with an average bulk density of 1.8 g cm^{-3}. The unit consists of 75 percent fine to medium-grained sub-rounded to sub-angular sand. At a depth

of 313 cm, there is a unit of wet, dark gray (GLEY 1 4/N), high plastic sandy clay. The sandy clay consists of 25 percent fine to medium-grained sub-rounded to sub-angular sand and has a bulk density of 1.9 g cm^{-3}. Below 363 cm in depth is a layer of wet, dark gray (GLEY 1 4/N), low plastic sandy clay loam with 68 percent fine to medium-grained sub-rounded to sub-angular sand and a bulk density of 2.0 g cm^{-3}. From a depth of 413 cm to 442 cm there is a layer of wet, dark gray (GLEY 1 4/N), high plastic clay with 30 percent fine to medium-grained sub-rounded to sub-angular sand. The clay unit has thin sand lenses throughout and a bulk density of 2.3 g cm^{-3}. The final stratigraphic unit in S8B1 is a wet, dark gray (GLEY 1 4/N), high plastic sandy clay loam with 55 percent fine to medium-grained rounded to sub-rounded sand. The unit has numerous *Mactra* shell fragments and a bulk density of 1.6 g cm^{-3}. The sandy clay loam unit extended to a depth of 563 cm which was the maximum depth of S8B1.

Due to transport and drying, sediment cores experienced some shrinkage during transport from the field to the laboratory. S7B1 was measured to be 491 cm at the time of analysis. This is 9 cm less than the 500 cm recovered in the field, and equates to a 2 percent sediment loss. S8B1 was measured to be 524.6 cm at the time of analysis. This is 38.4 cm less than the 563 total cm recovered in the field, and equates to a 7 percent sediment loss. With the error in each sediment core being small, the cores were not adjusted for depth. Each core was described from the top to the bottom of the sampling interval. The top of each sample was assigned to the start of the sampling interval, and the base of each sample was then extrapolated down to the bottom of the sampling interval.

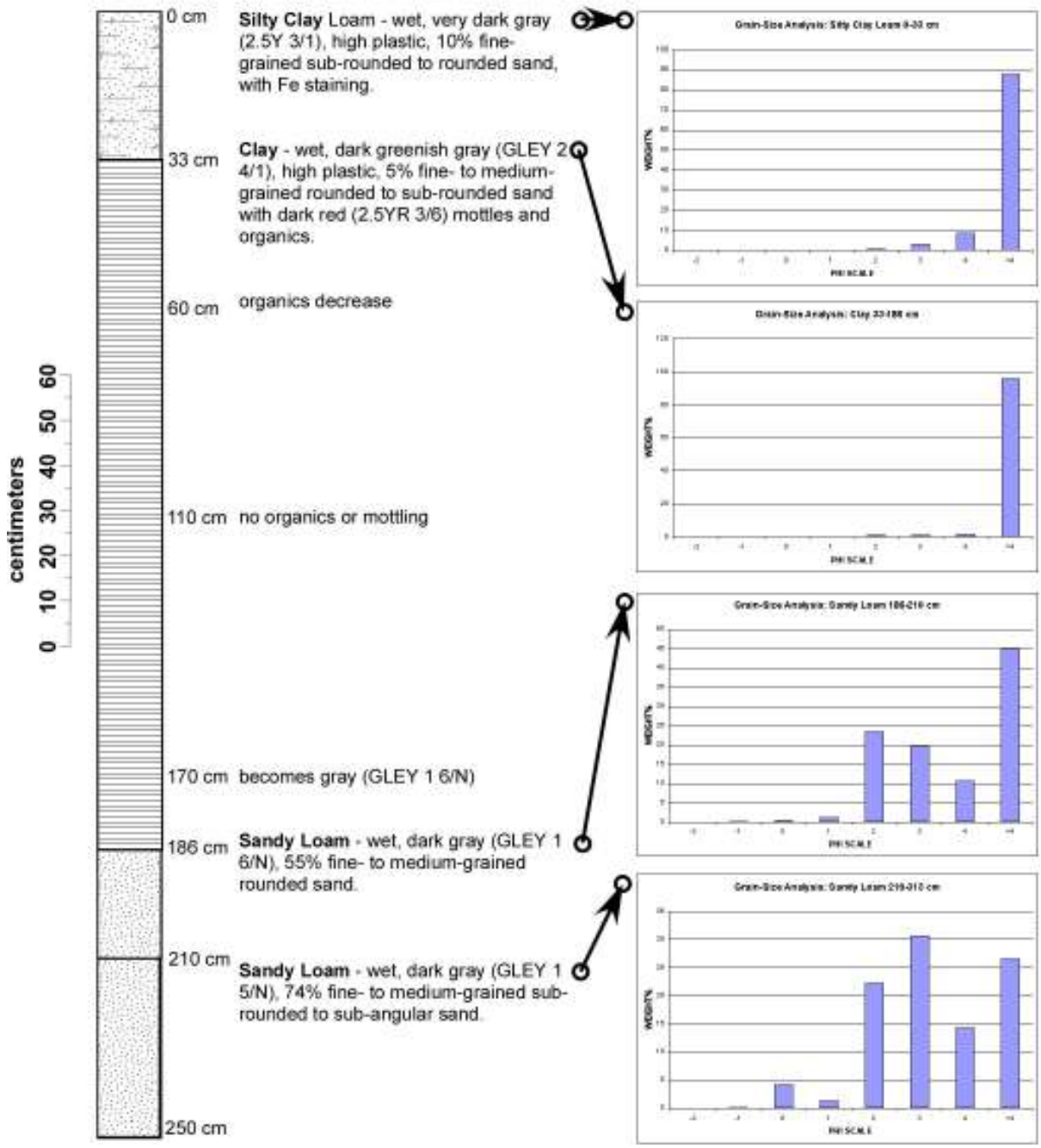

Figure 22. Stratigraphic column S8B1.

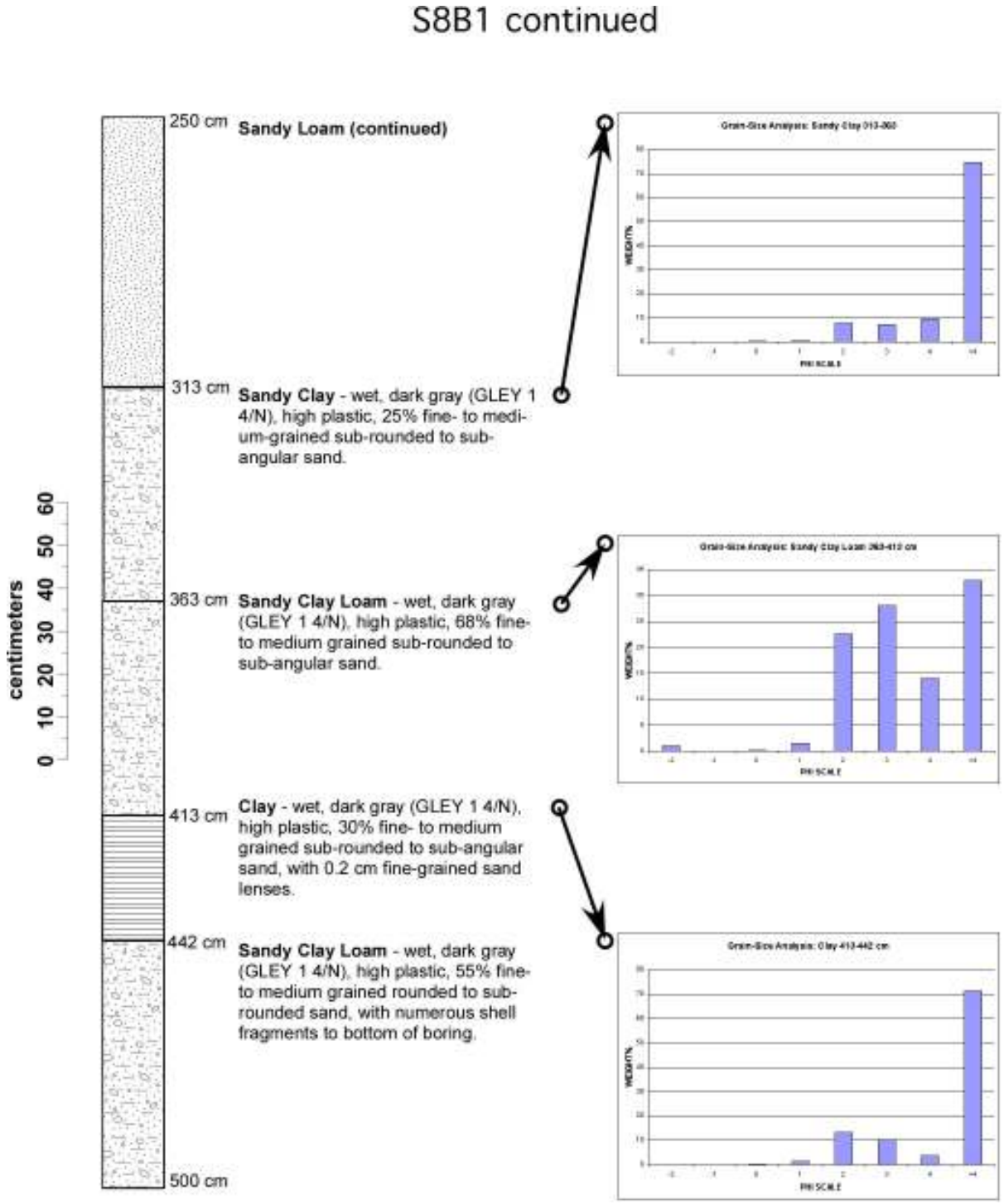

Figure 22 continued. Stratigraphic column S8B1 continued.

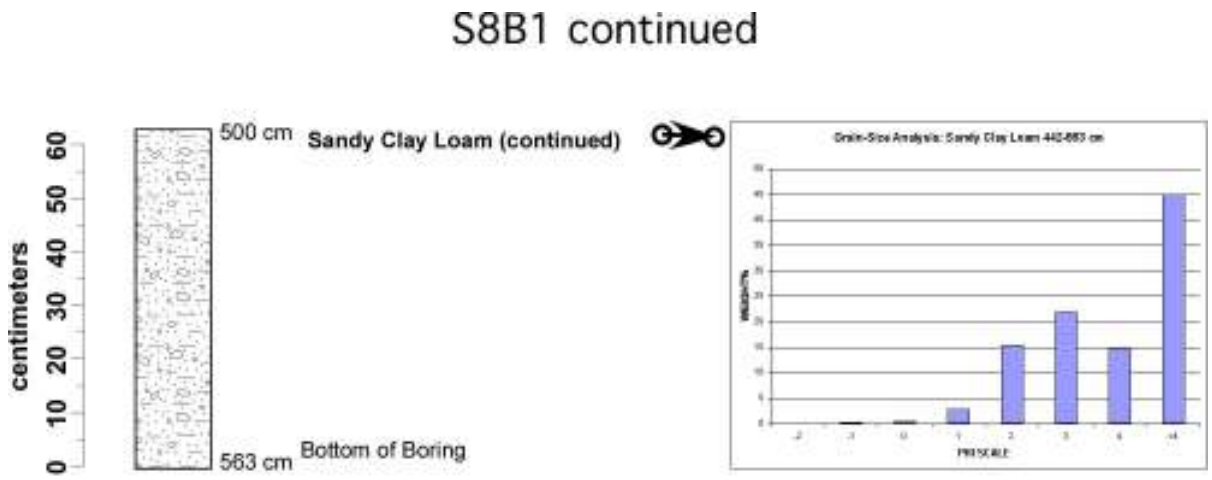

Figure 22 continued. Stratigraphic column S8B1 continued.

Grain-size analyses were made with wet and dry sieves. During this process, a limited amount of sediment can be lost through a process known as sieve loss. There were nine samples analyzed for grain-size from S7B1. There was a minimum sieve loss of 0.0 percent, a maximum of 6.5 percent, and the mean sieve loss for S7B1 was 1.0 percent. There were another nine samples analyzed for grain-size from S8B1. There was a minimum sieve loss of 0.1 percent, a maximum of 2.4 percent, and the mean sieve loss for S8B1 was 0.7 percent.

4.6 Radiocarbon Dating Methodology

Multiple shell and wood fragments were discovered in soil cores S7B1 and S8B1 (Figure 20 and Figure 22). The depths of the fragments were measured and recorded. After the fragments were extracted from the soil core, they were cleaned, labeled, and placed in plastic bags. Two shell fragments from each sediment core were selected based on size and position in the core and shipped to the Illinois State Geological Survey for radiocarbon dating

analysis. Standard procedures to pre-treat and analyze carbonate samples for Accelerator Mass Spectrometry (AMS) ^{14}C dating were used to analyze the four shell fragments (AMS Laboratory, 2008). The shell fragments were weighed and added to 2 ml of 100% phosphoric acid in a pyrex Rittenberg reaction vessel. The vessel was evacuated until the vacuum gauge dropped to 10 millitorr. Phosphoric acid was decanted from the side arm into the shell sample in the main chamber for reaction at 25 °C overnight. The CO_2 was then collected by cryogenic distillation for carbonate ($d^{13}C$) isotope and AMS ^{14}C dating analyses.

4.7 Radiocarbon Dating Results

The ages of the four radiocarbon dated samples range from 2.8 to 3.2 Ka (Table 1). The shallow sample (S7B1-S1) from S7B1 was sampled at a depth of 292 cm and was radiocarbon dated to be 2.83 Ka. This age produces a sediment accretion rate of 1.0 mm yr^{-1} for the last 2,830 years at Site 07. The deeper sample (S7B1-S12) was radiocarbon dated to be 3.23 Ka and was collected at a depth of 372 cm. Therefore, Site 07 has a mean sediment accretion rate of 1.2 mm yr^{-1} for the previous 3,230 years. The 400 year time gap between the deposition of S7B1-S1 and S7B1-S12 accumulated 80 cm of sediment with an accretion rate of 2.0 mm yr^{-1}. The shallow sample (S8B1-S1) from S8B1 was sampled at a depth of 454 cm and was radiocarbon dated to be 2.845 Ka. This age produces a sediment accretion rate of 1.6 mm yr^{-1} for the last 2,845 years at Site 08. The deeper sample (S8B1-S9) was radiocarbon dated to be 2.98 Ka and was collected at a depth of 536 cm. Therefore, Site 08 has a mean sediment accretion rate of 1.8 mm yr^{-1} for the previous 2980 years. The 135 year time gap between the deposition of S8B1-S1 and S8B1-S9 accumulated 82 cm of sediment with an accretion rate of 6.0 mm yr^{-1}. With mean accretion rates of 1.2 and 1.8 mm yr^{-1}, over

the length of the cores this study produced a mean sediment accretion rate of 1.5 mm yr^{-1} for the Trinity River delta.

Table 1. Accretion rates at sites 07 and 08.

Sample #	Depth (cm)	^{14}C age (yrs)	± (yrs)	Accretion Rate (mm yr^{-1})	Accretion Rate Between Samples (mm yr^{-1})
S7B1-S1	292	2830	20	1.0	2.0
S7B1-S12	372	3230	20	1.2	
S8B1-S1	454	2845	20	1.6	6.0
S8B1-S9	536	2980	20	1.8	

CHAPTER 5

DISCUSSION AND CONCLUSIONS

5.1 Ground Penetrating Radar Usefulness

The objectives of this thesis were (i) to document and quantify sediment accretion in the Trinity River delta using rapid, non-invasive ground penetrating radar (GPR) technology and traditional soil cores, and (ii) to test the usefulness of GPR in the interdistributary marshes of a fine-grained delta to determine subsurface stratigraphy. Although results indicate that stratigraphy can be constrained using GPR in coarse-grained environments, such as sand bars, it is not useful in determining the subsurface stratigraphy or accretion rates in interdistributary marshes of fine-grained deltas. Results show that the high dielectric constant of clay and water in the sediments completely attenuate the GPR signal masking the underlying stratigraphy. The high dielectric constant in the subsurface of the delta also generated multiple reflections, and in wooded areas, hyperbolic shaped air wave responses. Similar responses to fine-grained material and water content have been noted in previous GPR studies (Davis and Annan, 1989; Neal, 2004). Sass (2007) attempted to use GPR technology to determine depth of dam sediments in the Karoo, South Africa during the dry season, hoping that the dry sediment conditions would lead to a favorable GPR response. Sass (2007) found that even without saturated sediments, the electrical conductivity of the fine-grained silt and clay was enough to limit the GPR responses. Therefore, due to the results of this thesis and work by other authors, the study of highly vegetated, fine-grained deltas to determine sediment accretion rates and underlying stratigraphy with GPR technology is not viable.

5.2 Trinity River Delta Sediment Accumulation

Mactra shell fragments discovered in the sediment cores at sites 07 and 08 allowed the age of deposition (and hence accretion rates) within the delta to be determined, and gave insight into when alluvial sediment delivery to the coast started to exceed marine deposition of sediment at these locations. The marine bivalve *Mactra* is often found buried deeply in mud in estuaries and tidal flats. The presence of *Mactra* shells is evidence of inter-tidal deposition in the littoral zone (Pufahleta et al., 2004). According to the C_{14} dates, the Trinity River delta sediments started prograding out over marine deposits between 2.83 and 2.85 Ka at sites 07 and 08.

The sediment accretion results from this study display similar temporal and spatial variation in delta accretion rates as reported in previous studies (e.g., Rodriguez et al., 2005; Phillips, 2006). Site 08, the delta area near the main channel of the Trinity River, is accumulating sediment more rapidly than site 07 on the outer edge of the delta, and the sediment is coarser in texture (Figure 2). Phillips (2006) also noted that sites further from the Trinity River had lower sediment accretion rates. The observance of higher accumulation rates (1.2 mm yr^{-1} compared to 1.8 mm yr^{-1}) and coarser material at site 08 compared to site 07 is most likely the result of overbank flooding during high-energy sediment transport conditions along the main channel of the Trinity River.

The sediment accumulation rates calculated in this study range from 1.0 to 1.8 mm yr^{-1} with a mean of 1.5 mm yr^{-1}. These results are well within the range of accumulation rates cited in past studies of bayhead deltas in the Gulf Coast region which range from negligible to 16.7 mm yr^{-1} (Table 2). Where the results of this study differ from previous studies, however, is in the calculated mean accretion rates. With the exception of Rodriguez

et al. (2005), past studies have mean accretion rates ranging from 2.6 to 7.6 mm yr^{-1}. The reasons for the difference in mean accretion rates could be the depth at which samples were collected and their corresponding time intervals, or simply the number of sites sampled. Previous studies collected dateable material at depths of no more than one meter, but sampled many locations within the delta. However, in this study and that by Rodriguez et al. (2005), dateable samples were collected from depths significantly deeper than 1 m, but had a limited number of sampling locations. Despite this, our study and that by Rodriguez et al. (2005) had remarkably consistent Holocene sediment accretion rates of 1.5 and 1.58 mm yr^{-1}, respectively. The calculated mean accretion rates from surface samples (<1m) are providing better resolution in the short term, but are unrealistic as historic long term rates. In the short-term, however, the higher sediment accretion rates could be a signal of anthropogenic influence, such as intensive land use change and accelerated erosion.

Table 2. Delta accretion rates in southeast Texas.

Location	Range (mm yr^{-1})	Mean (mm yr^{-1})	Source
Trinity River, TX	1.0-1.8	1.5	this study
Trinity River, TX	0-16.7	3.3	Phillips, 2006
Trinity River, TX	0.52-5.68	1.58	Rodriguez et al., 2005
Trinity River, TX	1.6-13.0	5.1	White et al., 2002
Trinity River, TX		5.4	White and Calnan, 1990
Lavaca-Navidad, TX	0.9-10.3	3.3	White et al., 2002
Nueces, TX	0.7-7.6	2.6	White et al., 2002
Colorado River, TX		7.5	White and Calnan, 1990
Tensaw, AL		7.6	Aust et al., 1991

The amount of sediment needed to cover the surface area of the modern Trinity River delta was calculated to obtain the approximate amount necessary for accretion rates from 0.25 to 3.0 mm yr^{-1}. The surface area of the modern Trinity River delta is 126.1 km^2 and each mm yr^{-1} of sediment thickness over that area requires 126,100 m^3 yr^{-1} of sediment

(Phillips, 2006). Average bulk densities of floodplain and marsh deposits in the Trinity River delta are 1.4 Mg m^{-3} (Phillips, 2006). Therefore, the cubic meters necessary to cover the delta at a particular accretion rate was multiplied by 1.4 to obtain the Mg yr^{-1} required (Phillips, 2006). Figure 23 shows the megagrams required to cover 25-100% of the deltas surface at accretion rates from 0.25 to 3.0 mm yr^{-1}. Using the mean Holocene sediment accretion rate from this study (1.5 mm yr^{-1}) to cover 100% of the Trinity River delta, the amount of sediment needed per year was calculated to be 265,000 Mg yr^{-1}, which is 3.8 times the amount of sediment (70,000 Mg yr^{-1}) currently delivered to the delta by the Trinity River (Phillips, 2006; Phillips et al., 2004). At the current sediment delivery rate, the delta would be accreting at ± 0.4 mm yr^{-1}.

Modern fluvial sediment input from the Trinity River is thus inadequate to account for Holocene sedimentation rates in the delta. Pleistocene alluvial terraces and meander scars indicate higher discharges (and possibly higher sediment loads) in the past, but there is no evidence of different flow regimes the last 5 to 10 Ka (Phillips, 2006; Phillips et al., 2004). This leads one to believe that there are other non-fluvial sediment sources contributing to the accretion of sediment within the delta. Possible sediment sources accounting for the Trinity River delta accretion rates are slope wash from adjacent terraces, autochthonous organic matter, sediment delivery from tributaries within the delta area, and the reworking and resuspension of local Trinity Bay and delta sediments (Slattery and Phillips, 2005; Phillips, 2006). Recent work by Day et al. (2007) has shown that winter storms and hurricanes redeposit sediments eroded from nearby bays and wetlands. In fact, hurricanes Katrina and Rita deposited 5 to 10 cm of sediment on some coastal wetlands (Day et al., 2007).

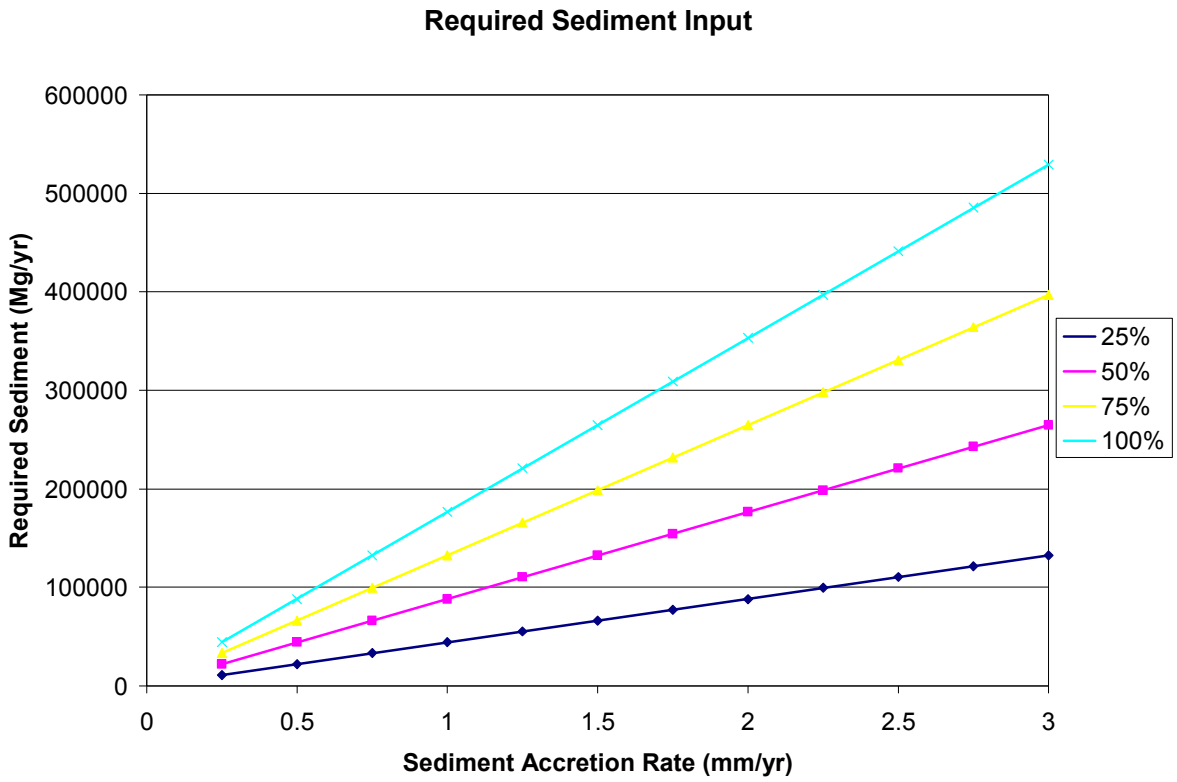

Figure 23. Sediment required to cover 25-100% of the delta surface at accretion rates from 0.25 to 3.0 mm yr^{-1}.

Modern fluvial sediment input from the Trinity River is also insufficient to combat subsidence and wetland loss. Eustatic sea level has been rising at a rate of 2.2 mm yr^{-1} and subsidence rates have been calculated to be 8.1 mm yr^{-1} (White et al., 2002). This produces a relative sea level rise of 10.3 mm yr^{-1} which far exceeds the mean accretion rate of 1.5 mm yr^{-1} from this study. The mean sediment accretion rates produced in this study and others are inadequate to combat the effects of long term, relative sea level rise. This has resulted in the disappearance of wetlands and erosion of shorelines. This erosion and land loss is often attributed to anthropogenic factors such as river closures, ground water withdrawal, and hydrocarbon production. Although groundwater withdrawal and hydrocarbon production have been found to accelerate subsidence in southeast Texas, the closure of Lake Livingston

on the Trinity River has not effected sediment delivery to the coast (Morton et al., 2001; White et al., 2002; Stork and Sneed, 2002; Phillips, 2004). The lower Trinity River is a sediment transport bottleneck, meaning that changes in sediment supply upstream have little impact on the delta (Phillips et al, 2004; Phillips and Slattery, 2006; Dollar, 2005; Wellmeyer et al., 2005).

In summary, the use of GPR was unsuccessful in determining the Holocene sediment accumulation rate in the Trinity River delta. However, traditional sediment coring methods produced sediment accretion rates for the past 3.2 Ka. Mean sediment accumulation rates of 1.2 and 1.8 mm yr^{-1} were attained for two interdistributary marshes in the Trinity River delta by radiocarbon dating shell fragments recovered from sediment cores. These accumulation rates are well within the ranges established in previous studies, and they extend beyond the time scope of past studies. Due to the limited sediment delivery in the lower Trinity River, the Holocene accretion rates provided by this study and others indicate that there are other sediment sources contributing to the accretion of sediment within the delta. Despite the supplemental sediment input from other sources, the sediment accretion rates in the Trinity River delta are insufficient to combat subsidence and wetland loss.

As stated previously, the Holocene sedimentation rate could not be determined through the use of GPR. The boundary between the Holocene deltaic sediments and the underlying Pleistocene deposits were masked due to the high dielectric constant of clay and water in the interdistributary marsh sediments. Material possessing high dielectric constants can completely attenuate the GPR signal, generate multiple reflections, or in wooded areas, produce hyperbolic shaped air wave responses. Although GPR is not useful in determining the subsurface stratigraphy or accretion rates in interdistributary marshes of fine-grained

deltas, results indicate that stratigraphy can be constrained using GPR in coarse-grained environments, such as sand bars.

APPENDIX A

GROUND PENETRATING RADAR PROFILES

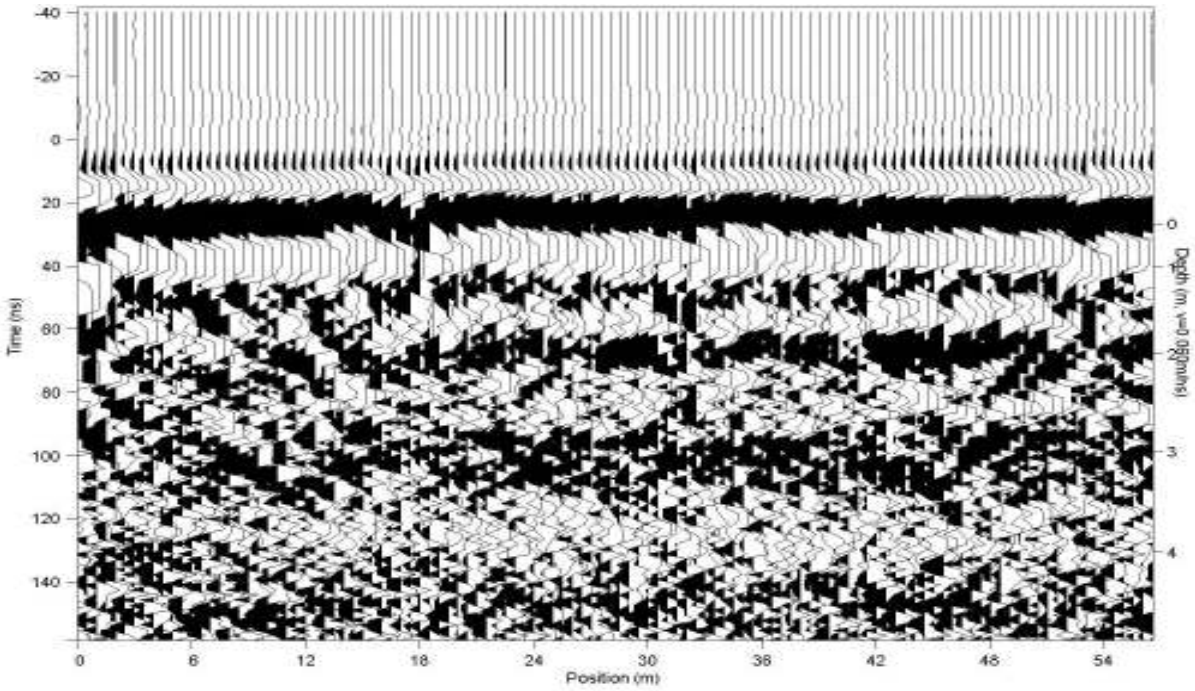

Site 01 line 01 wiggle trace

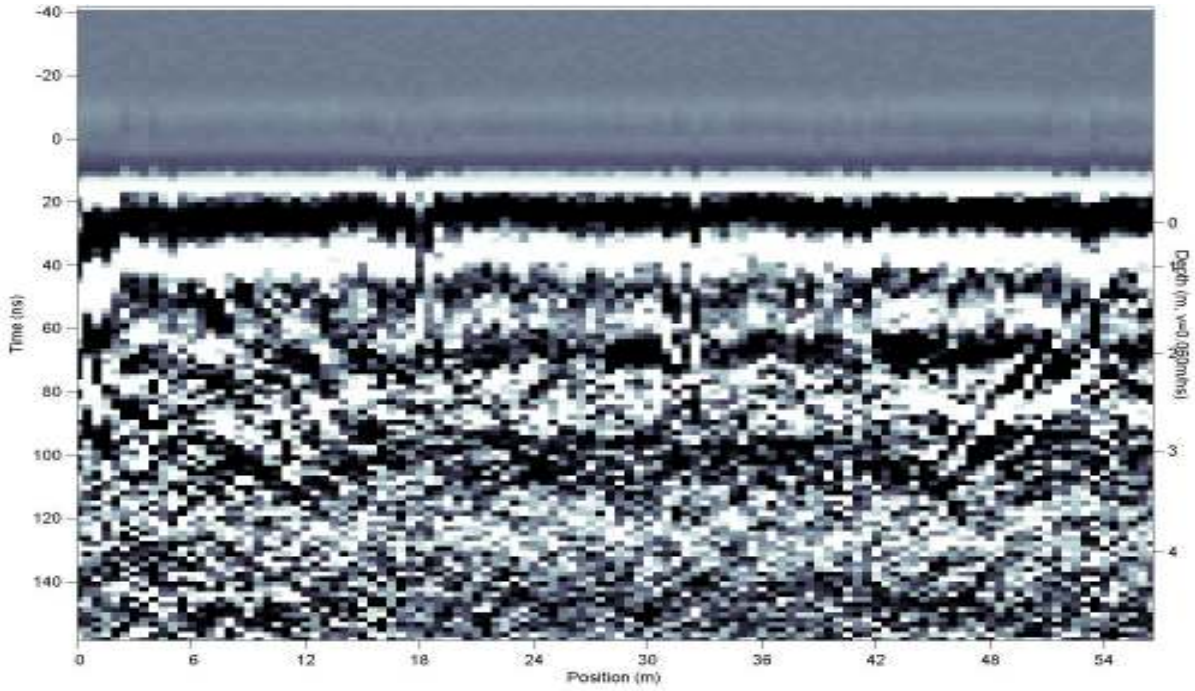

Site 01 line 01 color trace

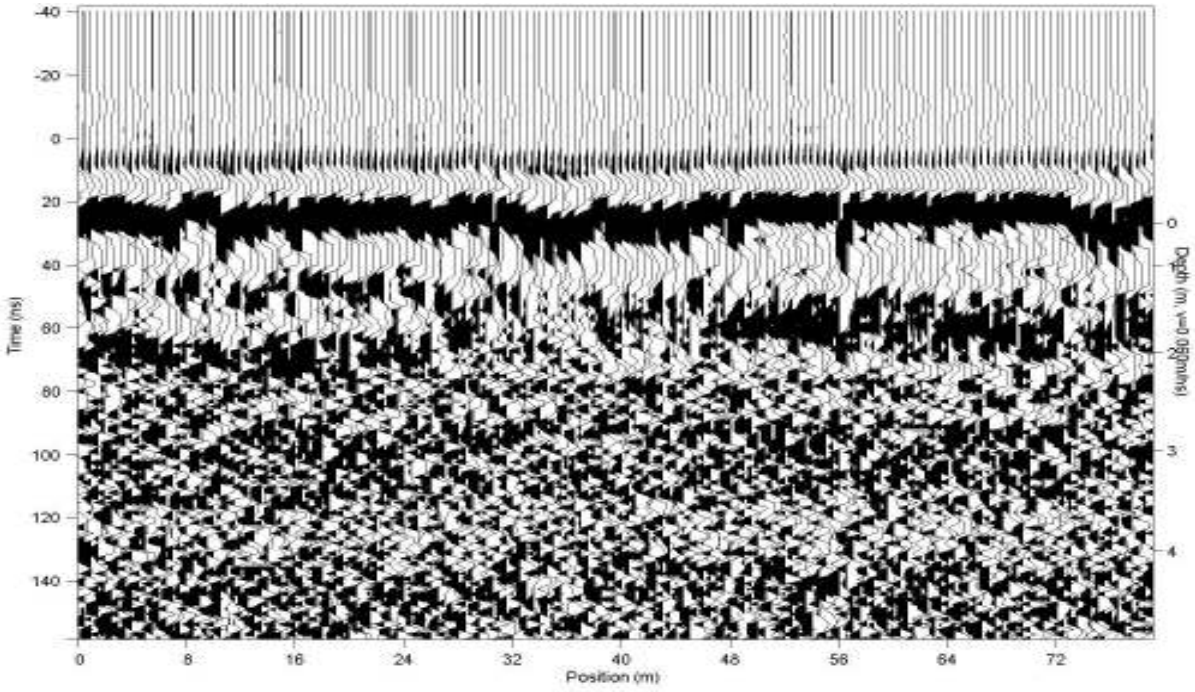

Site 01 line 02 wiggle trace

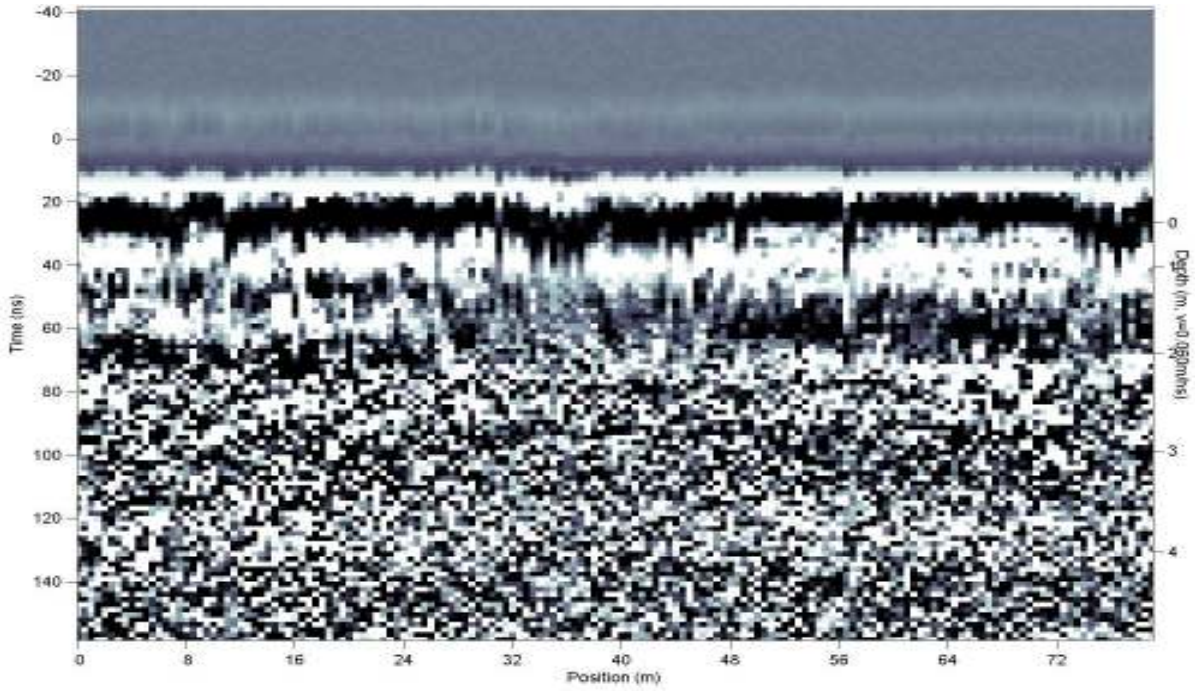

Site 01 line 02 color trace

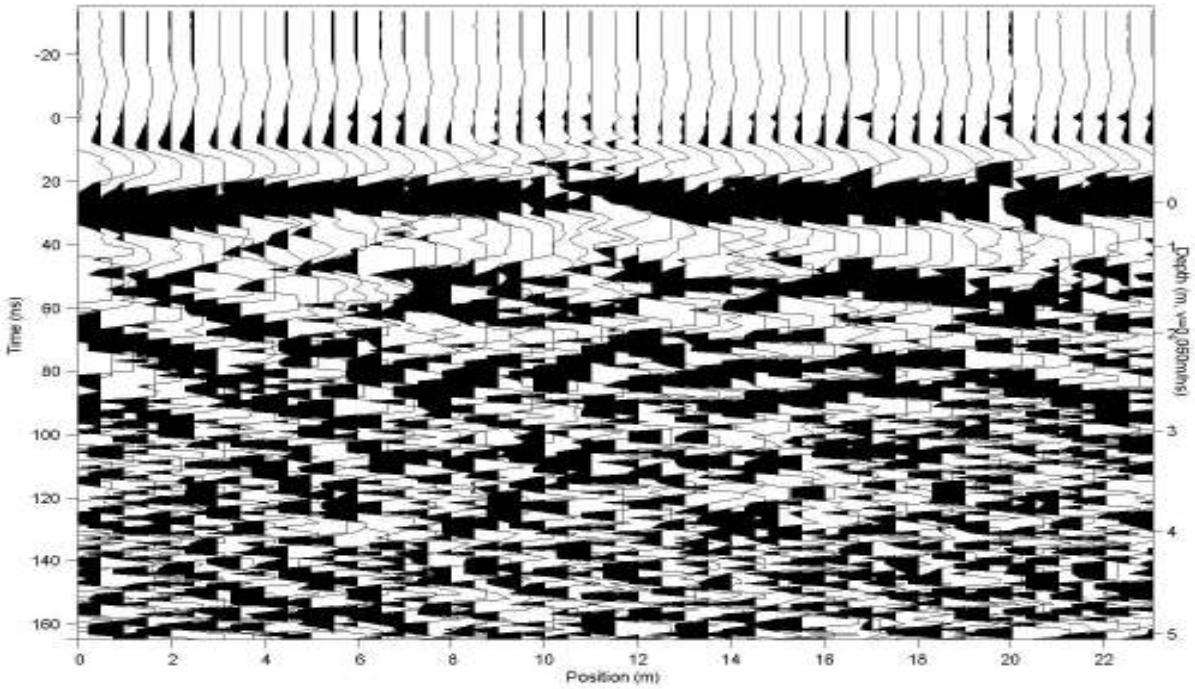

Site 01 line 03 wiggle trace

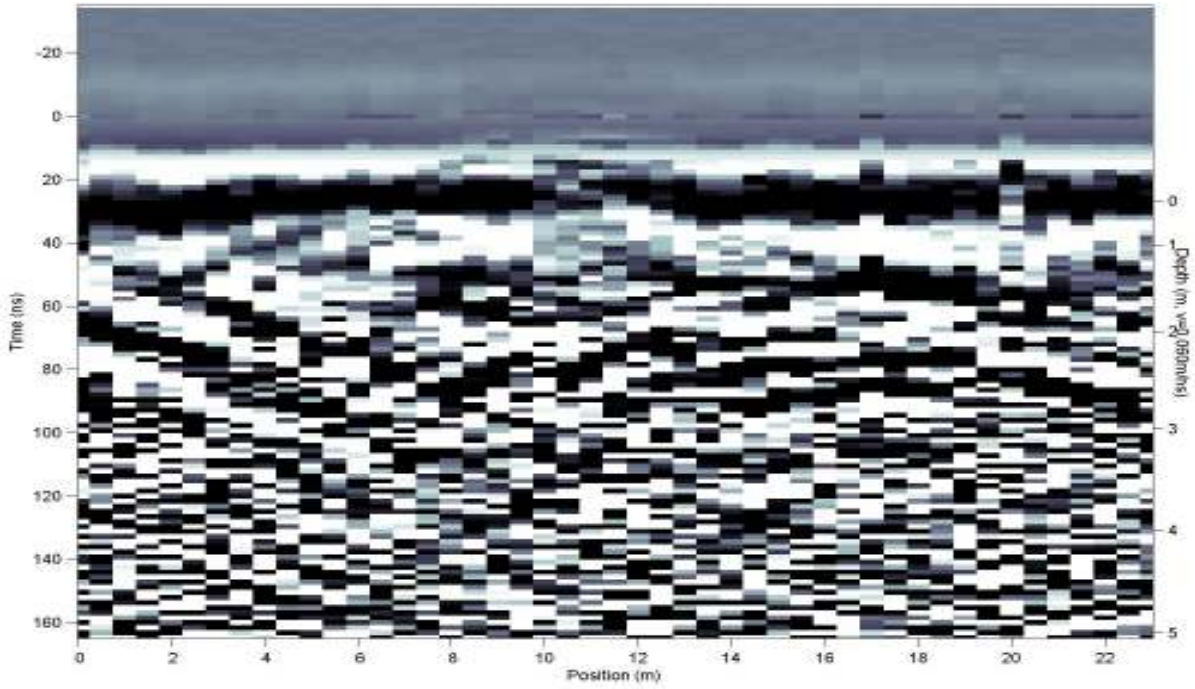

Site 01 line 03 color trace

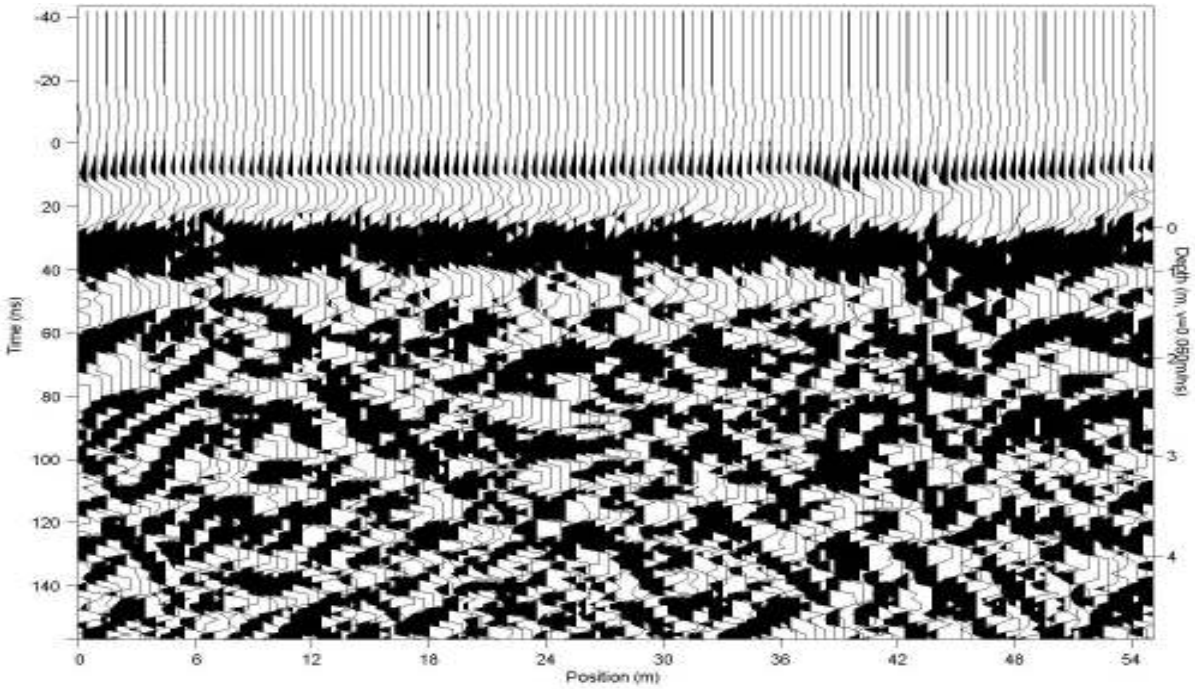

Site 01 line 04 wiggle trace

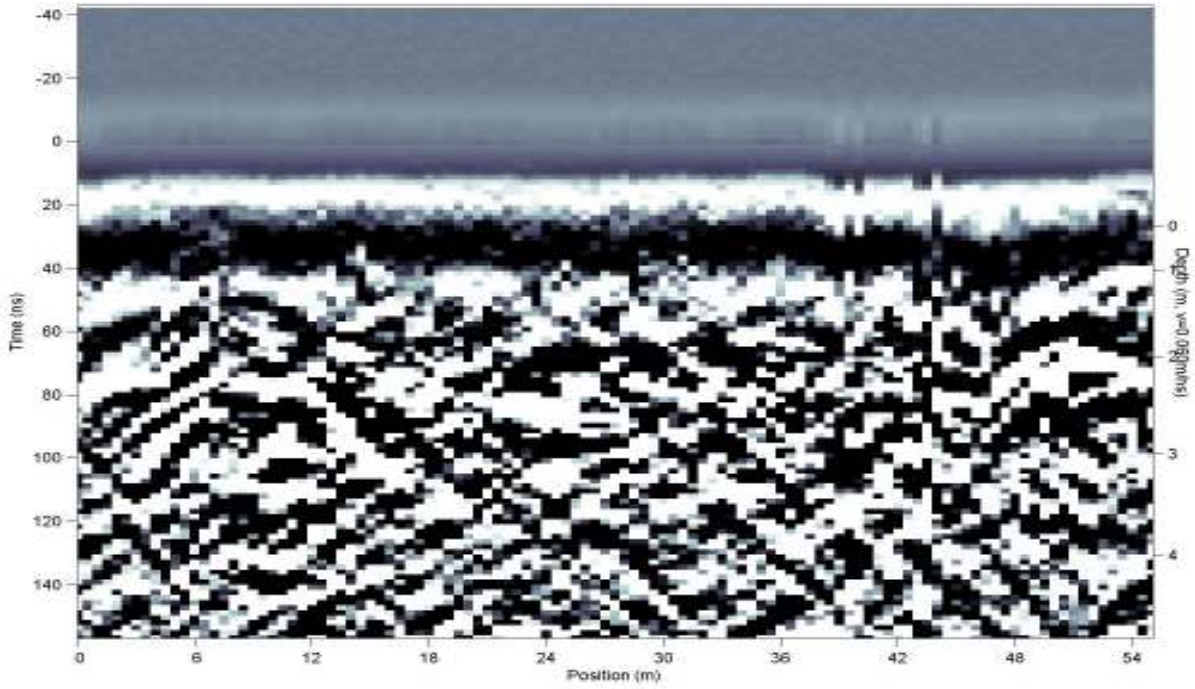

Site 01 line 04 color trace

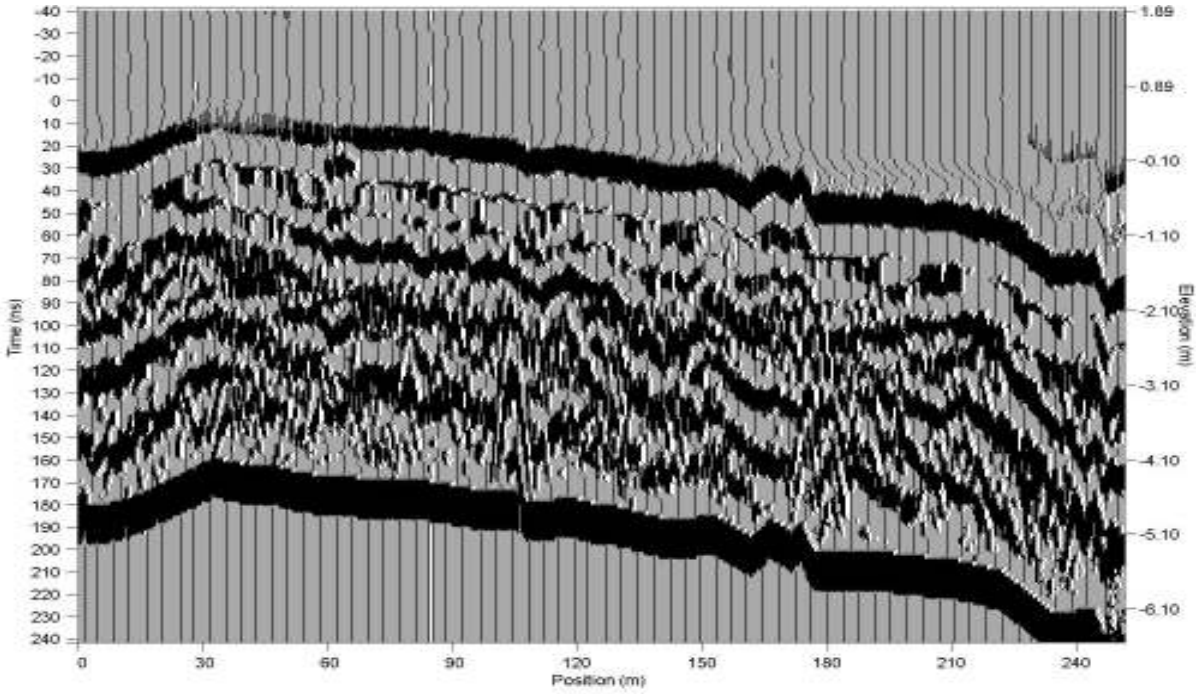

Site 01 lines 05 and 06 merged wiggle trace

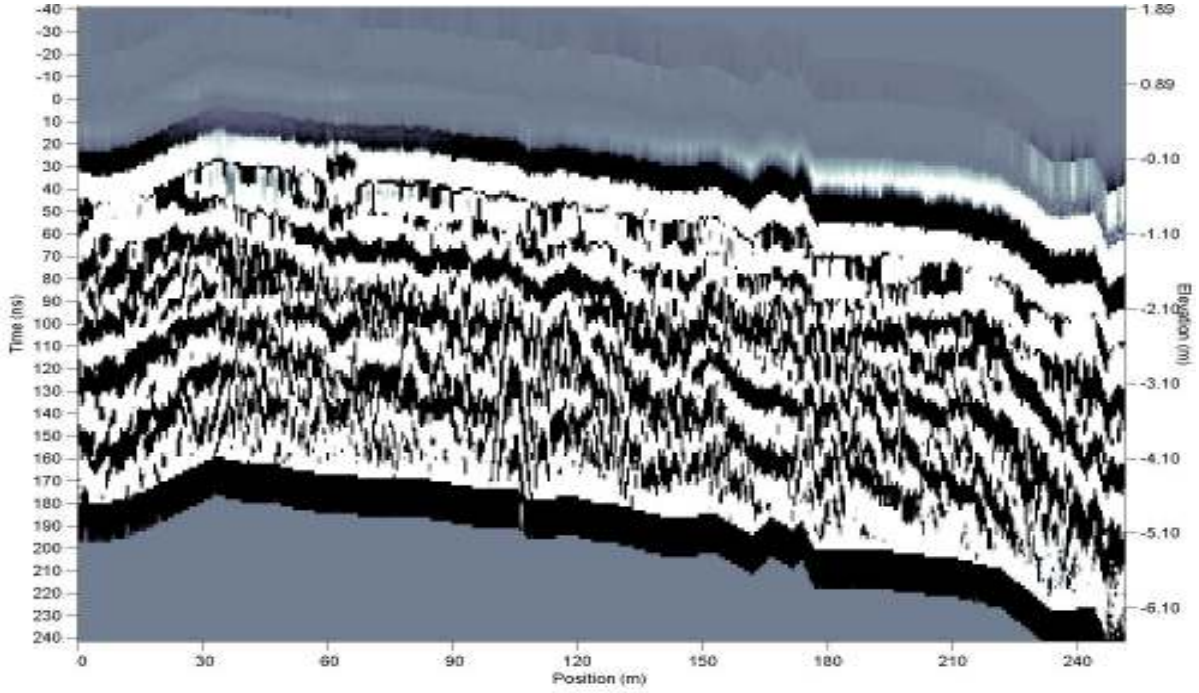

Site 01 lines 05 and 06 merged color trace

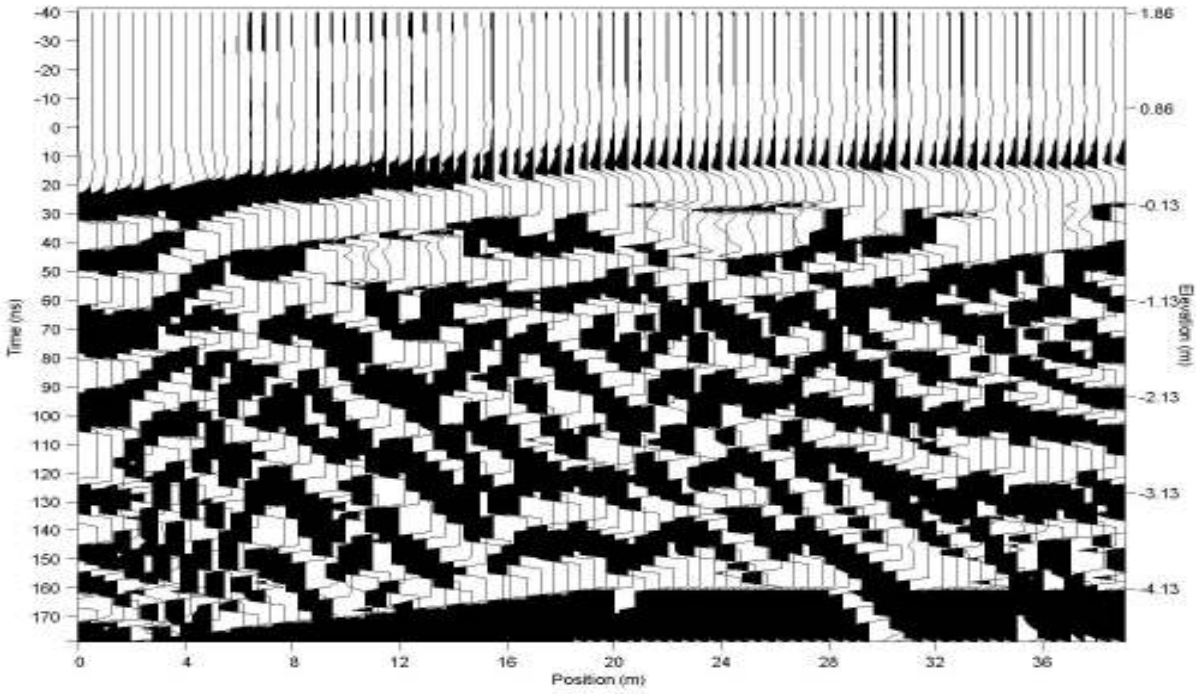

Site 01 line 07 wiggle trace

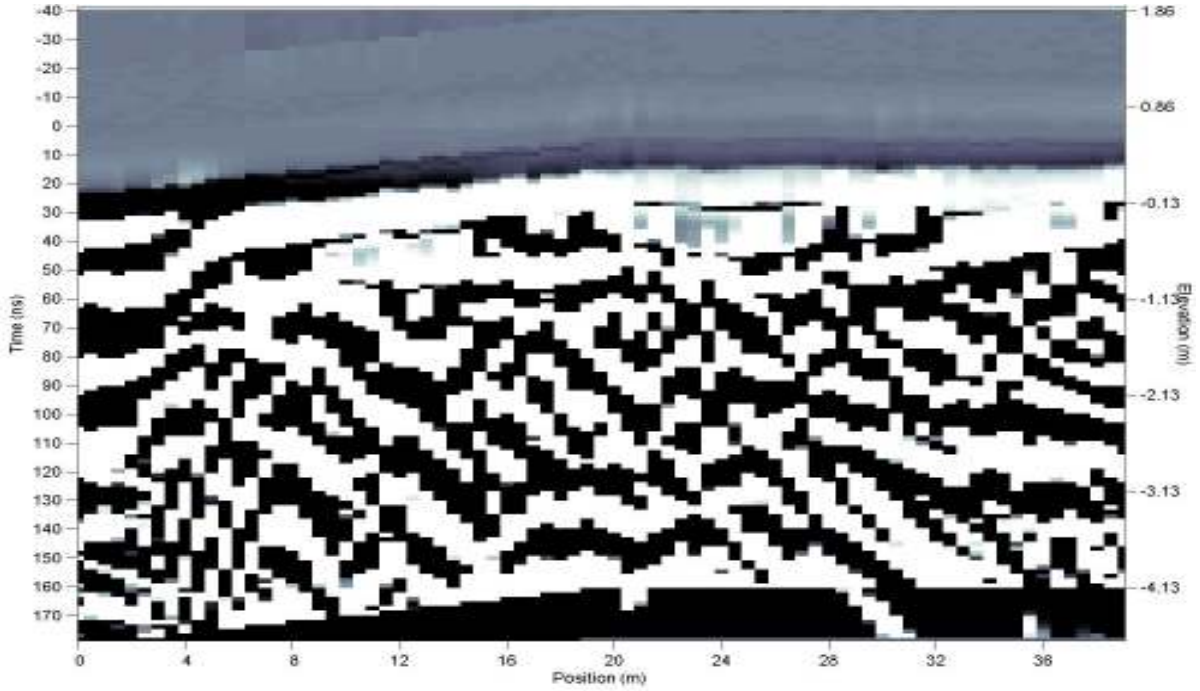

Site 01 line 07 color trace

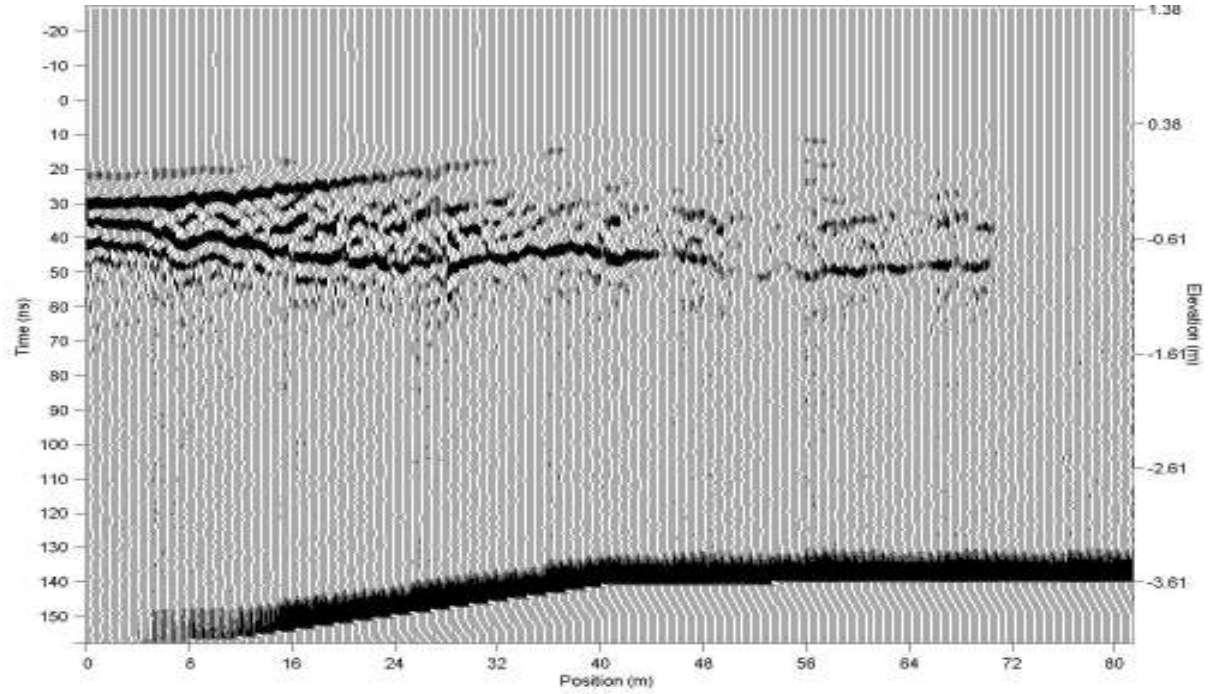

Site 01 line 08 wiggle trace

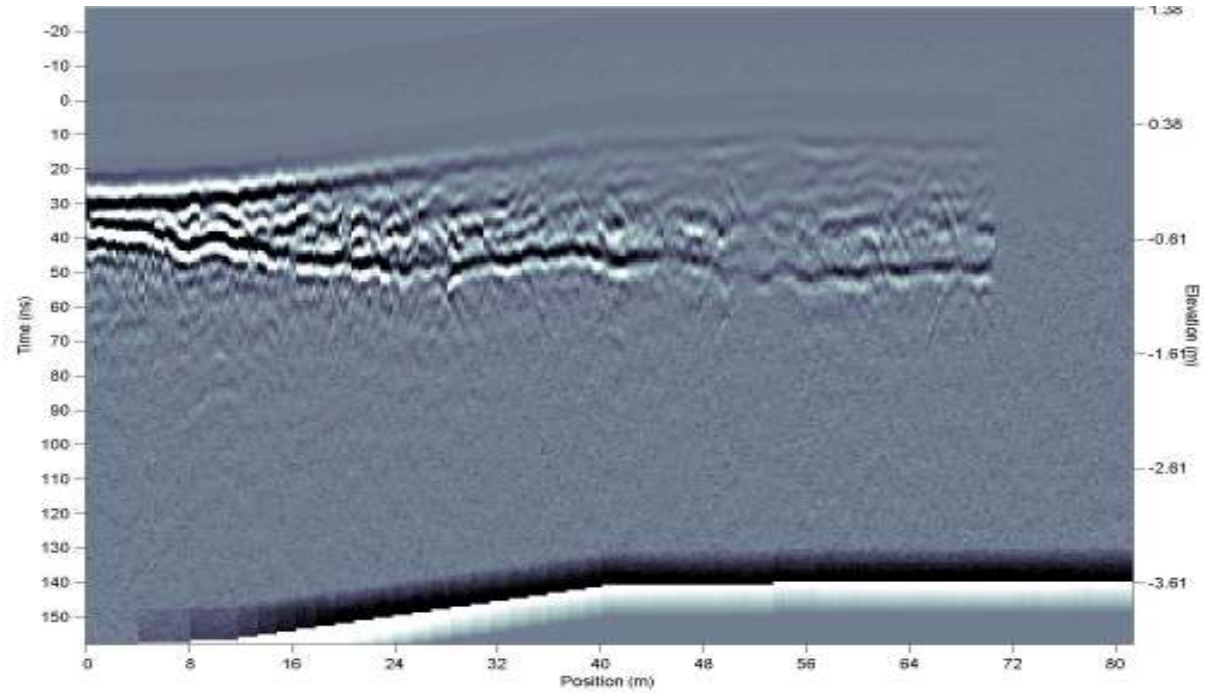

Site 01 line 08 color trace

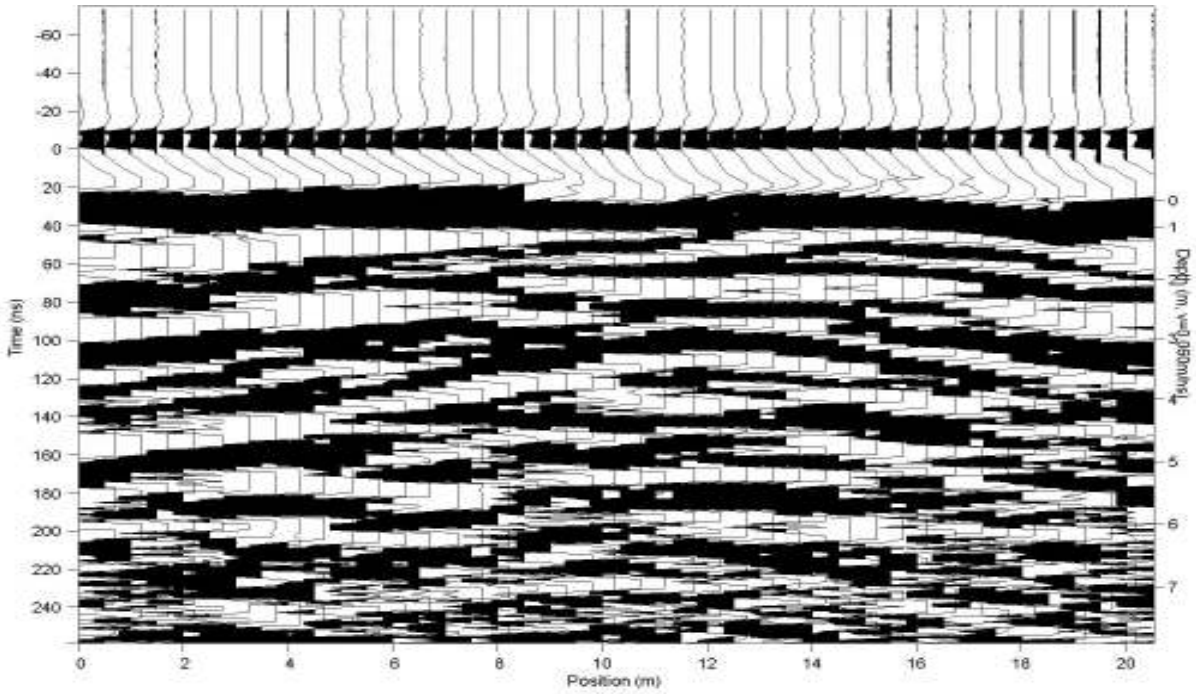

Site 02 line 01 wiggle trace

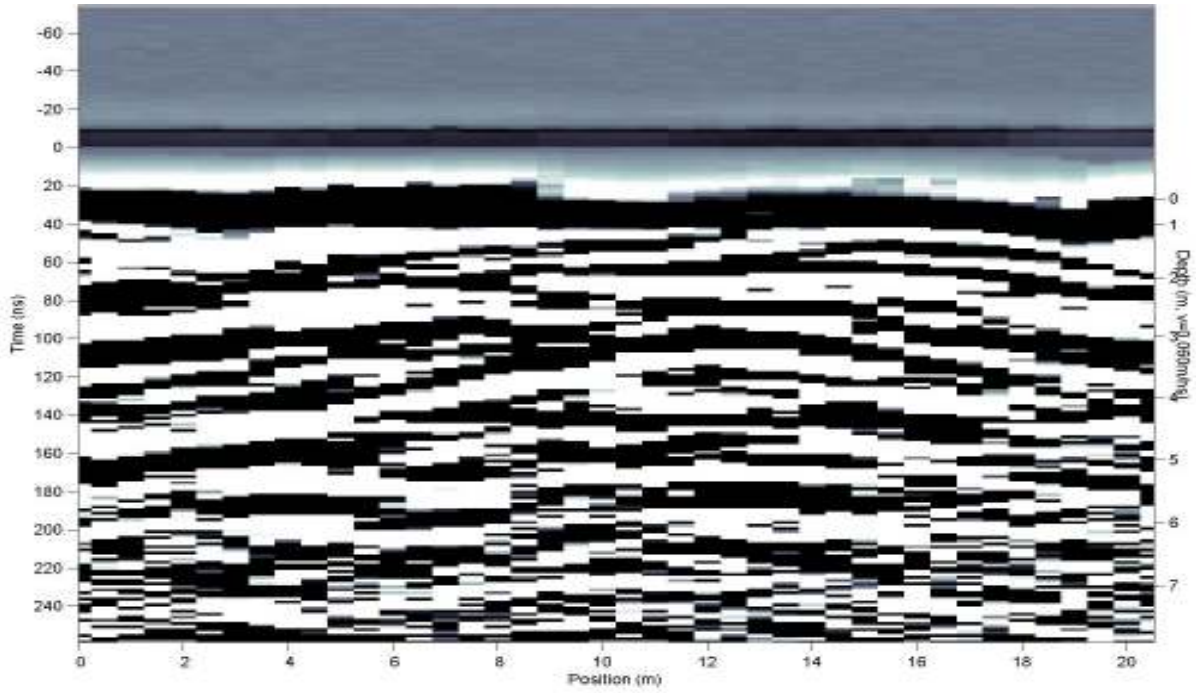

Site 02 line 01 color trace

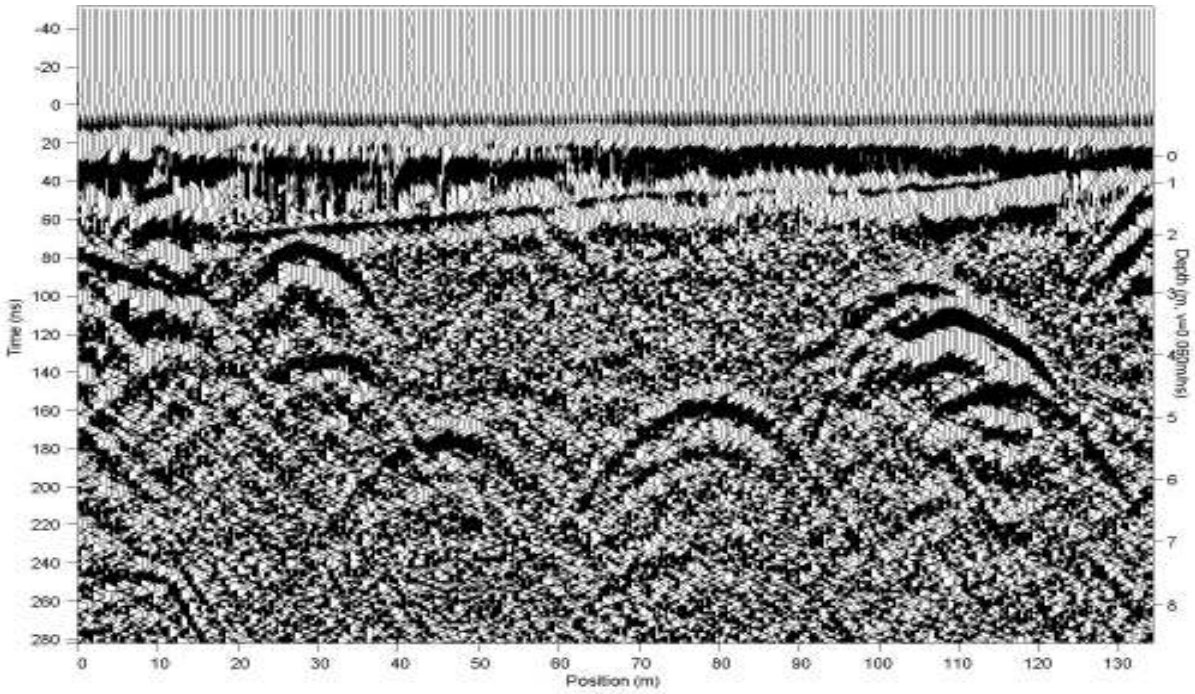

Site 03 lines 01 and 02 merged wiggle trace

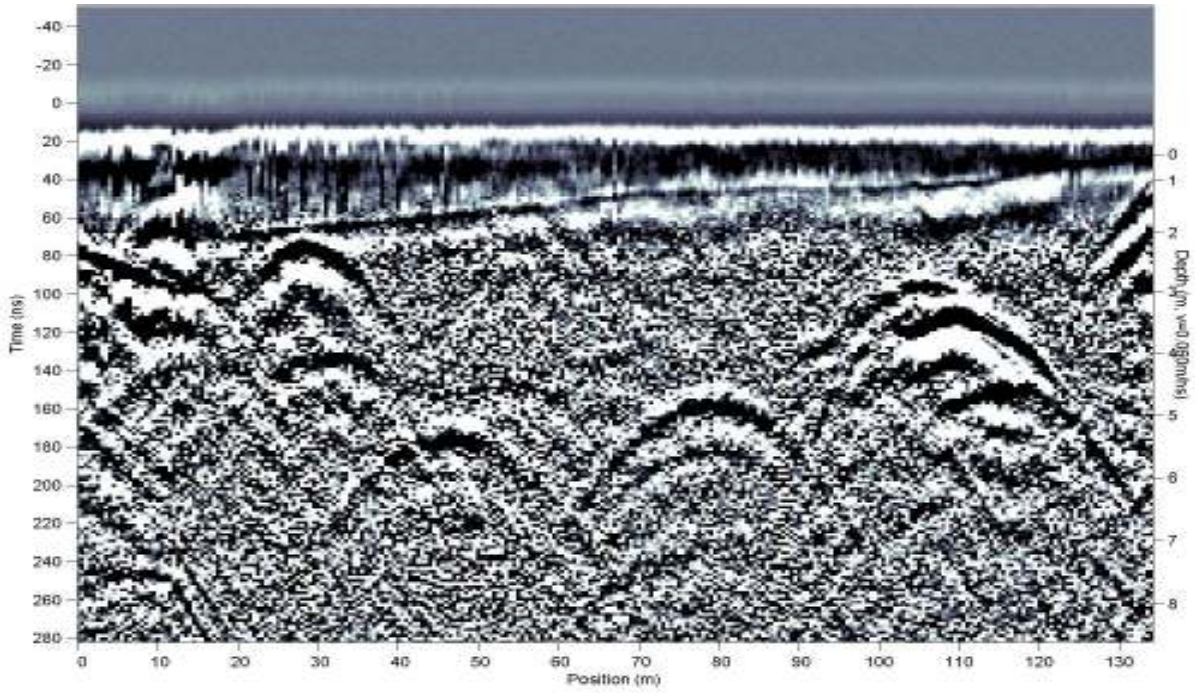

Site 03 lines 01 and 02 merged color trace

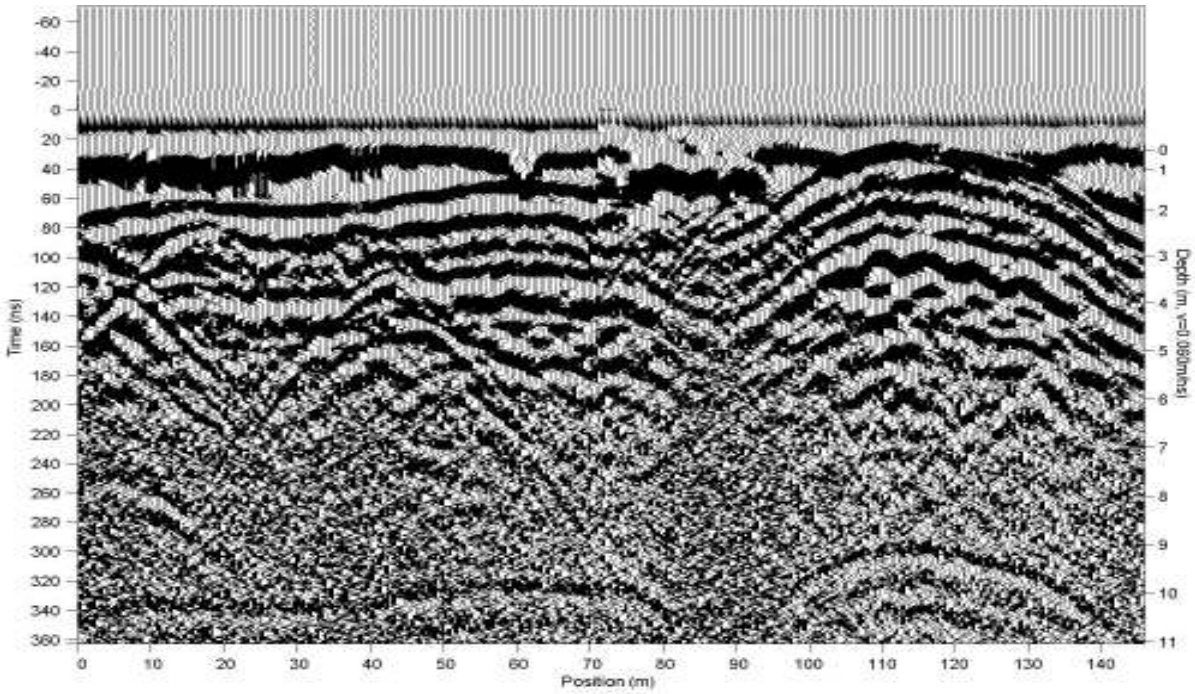

Site 05 line 01 wiggle trace

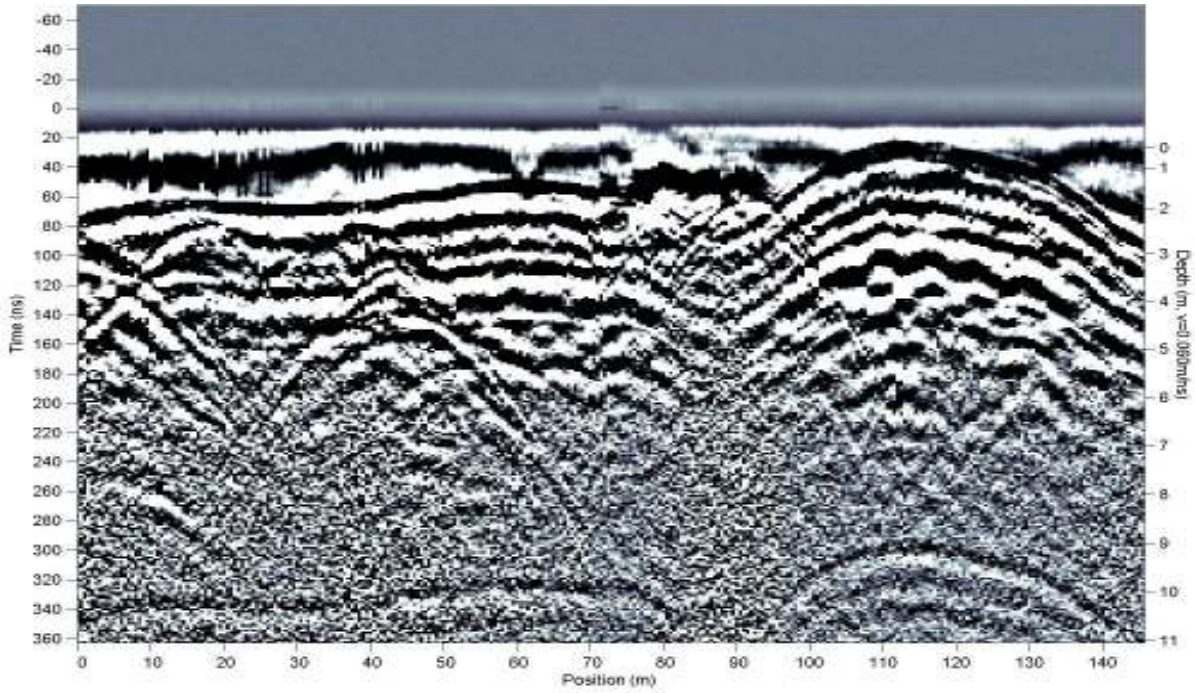

Site 05 line 01 color trace

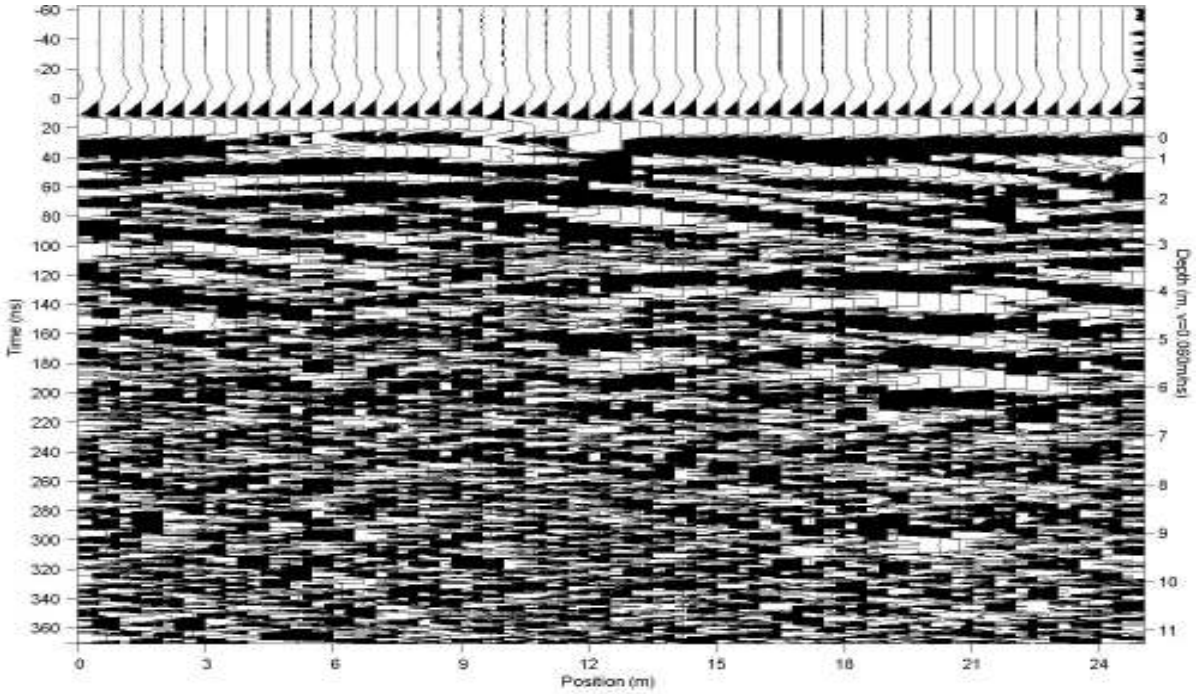

Site 06 line 01 wiggle trace

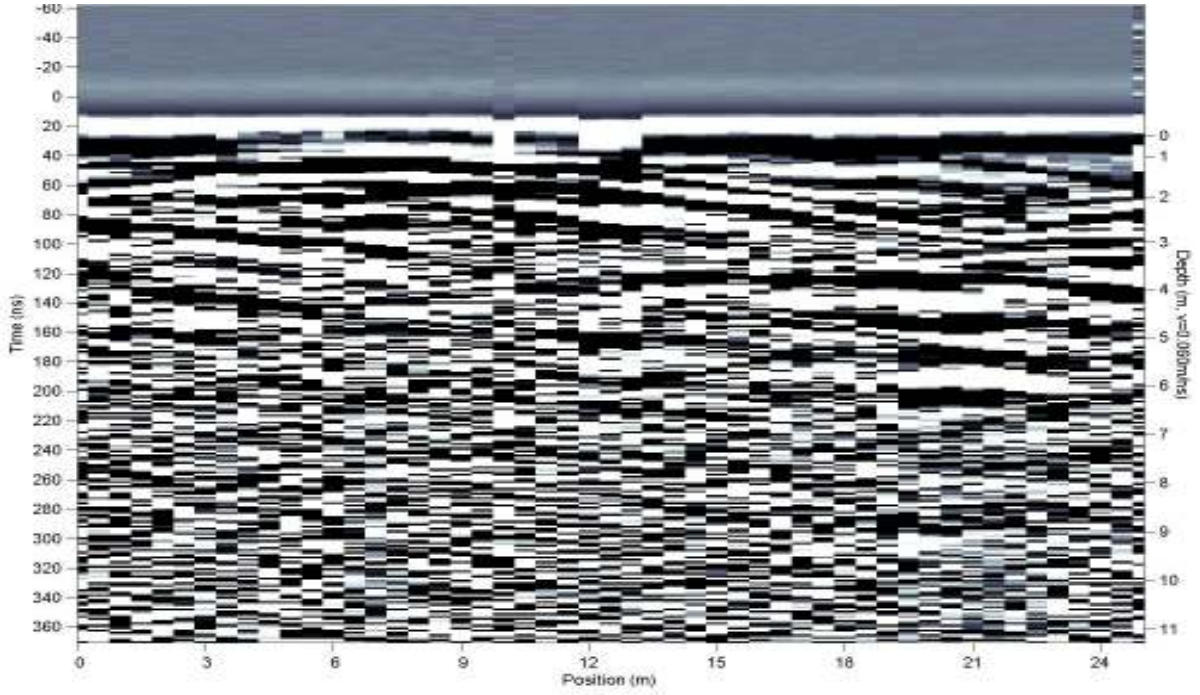

Site 06 line 01 color trace

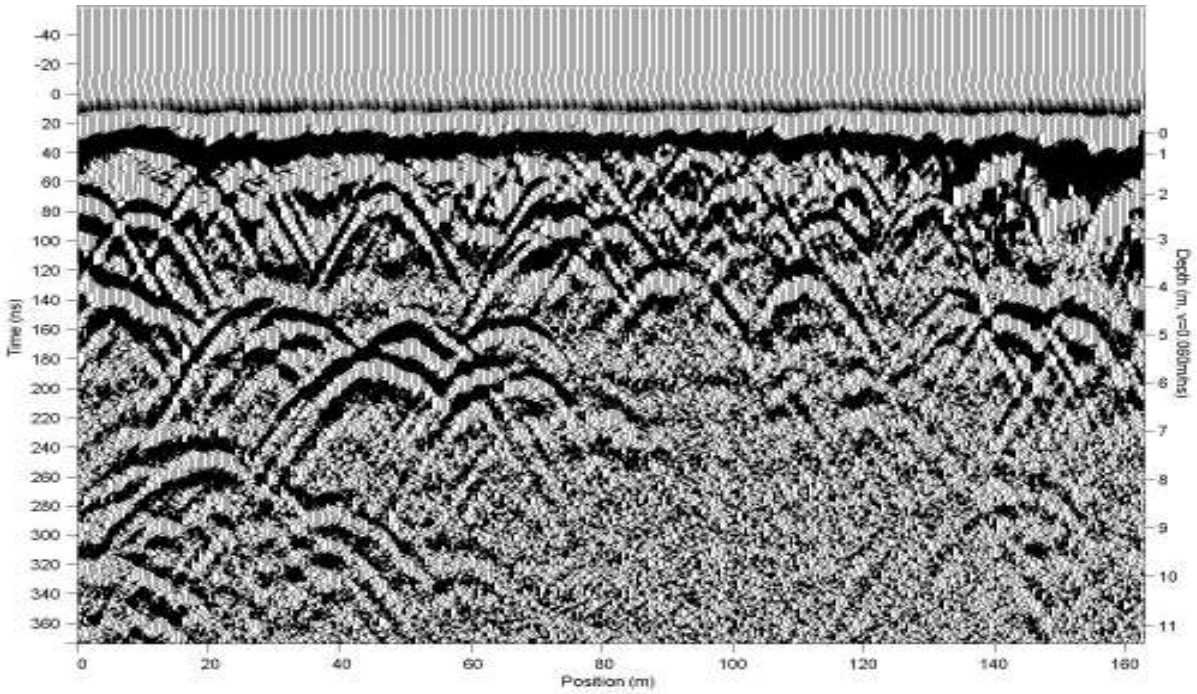

Site 07 line 01 wiggle trace

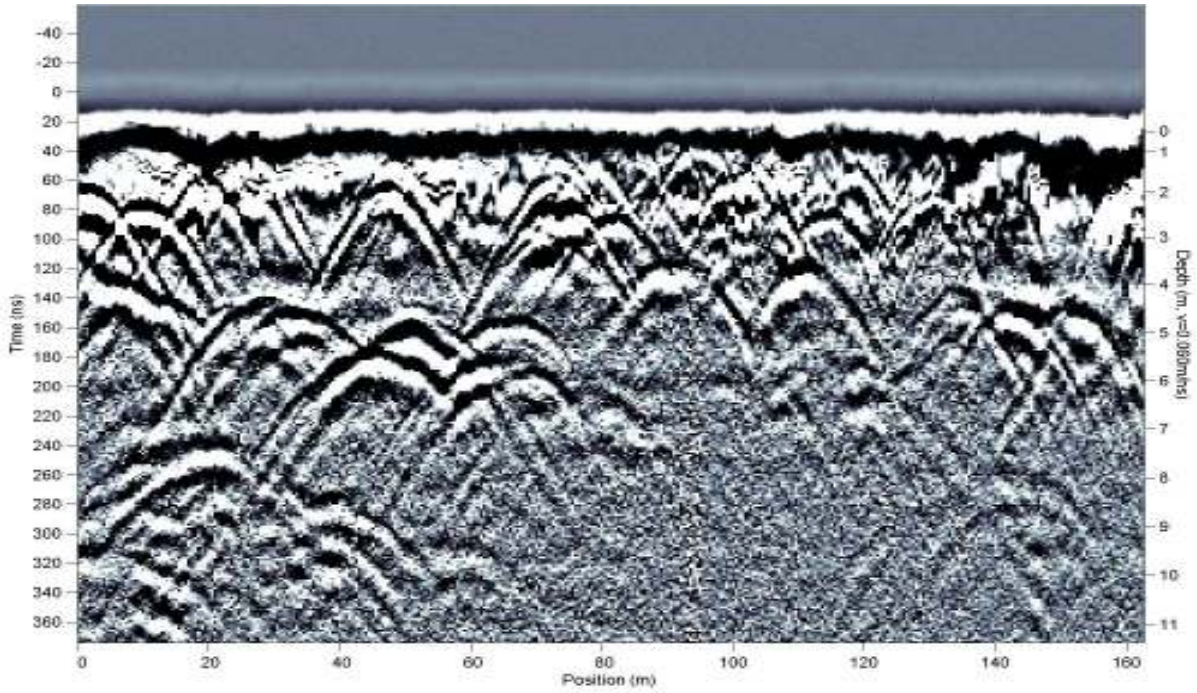

Site 07 line 01 color trace

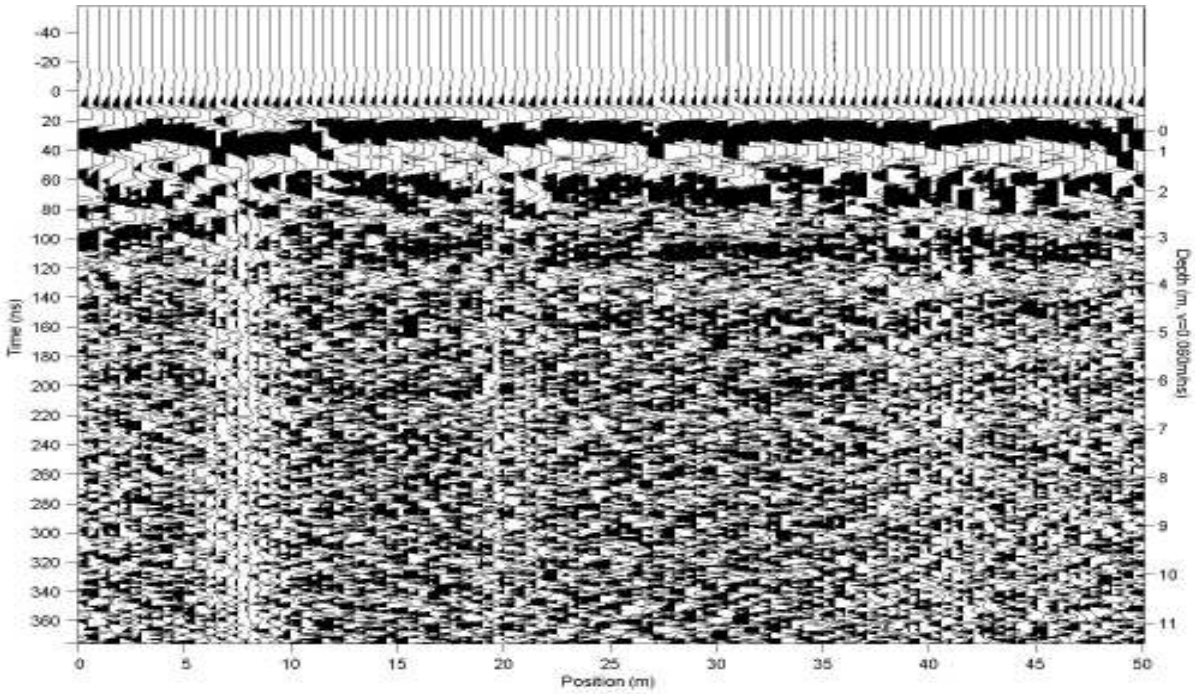

Site 07 line 02 wiggle trace

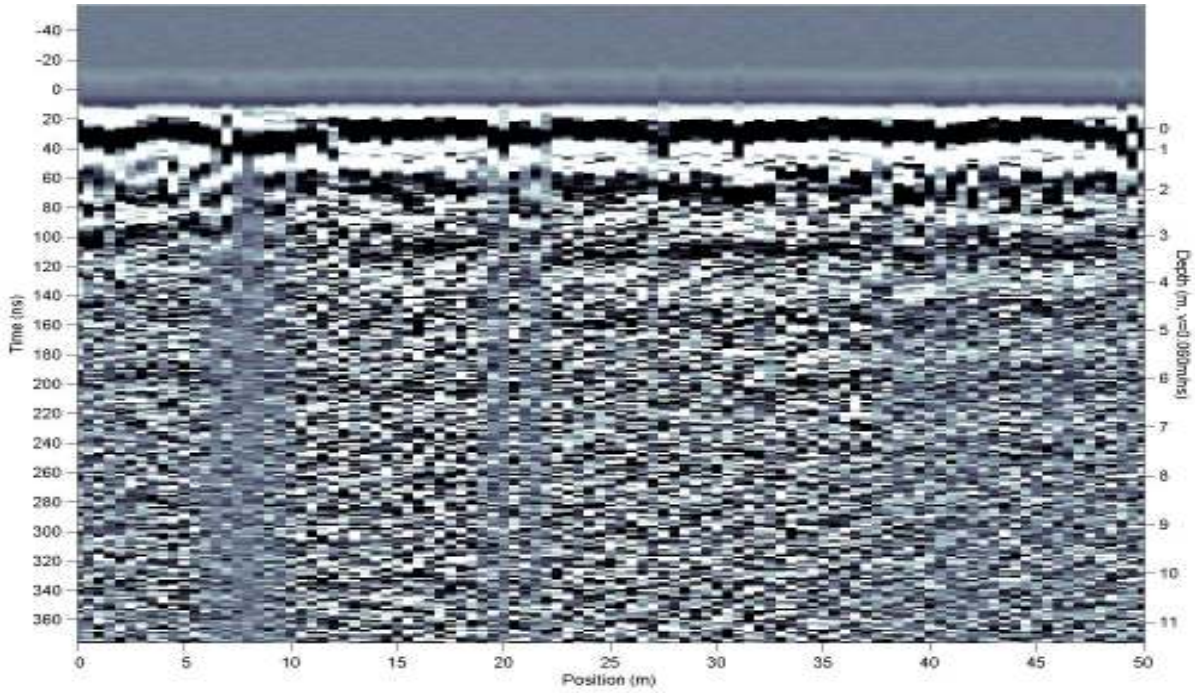

Site 07 line 02 color trace

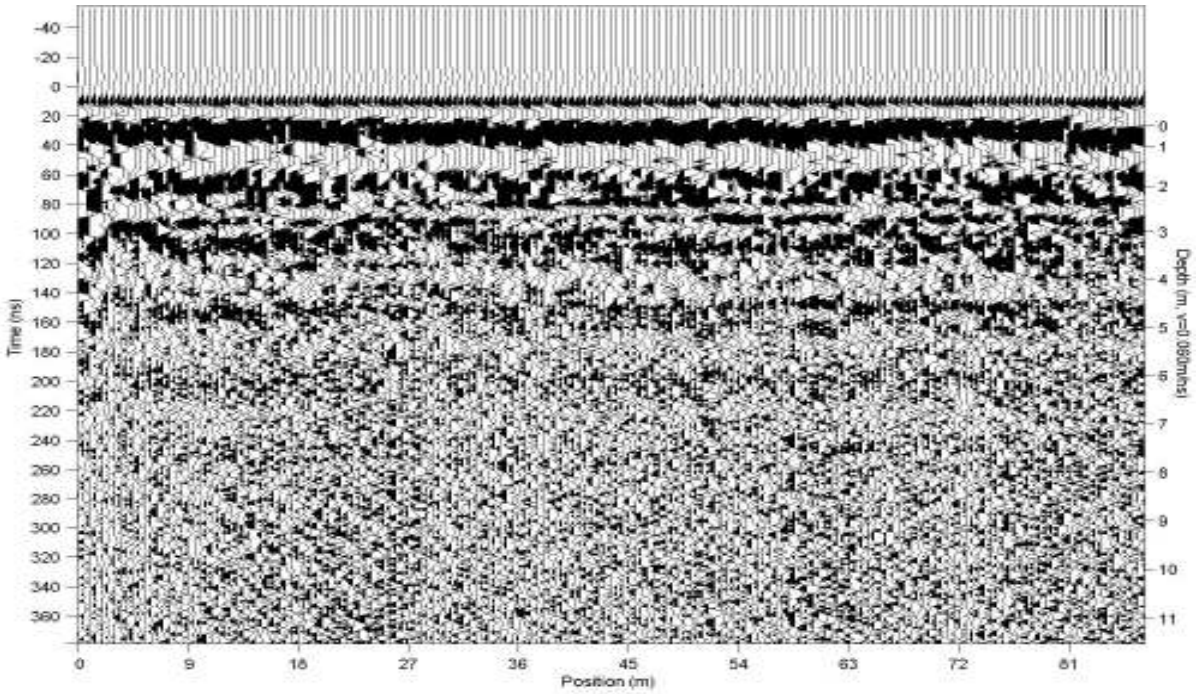

Site 07 line 03 wiggle trace

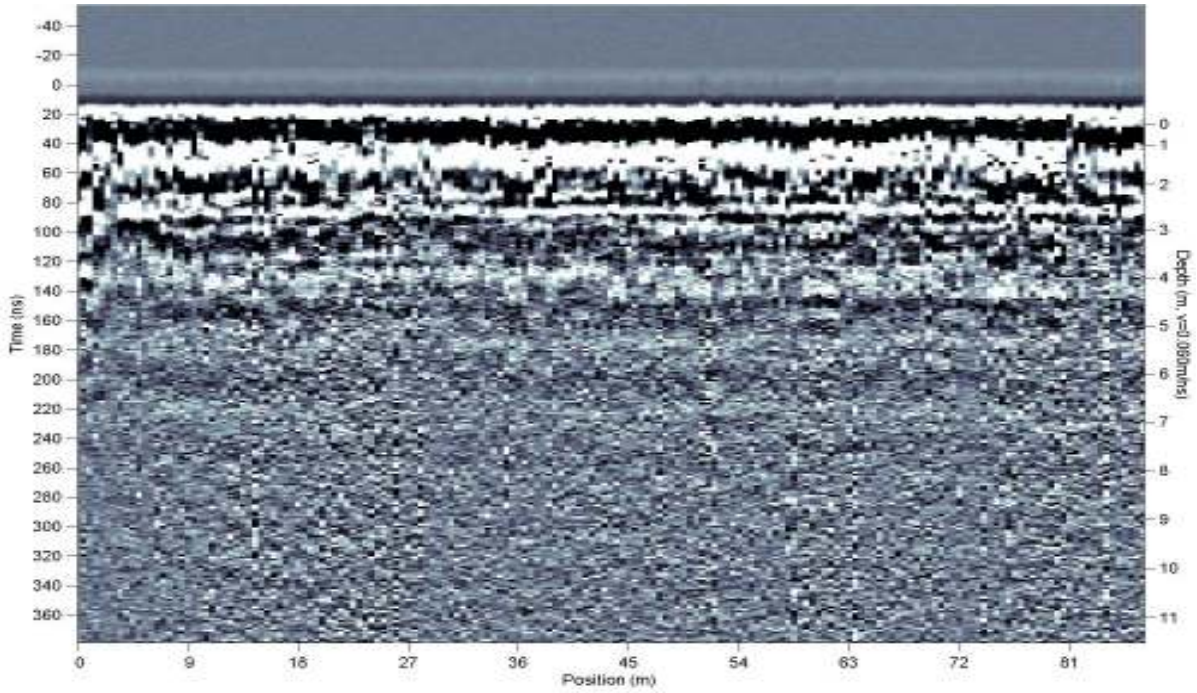

Site 07 line 03 color trace

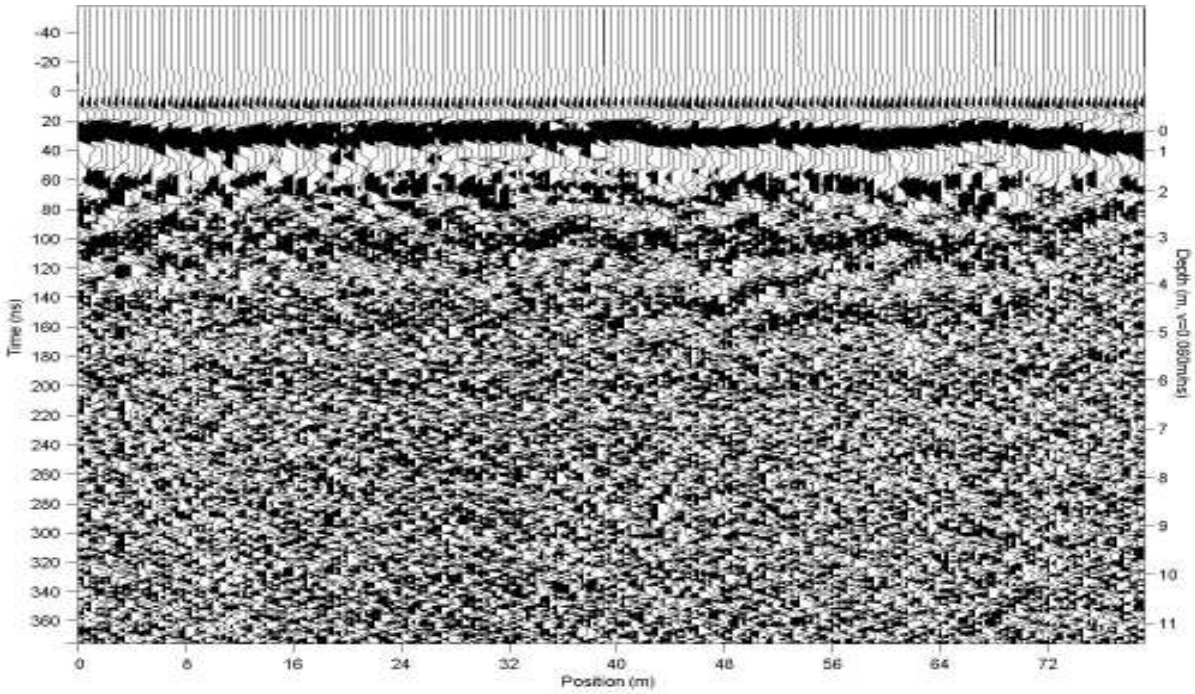

Site 07 line 04 wiggle trace

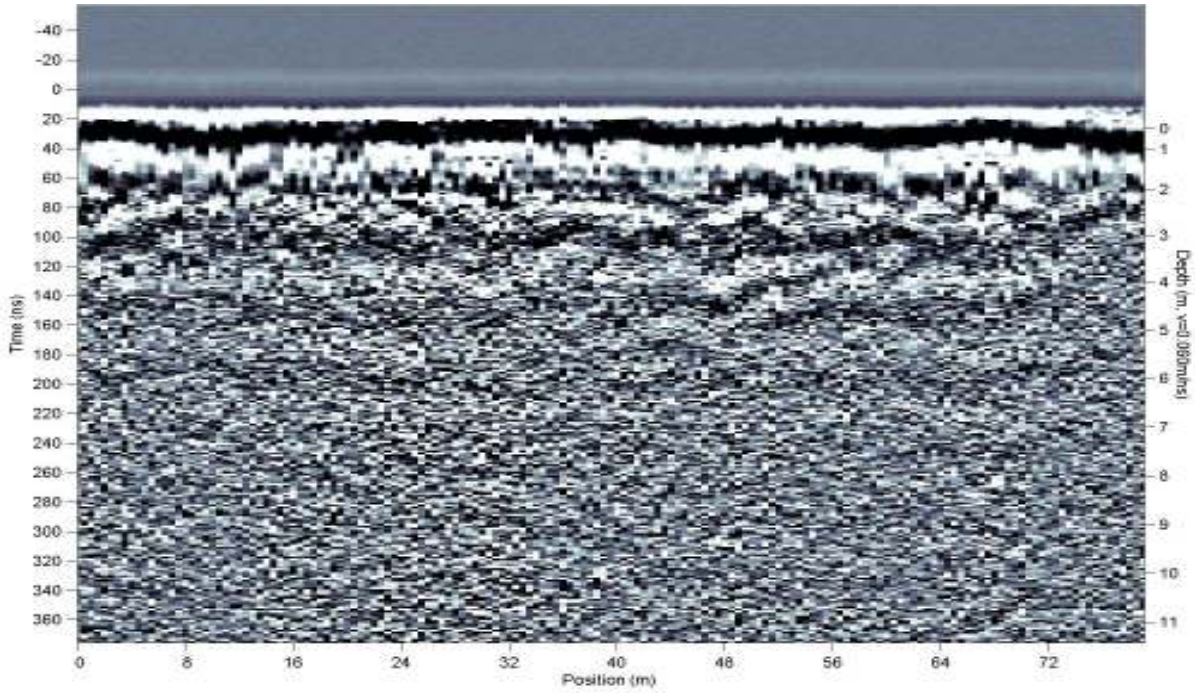

Site 07 line 04 color trace

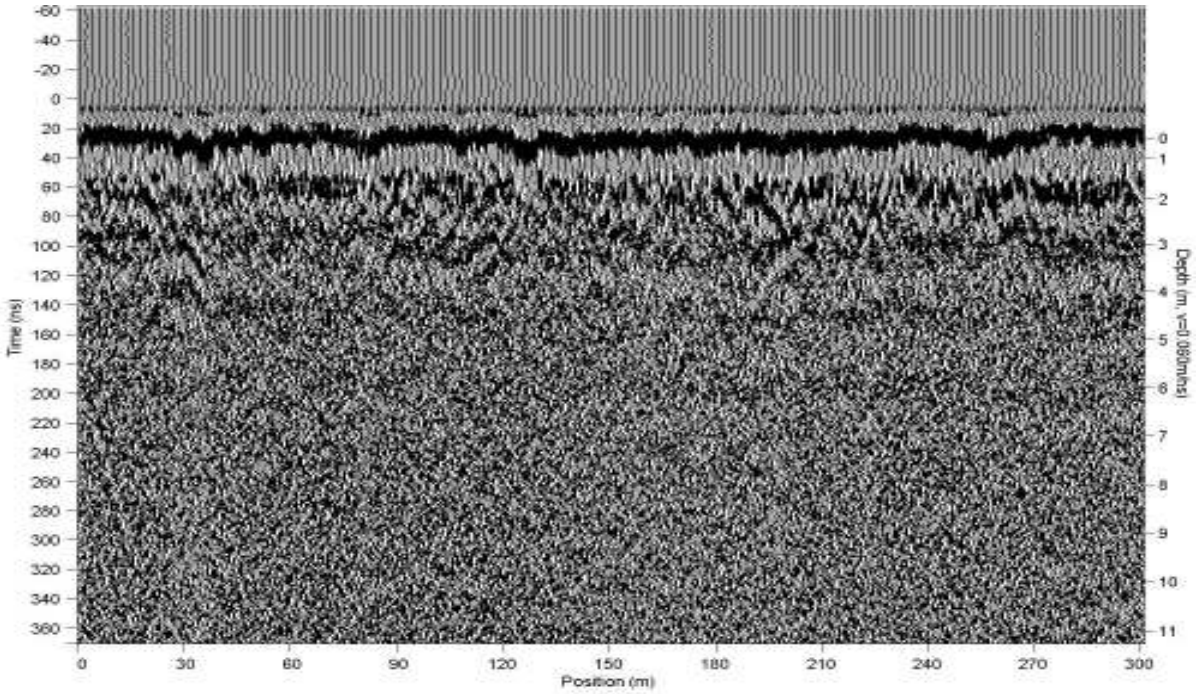

Site 08 line 01 wiggle trace

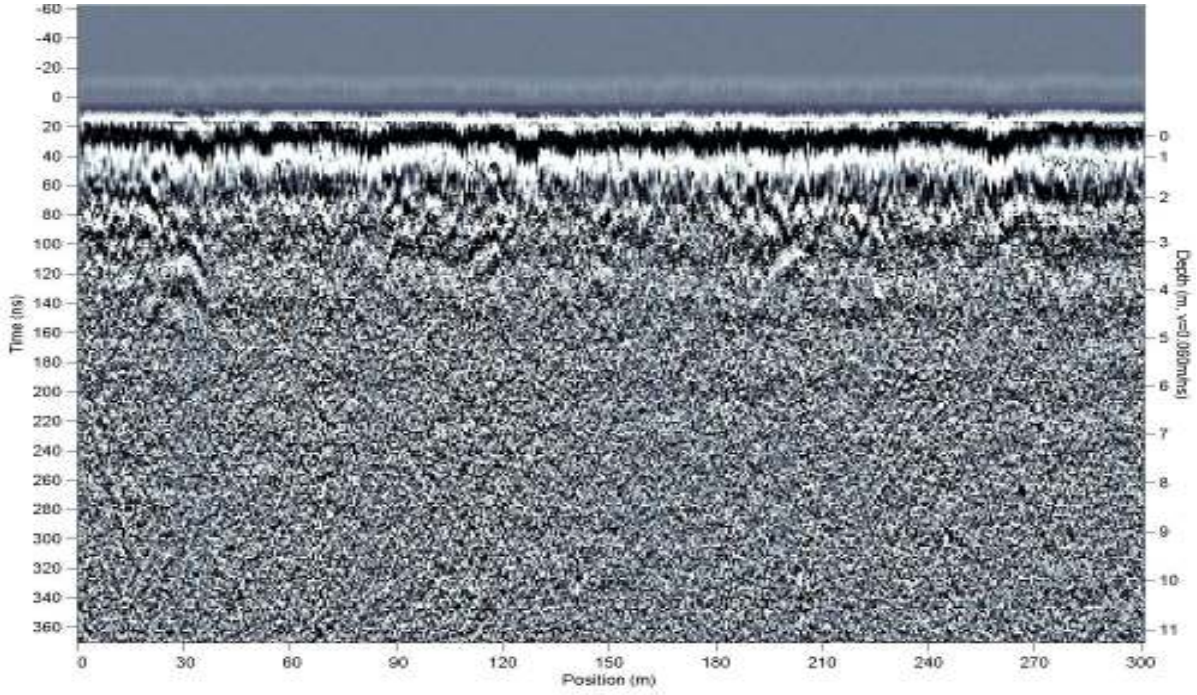

Site 08 line 01 color trace

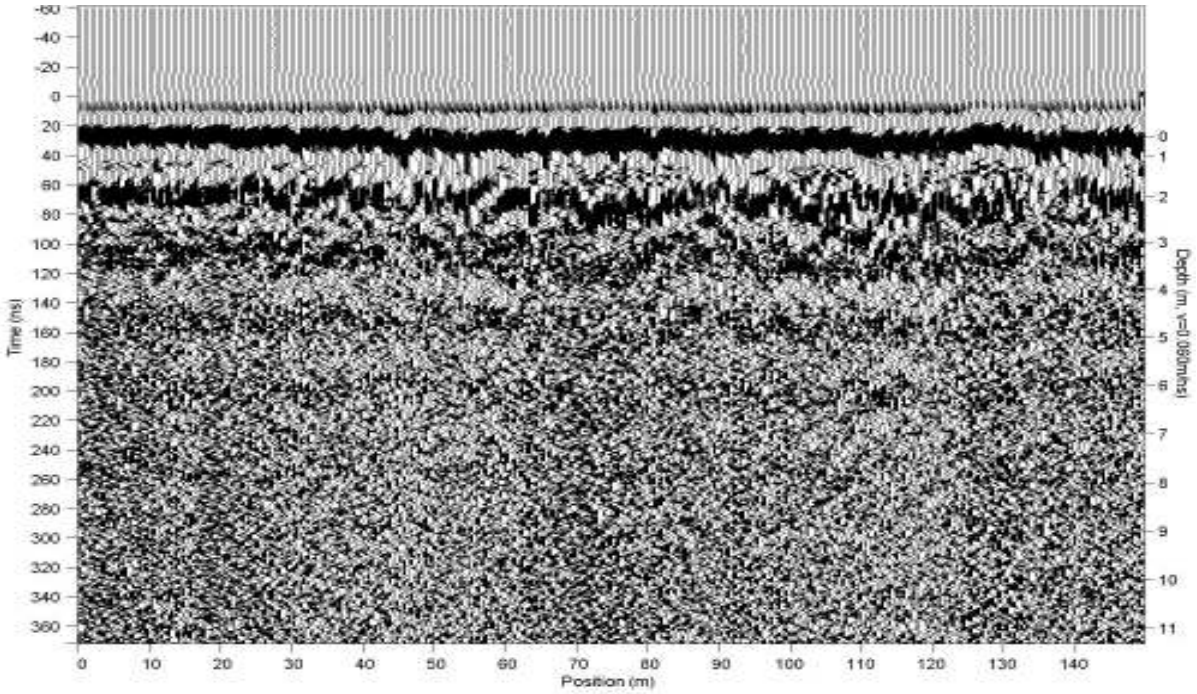

Site 08 line 02 wiggle trace

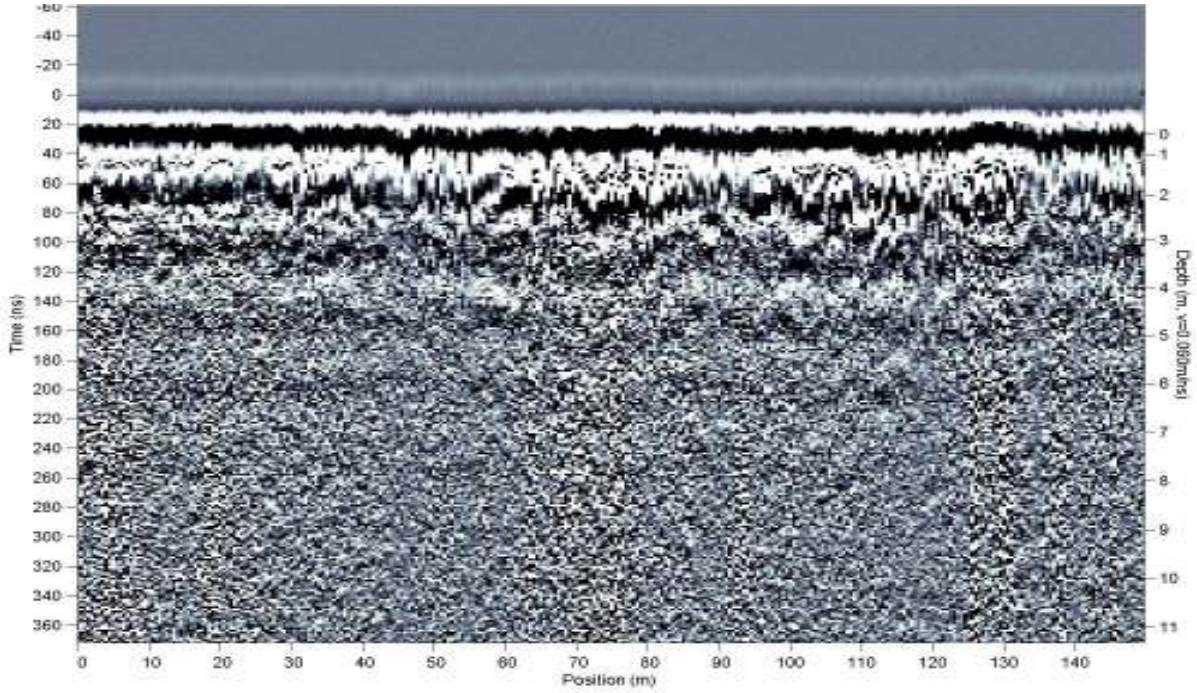

Site 08 line 02 color trace

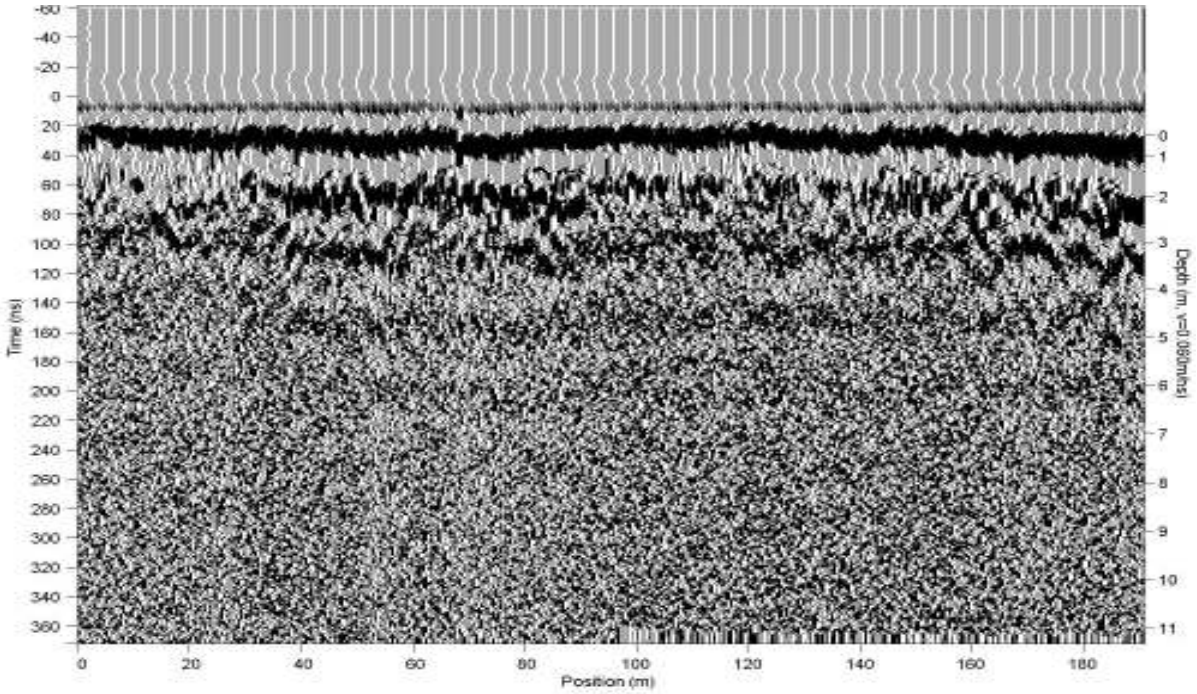

Site 08 lines 03 and 04 merged wiggle trace

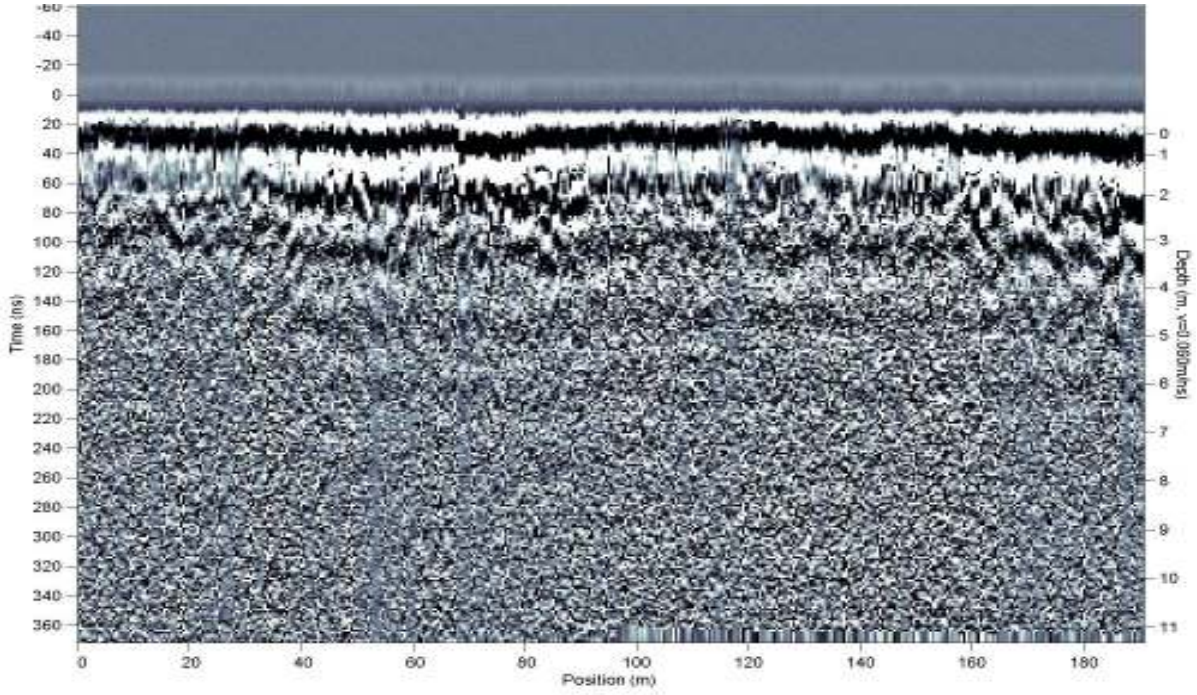

Site 08 lines 03 and 04 merged color trace

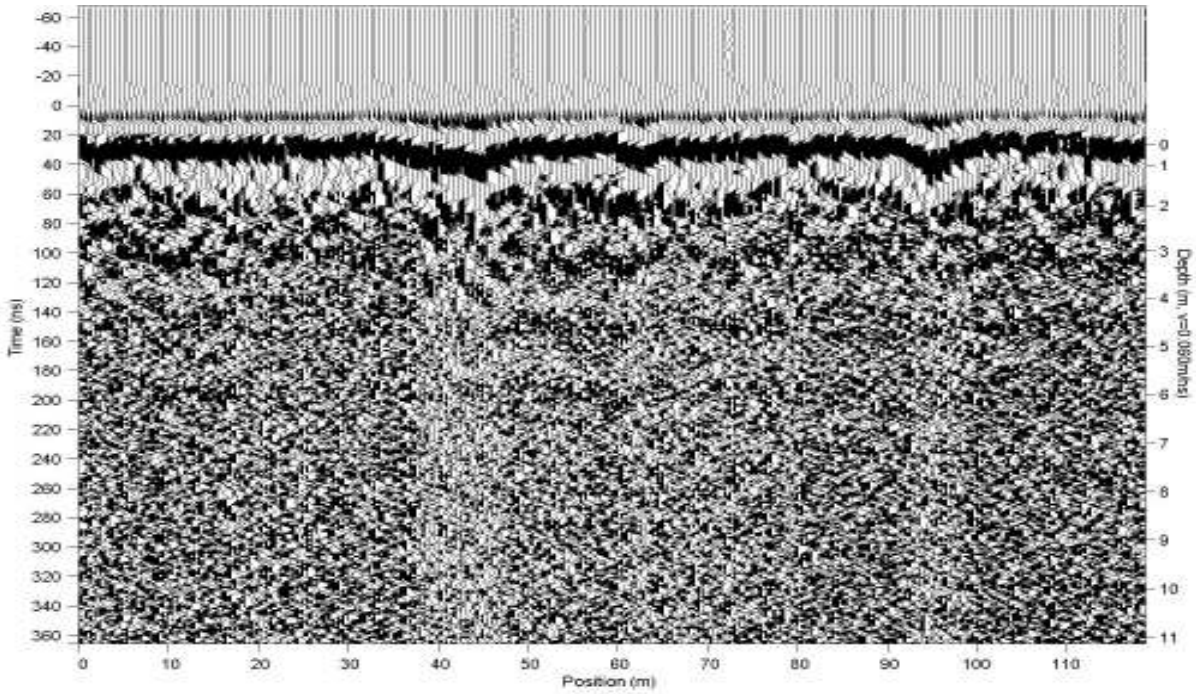

Site 08 line 05 wiggle trace

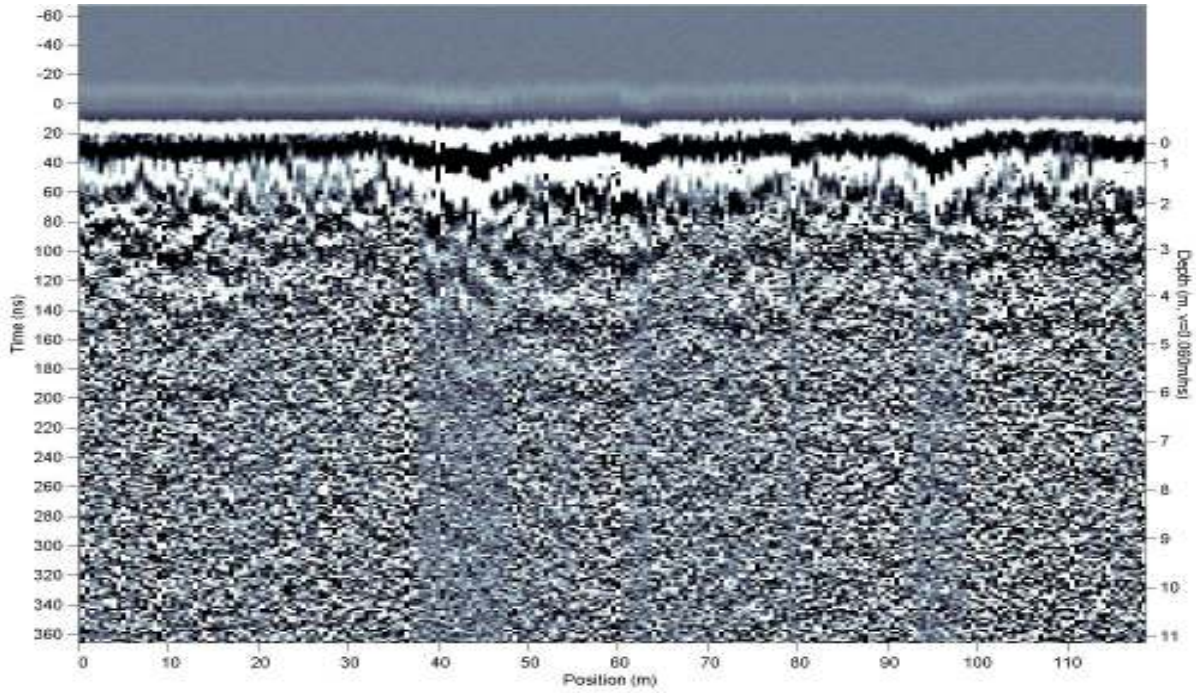

Site 08 line 05 color trace

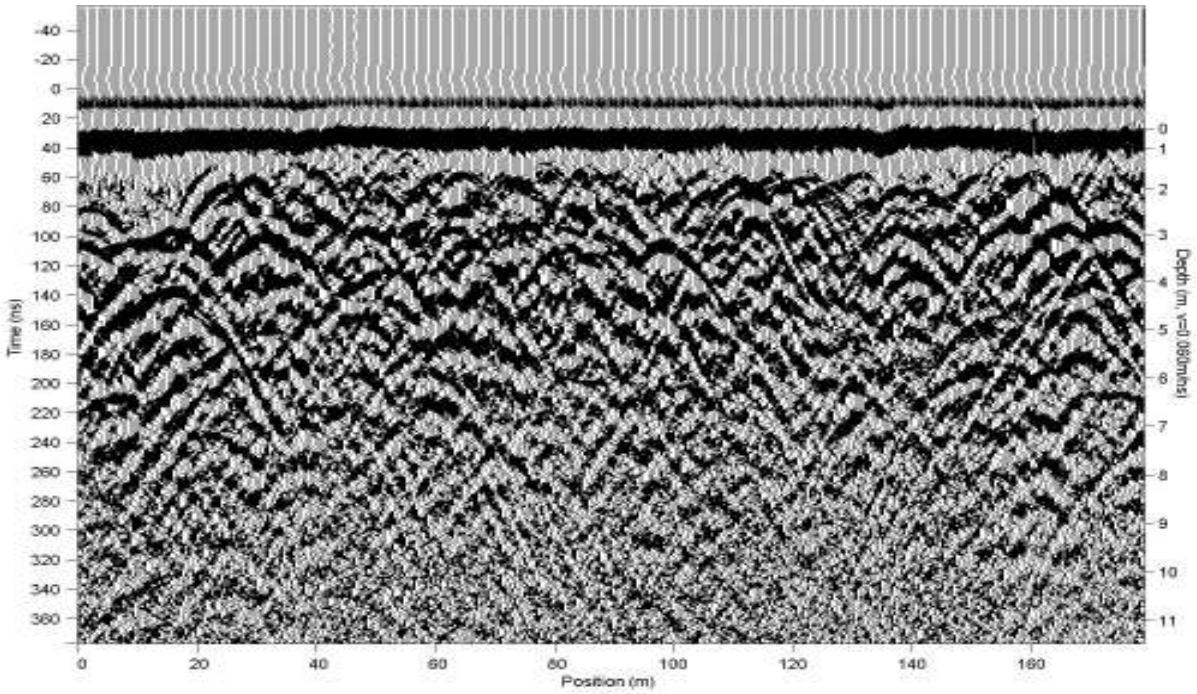

Site 09 line 01 wiggle trace

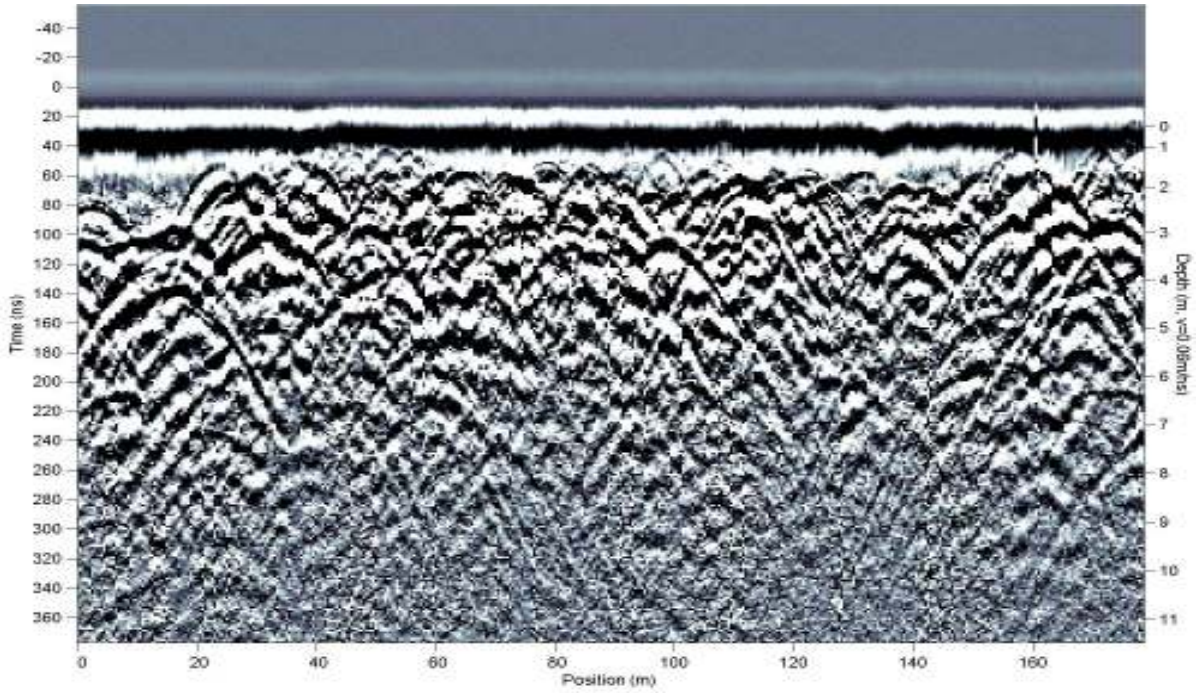

Site 09 line 01 color trace

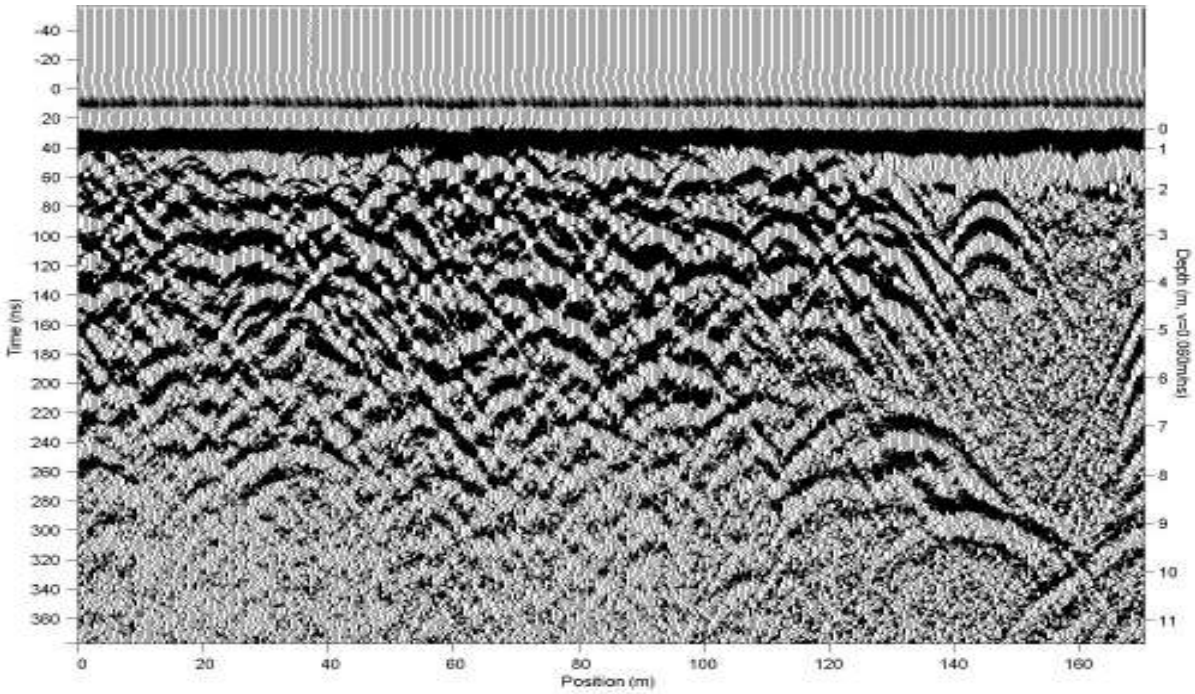

Site 09 lines 02 and 03 merged wiggle trace

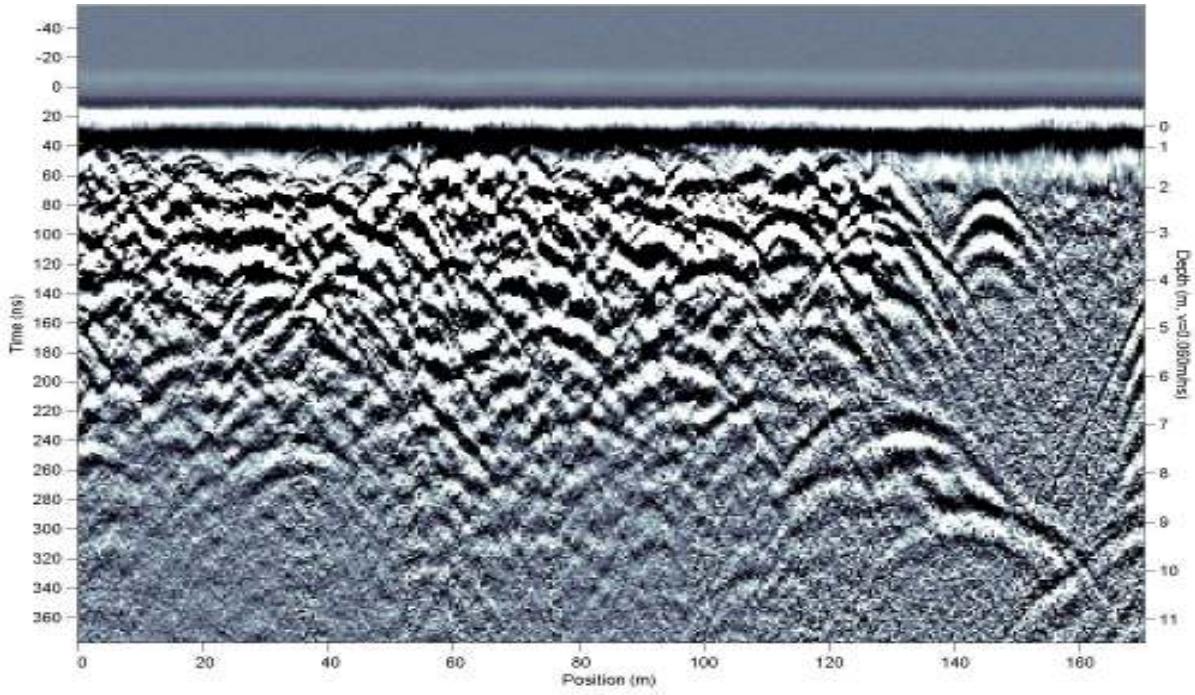

Site 09 lines 02 and 03 merged color trace

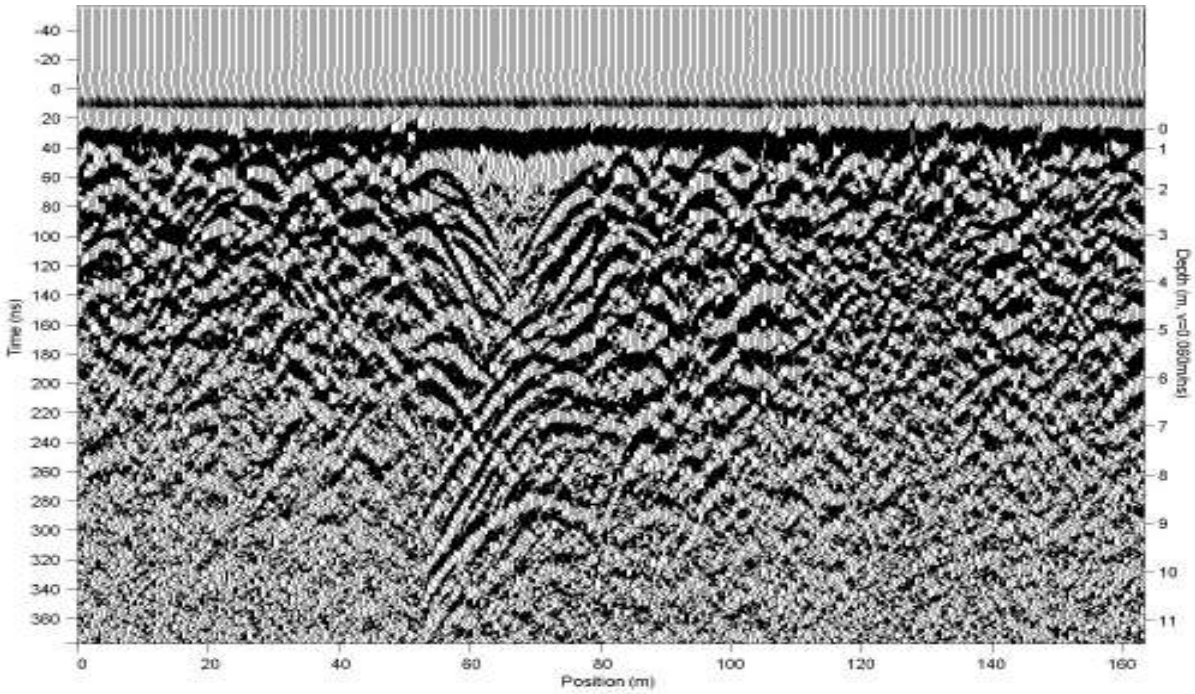

Site 09 line 04 wiggle trace

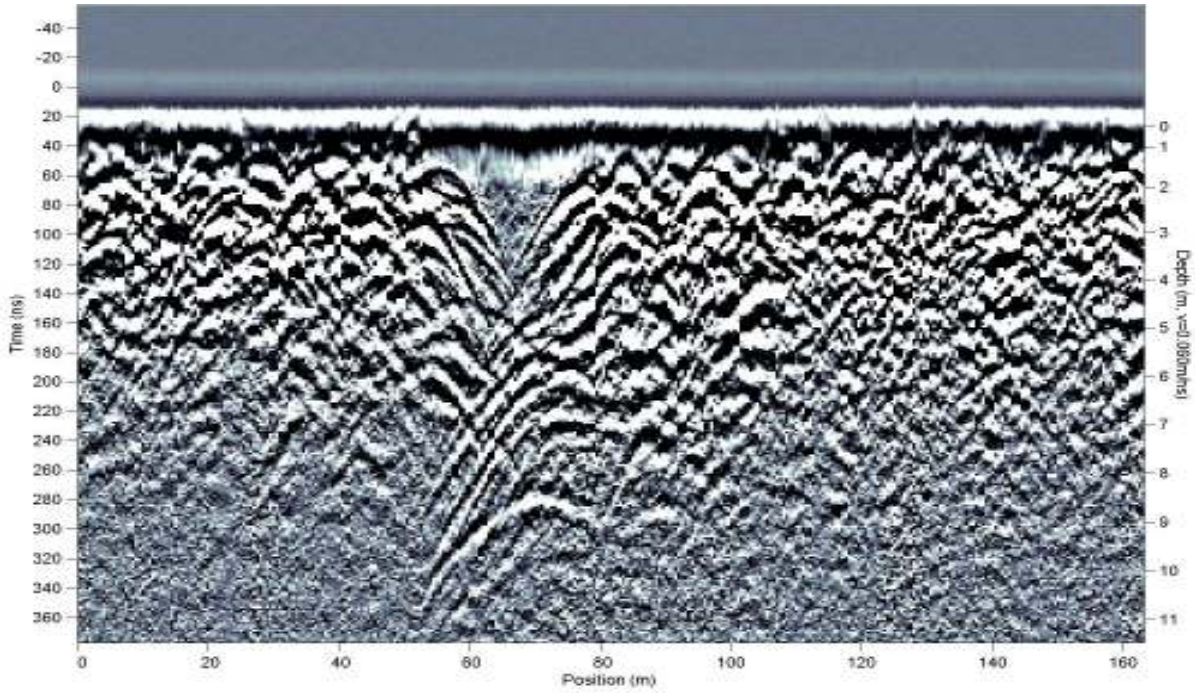

Site 09 line 04 color trace

APPENDIX B

GRAIN-SIZE ANALYSIS

S7-B1-GS1

DRY SAMPLE WEIGHT (g)	40.33	COARSE FRACTION WEIGHT (g)	3.88
DEPTH	10-20cm		

GRAIN-SIZE	PHI SCALE	US SEIVE	BEAKER + SAMPLE WEIGHT (g)	BEAKER WEIGHT (g)	SAMPLE WEIGHT (g)	WEIGHT %	CUM WEIGHT %
CG	-2	5	0.00	0.00	0.00	0.00	0.00
MG	-1	10	0.00	0.00	0.00	0.00	0.00
FG	0	18	0.00	0.00	0.00	0.00	0.00
CS	1	35	53.22	53.13	0.09	0.22	0.22
MS	2	60	53.95	53.84	0.11	0.27	0.50
FS	3	120	58.18	57.47	0.71	1.76	2.26
VFS	4	230	58.09	55.76	2.33	5.78	8.03
M	PAN	PAN	53.80	53.25	0.55		
M+CL					37.00	91.74	99.78

TOTAL COARSE FRACTION WEIGHT (g)	3.33
POST ANALYTICAL WEIGHT (g)	3.79
STARTING COARSE FRACTION WEIGHT (g)	3.88
SEIVE LOSS (g)	0.09
% LOSS	2.32

S7-B1-GS2

DRY SAMPLE WEIGHT (g)	51.09	COARSE FRACTION WEIGHT (g)	1.48
DEPTH	110-126cm		

GRAIN-SIZE	PHI SCALE	US SEIVE	BEAKER + SAMPLE WEIGHT (g)	BEAKER WEIGHT (g)	SAMPLE WEIGHT (g)	WEIGHT %	CUM WEIGHT %
CG	-2	5	0.00	0.00	0.00	0.00	0.00
MG	-1	10	0.00	0.00	0.00	0.00	0.00
FG	0	18	0.00	0.00	0.00	0.00	0.00
CS	1	35	53.02	53.00	0.02	0.04	0.04
MS	2	60	53.61	53.57	0.04	0.08	0.12
FS	3	120	53.78	53.73	0.05	0.10	0.22
VFS	4	230	57.49	56.20	1.29	2.52	2.74
M	PAN	PAN	54.88	54.80	0.08		
M+CL					49.69	97.26	100.00

TOTAL COARSE FRACTION WEIGHT (g)	1.40
POST ANALYTICAL WEIGHT (g)	1.48
STARTING COARSE FRACTION WEIGHT (g)	1.48
SEIVE LOSS (g)	0.00
% LOSS	0.00

S7-B1-GS3

DRY SAMPLE WEIGHT (g)	60.47	COARSE FRACTION WEIGHT (g)	27.96
DEPTH	191-200cm		

GRAIN-SIZE	PHI SCALE	US SEIVE	BEAKER + SAMPLE WEIGHT (g)	BEAKER WEIGHT (g)	SAMPLE WEIGHT (g)	WEIGHT %	CUM WEIGHT %
CG	-2	5	0.00	0.00	0.00	0.00	0.00
MG	-1	10	0.00	0.00	0.00	0.00	0.00
FG	0	18	54.86	54.78	0.08	0.13	0.13
CS	1	35	55.92	55.37	0.55	0.91	1.04
MS	2	60	63.18	56.20	6.98	11.54	12.58
FS	3	120	64.61	53.72	10.89	18.01	30.59
VFS	4	230	62.04	53.59	8.45	13.97	44.57
M	PAN	PAN	53.98	53.00	0.98		
M+CL					33.49	55.38	99.95

TOTAL COARSE FRACTION WEIGHT (g)	26.98
POST ANALYTICAL WEIGHT (g)	27.93
STARTING COARSE FRACTION WEIGHT (g)	27.96
SEIVE LOSS (g)	0.03
% LOSS	0.11

S7-B1-GS4

DRY SAMPLE WEIGHT (g)	60.41	COARSE FRACTION WEIGHT (g)	15.07
DEPTH	207-217cm		

GRAIN-SIZE	PHI SCALE	US SEIVE	BEAKER + SAMPLE WEIGHT (g)	BEAKER WEIGHT (g)	SAMPLE WEIGHT (g)	WEIGHT %	CUM WEIGHT %
CG	-2	5	0.00	0.00	0.00	0.00	0.00
MG	-1	10	0.00	0.00	0.00	0.00	0.00
FG	0	18	54.86	54.78	0.08	0.13	0.13
CS	1	35	55.68	55.36	0.32	0.53	0.66
MS	2	60	59.63	55.20	4.43	7.33	8.00
FS	3	120	58.88	53.72	5.16	8.54	16.54
VFS	4	230	59.13	53.59	5.54	9.17	25.71
M	PAN	PAN	53.52	53.00	0.52		
M+CL					45.86	75.91	101.62

TOTAL COARSE FRACTION WEIGHT (g)	14.55
POST ANALYTICAL WEIGHT (g)	16.05
STARTING COARSE FRACTION WEIGHT (g)	15.07
SEIVE LOSS (g)	-0.98
% LOSS	-6.50

S7-B1-GS5

DRY SAMPLE WEIGHT (g)	55.32	COARSE FRACTION WEIGHT (g)	24.51
DEPTH	282-291cm		

GRAIN-SIZE	PHI SCALE	US SEIVE	BEAKER + SAMPLE WEIGHT (g)	BEAKER WEIGHT (g)	SAMPLE WEIGHT (g)	WEIGHT %	CUM WEIGHT %
CG	-2	5	0.00	0.00	0.00	0.00	0.00
MG	-1	10	54.82	54.78	0.04	0.07	0.07
FG	0	18	55.40	55.36	0.04	0.07	0.14
CS	1	35	56.59	56.20	0.39	0.70	0.85
MS	2	60	57.46	53.72	3.74	6.76	7.61
FS	3	120	60.69	53.59	7.10	12.83	20.44
VFS	4	230	64.96	53.00	11.96	21.62	42.06
M	PAN	PAN	53.16	51.93	1.23		
M+CL					32.04	57.92	99.98

TOTAL COARSE FRACTION WEIGHT (g)	23.28
POST ANALYTICAL WEIGHT (g)	24.50
STARTING COARSE FRACTION WEIGHT (g)	24.51
SEIVE LOSS (g)	0.01
% LOSS	0.04

S7-B1-GS6

DRY SAMPLE WEIGHT (g)	63.40	COARSE FRACTION WEIGHT (g)	23.61
DEPTH	314-323cm		

GRAIN-SIZE	PHI SCALE	US SEIVE	BEAKER + SAMPLE WEIGHT (g)	BEAKER WEIGHT (g)	SAMPLE WEIGHT (g)	WEIGHT %	CUM WEIGHT %
CG	-2	5	54.88	54.79	0.09	0.14	0.14
MG	-1	10	55.54	55.36	0.18	0.28	0.43
FG	0	18	56.39	56.19	0.20	0.32	0.74
CS	1	35	54.39	53.72	0.67	1.06	1.80
MS	2	60	57.92	53.58	4.34	6.85	8.64
FS	3	120	59.87	53.00	6.87	10.84	19.48
VFS	4	230	62.12	51.92	10.20	16.09	35.57
M	PAN	PAN	54.19	53.13	1.06		
M+CL					40.85	64.43	100.00

TOTAL COARSE FRACTION WEIGHT (g)	22.55
POST ANALYTICAL WEIGHT (g)	23.61
STARTING COARSE FRACTION WEIGHT (g)	23.61
SEIVE LOSS (g)	0.00
% LOSS	0.00

S7-B1-GS7

DRY SAMPLE WEIGHT (g)	57.65	COARSE FRACTION WEIGHT (g)	27.44
DEPTH	350-360cm		

GRAIN-SIZE	PHI SCALE	US SEIVE	BEAKER + SAMPLE WEIGHT (g)	BEAKER WEIGHT (g)	SAMPLE WEIGHT (g)	WEIGHT %	CUM WEIGHT %
CG	-2	5	0.00	0.00	0.00	0.00	0.00
MG	-1	10	54.99	54.78	0.21	0.36	0.36
FG	0	18	55.63	55.37	0.26	0.45	0.82
CS	1	35	56.83	56.20	0.63	1.09	1.91
MS	2	60	58.09	53.72	4.37	7.58	9.49
FS	3	120	62.84	53.59	9.25	16.05	25.53
VFS	4	230	64.50	53.01	11.49	19.93	45.46
M	PAN	PAN	53.11	51.94	1.17		
M+CL					31.38	54.43	99.90

TOTAL COARSE FRACTION WEIGHT (g)	26.27
POST ANALYTICAL WEIGHT (g)	27.38
STARTING COARSE FRACTION WEIGHT (g)	27.44
SEIVE LOSS (g)	0.06
% LOSS	0.22

S7-B1-GS8

DRY SAMPLE WEIGHT (g)	66.52	COARSE FRACTION WEIGHT (g)	28.47
DEPTH	420-427cm		

GRAIN-SIZE	PHI SCALE	US SEIVE	BEAKER + SAMPLE WEIGHT (g)	BEAKER WEIGHT (g)	SAMPLE WEIGHT (g)	WEIGHT %	CUM WEIGHT %
CG	-2	5	0.00	0.00	0.00	0.00	0.00
MG	-1	10	54.78	54.78	0.00	0.00	0.00
FG	0	18	55.40	55.36	0.04	0.06	0.06
CS	1	35	56.42	56.19	0.23	0.35	0.41
MS	2	60	56.91	53.72	3.19	4.80	5.20
FS	3	120	64.40	53.60	10.80	16.24	21.44
VFS	4	230	65.87	53.00	12.87	19.35	40.78
M	PAN	PAN	53.24	51.93	1.31		
M+CL					39.36	59.17	99.95

TOTAL COARSE FRACTION WEIGHT (g)	27.16
POST ANALYTICAL WEIGHT (g)	28.44
STARTING COARSE FRACTION WEIGHT (g)	28.47
SEIVE LOSS (g)	0.03
% LOSS	0.11

S7-B1-GS9

DRY SAMPLE WEIGHT (g)	60.80	COARSE FRACTION WEIGHT (g)	25.34
DEPTH	480-487cm		

GRAIN-SIZE	PHI SCALE	US SEIVE	BEAKER + SAMPLE WEIGHT (g)	BEAKER WEIGHT (g)	SAMPLE WEIGHT (g)	WEIGHT %	CUM WEIGHT %
CG	-2	5	0.00	0.00	0.00	0.00	0.00
MG	-1	10	54.80	54.78	0.02	0.03	0.03
FG	0	18	55.47	55.36	0.11	0.18	0.21
CS	1	35	56.59	56.20	0.39	0.64	0.86
MS	2	60	57.48	53.72	3.76	6.18	7.04
FS	3	120	63.51	53.59	9.92	16.32	23.36
VFS	4	230	63.36	53.00	10.36	17.04	40.39
M	PAN	PAN	52.69	51.93	0.76		
M+CL					36.22	59.57	99.97

TOTAL COARSE FRACTION WEIGHT (g)	24.58
POST ANALYTICAL WEIGHT (g)	25.32
STARTING COARSE FRACTION WEIGHT (g)	25.34
SEIVE LOSS (g)	0.02
% LOSS	0.08

S8-B1-GS1

DRY SAMPLE WEIGHT (g)	52.06	COARSE FRACTION WEIGHT (g)	6.66
DEPTH	0-20cm		

GRAIN-SIZE	PHI SCALE	US SEIVE	BEAKER + SAMPLE WEIGHT (g)	BEAKER WEIGHT (g)	SAMPLE WEIGHT (g)	WEIGHT %	CUM WEIGHT %
CG	-2	5	0.00	0.00	0.00	0.00	0.00
MG	-1	10	0.00	0.00	0.00	0.00	0.00
FG	0	18	55.48	55.47	0.01	0.02	0.02
CS	1	35	53.25	53.22	0.03	0.06	0.08
MS	2	60	56.06	55.78	0.28	0.54	0.61
FS	3	120	59.10	57.48	1.62	3.11	3.73
VFS	4	230	58.21	53.85	4.36	8.37	12.10
M	PAN	PAN	53.35	53.15	0.20		
M+CL					45.60	87.59	99.69

TOTAL COARSE FRACTION WEIGHT (g)	6.46
POST ANALYTICAL WEIGHT (g)	6.50
STARTING COARSE FRACTION WEIGHT (g)	6.66
SEIVE LOSS (g)	0.16
% LOSS	2.40

S8-B1-GS2

DRY SAMPLE WEIGHT (g)	59.62	COARSE FRACTION WEIGHT (g)	2.57
DEPTH	114-134cm		

GRAIN-SIZE	PHI SCALE	US SEIVE	BEAKER + SAMPLE WEIGHT (g)	BEAKER WEIGHT (g)	SAMPLE WEIGHT (g)	WEIGHT %	CUM WEIGHT %
CG	-2	5	0.00	0.00	0.00	0.00	0.00
MG	-1	10	0.00	0.00	0.00	0.00	0.00
FG	0	18	0.00	0.00	0.00	0.00	0.00
CS	1	35	53.18	53.16	0.02	0.03	0.03
MS	2	60	55.58	54.82	0.76	1.27	1.31
FS	3	120	52.65	51.96	0.69	1.16	2.47
VFS	4	230	56.43	55.39	1.04	1.74	4.21
M	PAN	PAN	53.90	53.87	0.03		
M+CL					57.08	95.74	99.95

TOTAL COARSE FRACTION WEIGHT (g)	2.54
POST ANALYTICAL WEIGHT (g)	2.54
STARTING COARSE FRACTION WEIGHT (g)	2.57
SEIVE LOSS (g)	0.03
% LOSS	1.17

S8-B1-GS3

DRY SAMPLE WEIGHT (g)	61.58	COARSE FRACTION WEIGHT (g)	34.94
DEPTH	190-205cm		

GRAIN-SIZE	PHI SCALE	US SEIVE	BEAKER + SAMPLE WEIGHT (g)	BEAKER WEIGHT (g)	SAMPLE WEIGHT (g)	WEIGHT %	CUM WEIGHT %
CG	-2	5	0.00	0.00	0.00	0.00	0.00
MG	-1	10	55.43	55.39	0.04	0.06	0.06
FG	0	18	56.28	56.20	0.08	0.13	0.19
CS	1	35	54.40	53.74	0.66	1.07	1.27
MS	2	60	67.47	53.01	14.46	23.48	24.75
FS	3	120	65.69	53.61	12.08	19.62	44.37
VFS	4	230	58.50	51.95	6.55	10.64	55.00
M	PAN	PAN	55.69	54.78	0.91		
M+CL					27.55	44.74	99.74

TOTAL COARSE FRACTION WEIGHT (g)	34.03
POST ANALYTICAL WEIGHT (g)	34.78
STARTING COARSE FRACTION WEIGHT (g)	34.94
SEIVE LOSS (g)	0.16
% LOSS	0.46

S8-B1-GS4

DRY SAMPLE WEIGHT (g)	61.05	COARSE FRACTION WEIGHT (g)	45.36
DEPTH	215-225cm		

GRAIN-SIZE	PHI SCALE	US SEIVE	BEAKER + SAMPLE WEIGHT (g)	BEAKER WEIGHT (g)	SAMPLE WEIGHT (g)	WEIGHT %	CUM WEIGHT %
CG	-2	5	0.00	0.00	0.00	0.00	0.00
MG	-1	10	56.21	56.20	0.01	0.02	0.02
FG	0	18	56.22	53.73	2.49	4.08	4.10
CS	1	35	55.52	54.78	0.74	1.21	5.31
MS	2	60	66.71	53.14	13.57	22.23	27.53
FS	3	120	73.16	54.45	18.71	30.65	58.18
VFS	4	230	61.86	53.21	8.65	14.17	72.35
M	PAN	PAN	55.85	55.38	0.47		
M+CL					16.16	26.47	98.82

TOTAL COARSE FRACTION WEIGHT (g)	44.89
POST ANALYTICAL WEIGHT (g)	44.64
STARTING COARSE FRACTION WEIGHT (g)	45.36
SEIVE LOSS (g)	0.72
% LOSS	1.59

S8-B1-GS5

DRY SAMPLE WEIGHT (g)	59.31	COARSE FRACTION WEIGHT (g)	45.82
DEPTH	265-275cm		

GRAIN-SIZE	PHI SCALE	US SEIVE	BEAKER + SAMPLE WEIGHT (g)	BEAKER WEIGHT (g)	SAMPLE WEIGHT (g)	WEIGHT %	CUM WEIGHT %
CG	-2	5	0.00	0.00	0.00	0.00	0.00
MG	-1	10	0.00	0.00	0.00	0.00	0.00
FG	0	18	53.07	53.01	0.06	0.10	0.10
CS	1	35	54.32	53.61	0.71	1.20	1.30
MS	2	60	68.09	54.71	13.38	22.56	23.86
FS	3	120	78.89	54.79	24.10	40.63	64.49
VFS	4	230	61.56	54.45	7.11	11.99	76.48
M	PAN	PAN	55.87	55.47	0.40		
M+CL					13.89	23.42	99.90

TOTAL COARSE FRACTION WEIGHT (g)	45.42
POST ANALYTICAL WEIGHT (g)	45.76
STARTING COARSE FRACTION WEIGHT (g)	45.82
SEIVE LOSS (g)	0.06
% LOSS	0.13

S8-B1-GS6

DRY SAMPLE WEIGHT (g)	53.73	COARSE FRACTION WEIGHT (g)	13.9
DEPTH	320-340cm		

GRAIN-SIZE	PHI SCALE	US SEIVE	BEAKER + SAMPLE WEIGHT (g)	BEAKER WEIGHT (g)	SAMPLE WEIGHT (g)	WEIGHT %	CUM WEIGHT %
CG	-2	5	0.00	0.00	0.00	0.00	0.00
MG	-1	10	0.00	0.00	0.00	0.00	0.00
FG	0	18	54.55	54.46	0.09	0.17	0.17
CS	1	35	57.80	57.48	0.32	0.60	0.76
MS	2	60	57.39	53.24	4.15	7.72	8.49
FS	3	120	57.54	53.74	3.80	7.07	15.56
VFS	4	230	58.39	53.19	5.20	9.68	25.24
M	PAN	PAN	56.08	55.77	0.31		
M+CL					40.14	74.71	99.94

TOTAL COARSE FRACTION WEIGHT (g)	13.59
POST ANALYTICAL WEIGHT (g)	13.87
STARTING COARSE FRACTION WEIGHT (g)	13.90
SEIVE LOSS (g)	0.03
% LOSS	0.22

S8-B1-GS7

DRY SAMPLE WEIGHT (g)	56.73	COARSE FRACTION WEIGHT (g)	38.6
DEPTH	370-390cm		

GRAIN-SIZE	PHI SCALE	US SEIVE	BEAKER + SAMPLE WEIGHT (g)	BEAKER WEIGHT (g)	SAMPLE WEIGHT (g)	WEIGHT %	CUM WEIGHT %
CG	-2	5	0.00	0.00	0.52	0.92	0.92
MG	-1	10	55.78	55.76	0.02	0.04	0.95
FG	0	18	53.63	53.60	0.03	0.05	1.00
CS	1	35	55.26	54.44	0.82	1.45	2.45
MS	2	60	66.51	53.72	12.79	22.55	25.00
FS	3	120	68.89	53.01	15.88	27.99	52.99
VFS	4	230	62.71	54.77	7.94	14.00	66.98
M	PAN	PAN	53.68	53.13	0.55		
M+CL					18.68	32.93	99.91

TOTAL COARSE FRACTION WEIGHT (g)	38.05
POST ANALYTICAL WEIGHT (g)	38.55
STARTING COARSE FRACTION WEIGHT (g)	38.60
SEIVE LOSS (g)	0.05
% LOSS	0.13

S8-B1-GS8

DRY SAMPLE WEIGHT (g)	58.68	COARSE FRACTION WEIGHT (g)	17.02
DEPTH	415-435cm		

GRAIN-SIZE	PHI SCALE	US SEIVE	BEAKER + SAMPLE WEIGHT (g)	BEAKER WEIGHT (g)	SAMPLE WEIGHT (g)	WEIGHT %	CUM WEIGHT %
CG	-2	5	0.00	0.00	0.00	0.00	0.00
MG	-1	10	0.00	0.00	0.00	0.00	0.00
FG	0	18	53.32	53.24	0.08	0.14	0.14
CS	1	35	54.65	53.83	0.82	1.40	1.53
MS	2	60	65.23	57.49	7.74	13.19	14.72
FS	3	120	57.98	51.92	6.06	10.33	25.05
VFS	4	230	57.67	55.45	2.22	3.78	28.83
M	PAN	PAN	53.28	53.20	0.08		
M+CL					41.74	71.13	99.97

TOTAL COARSE FRACTION WEIGHT (g)	16.94
POST ANALYTICAL WEIGHT (g)	17.00
STARTING COARSE FRACTION WEIGHT (g)	17.02
SEIVE LOSS (g)	0.02
% LOSS	0.12

S8-B1-GS9

DRY SAMPLE WEIGHT (g)	55.32	COARSE FRACTION WEIGHT (g)	30.91
DEPTH	475-495cm		

GRAIN-SIZE	PHI SCALE	US SEIVE	BEAKER + SAMPLE WEIGHT (g)	BEAKER WEIGHT (g)	SAMPLE WEIGHT (g)	WEIGHT %	CUM WEIGHT %
CG	-2	5	0.00	0.00	0.00	0.00	0.00
MG	-1	10	53.88	53.82	0.06	0.11	0.11
FG	0	18	55.66	55.46	0.20	0.36	0.47
CS	1	35	54.54	53.01	1.53	2.77	3.24
MS	2	60	62.08	53.59	8.49	15.35	18.58
FS	3	120	63.97	51.94	12.03	21.75	40.33
VFS	4	230	65.56	57.50	8.06	14.57	54.90
M	PAN	PAN	53.70	53.25	0.45		
M+CL					24.86	44.94	99.84

TOTAL COARSE FRACTION WEIGHT (g)	30.46
POST ANALYTICAL WEIGHT (g)	30.82
STARTING COARSE FRACTION WEIGHT (g)	30.91
SEIVE LOSS (g)	0.09
% LOSS	0.29

APPENDIX C

BULK DENSITY ANALYSIS

SAMPLE	DEPTH	VOLUME	BEAKER WT	BEAKER AND SAMPLE WT	DRY BEAKER AND SAMPLE WT	DRY SAMPLE WT	BULK DENSITY
S7-B1-BD1	18.0	6.23	53.13	62.78	58.38	5.25	0.84
S7-B1-BD2	56.0	6.23	53.85	64.67	60.79	6.94	1.11
S7-B1-BD3	194.0	6.23	57.48	70.15	67.06	9.58	1.54
S7-B1-BD4	240.0	6.23	55.76	68.07	64.97	9.21	1.48
S7-B1-BD5	272.0	6.23	53.20	66.34	63.86	10.66	1.71
S7-B1-BD6	315.0	6.23	55.46	68.03	65.16	9.70	1.56
S7-B1-BD7	389.0	6.23	53.25	65.49	62.30	9.05	1.45
S7-B1-BD8	419.0	6.23	54.46	67.44	64.32	9.86	1.58
S7-B1-BD9	479.0	6.23	54.72	67.53	64.59	9.87	1.58
S8-B1-BD1	20.0	5.2	53.14	63.31	63.01	9.87	1.9
S8-B1-BD2	88.8	3.1	53.84	60.49	59.83	5.99	1.9
S8-B1-BD3	186.4	3.6	57.48	64.73	64.65	7.17	2.0
S8-B1-BD4	213.4	3.5	55.80	62.43	62.36	6.56	1.9
S8-B1-BD5	237.2	2.2	53.20	56.98	56.94	3.74	1.7
S8-B1-BD6	315.2	3.1	55.45	61.42	61.33	5.88	1.9
S8-B1-BD7	356.0	2.7	53.24	58.60	58.56	5.32	2.0
S8-B1-BD8	397.6	5.4	54.47	67.70	66.67	12.20	2.3
S8-B1-BD9	456.2	4.1	54.72	61.82	61.27	6.55	1.6

APPENDIX D

RADIOCARBON DATING ANALYSIS

February 5, 2008

AMS ^{14}C assays of marine shells, TX for Todd and Slattery:

ISGS #	Sample #	$\delta^{13}C$	pMC	±	$D^{14}C$	±	^{14}C age	±
A1037	S7B1-S1	-0.9	0.7029	0.0016	-297.1	1.6	**2830**	**20**
A1038	S7B1-S12	-6.3	0.6689	0.0015	-331.1	1.5	**3230**	**20**
A1039	S8B1-S1	-7.8	0.7018	0.0015	-298.2	1.5	**2845**	**20**
A1040	S8B1-S9	-8.7	0.6899	0.0015	-310.1	1.5	**2980**	**20**

Hong Wang
Director of Radiocarbon Dating Laboratory
Illinois State Geological Survey
University of Illinois at Urbana-Champaign
Tel-217-244-7692
wang@isgs.uiuc.edu

REFERENCES

Accelerator Mass Spectrometry Laboratory, University of Arizona, 2008. Sample Preparation. URL: http://www.physics.arizona.edu/ams/education/pretreat.htm.

Annan, A.P., 1999. Practical processing of GPR data. Proceedings of the Second Government Workshop on Ground Penetrating Radar. Sensors and Software, Ontario. 16 pp.

Augustinus, P.C., Nichol, S., 1999. Ground-penetrating radar imaging of Pleistocene sediments, Boco Plain, western Tasmania. Australian Journal of Earth Science. 46, 275-282.

Aust, W.M., Lea, R., Gregory, J.D., 1991. Removal of floodwater sediments by a clearcut tupelo-cypress wetland. Water Resources Bulletin 27, 111-116.

Barnhardt, W.A., Sherrod, B.L., 2006. Evolution of a Holocene delta driven by episodic sediment delivery and coseismic deformation, Puget Sound, Washington, USA. Sedimentology. 53, 1211-1228.

Blum, M.D., Tornqvist, T.E., 2000. Fluvial responses to climate and sea-level change: a review and look forward. Sedimentology. 47 (Suppl. 1), 2-48.

Blum, M.D., Misner, T.J., Collins, E.S., Scott, D.B., Morton, R.A., Aslan, A., 2001. Middle Holocene sea-level rise and highstand at +2 M, central Texas coast. Journal of Sedimentary Research. 71, 581-588.

Brandt, S.A., 2000. Classification of geomorphological effects downstream of dams. Catena. 40, 375-401.

Bridge, J., Collier, R., Alexander, J., 1998. Large-scale structure of Calamus River deposits (Nebraska, USA) revealed using ground-penetrating radar. Sedimentology. 45, 977-986.

Bristow, C.S., Skelly, R.L., Ethridge, F.G., 1999. Crevasse splays from the rapidly aggrading, sand-bed, braided Niobrara River, Nebraska: effect of base level rise. Sedimentology. 46, 1029-1047.

Bristow, C.S., Jol, H.M. (Eds.), 2003. Ground Penetrating Radar in Sediments. Geololgical Society of London Special Publication. 211, 330 pp.

Butnor, J.R., Doolittle, J.A., Kress, L., Cohen, S., Johnsen, K.H., 2001. Use of ground-penetrating radar to study tree roots in the southeastern United States. Tree Physiology. 21, 1269-1278.

Conyers, L.B., Goodman, D., 1997. Ground-Penetrating Radar: An Introduction for Archaeologists. Altamira Press, London. 232 pp.

Crout, J.D., 1976. Soil Survey of Chambers County, Texas. Washington: USDA Soil Conservation Service. 53 pp.

Davis, J.L., Annan, A.P., 1989. Ground-penetrating radar for high-resolution mapping of soil and rock stratigraphy. Geophysical Prospecting. 3, 531-551.

Day, J.W., Boesch, D.F., Clairain, E.J., Kemp, G.P., Laska, S.B., Mitsch, W.J., Orth, K., Mashriqui, H., Reed, D.J., Shabman, L., Simenstad, C.A., Streever, B.J., Twilley, R.R., Watson, C.C., Wells, J.T., Whigham, D.F., 2007. Restoration of the Mississippi Delta: Lessons from Hurricanes Katrina and Rita. Science. 5819, 1679-1684.

Dollar, D.B., 2005. Quantifying sediment delivery to the lower Trinity River channel below Livingston Dam, south Texas. M.S. Thesis, Texas Christian University, Fort Worth, 58 pp.

Ezzy, T.R., Cox, M.E., O'Rourke, A.J., Huftile, G.J., 2006. Groundwater flow modeling within a coastal alluvial plain setting using a high resolution hydrofacies approach; Bells Creek plain, Australia. Hydrology Journal. 14, 675-688.

Fisher, S.C., Stewart, R.R., and Jol, H.M., 1992. Processing ground penetrating radar (GPR) data. CREWES Research Report. 4, 1-22.

Fryirs, K., Brierley, G.J., 1999. Slope-channel decoupling in Wolumla catchment, New South Wales, Australia: the changing nature of sediment sources following European settlement. Catena. 35, 41-63.

Griffith, K.L., 1996. Soil Survey of Liberty County, Texas. Washington: USDA Soil Conservation Service. 192 pp.

Johnston, G., 2007. Personal communication, Sensors and Software, Ontario.

Jol, H.M., Smith, D.G., 1991. Ground penetrating radar of northern lacustrine deltas. Canadian Journal of Earth Science. 28(12), 1939-1947.

Lankford, R.R., Rehkemper, L.J., 1969. The Galveston Bay complex: a summary of characteristics. In: Lankford, R.R., Rogers, J.J.W. (Eds.), Holocene Geology of the Bay Area. Houston Geological Society, Houston, 1-11.

Levine, E., 2001. Soil characterization protocols: A step by step guide. NASA's Goddard Space Flight Center. URL: http://soil.gsfc.nasa.gov/pvg/texture2.htm

McEwan, M.C., 1963. Sedimentary Facies of the Trinity River Delta, Texas. PhD dissertation, Rice University, Houston, 99 pp.

Morton, R.A., 1977. Historical shoreline changes and their causes, Texas Gulf Coast. Transactions of the Gulf Coast Association of Geological Societies. 27, 321-331.

Morton, R.A., Payne, J.G., 1990. Coastal land loss in Texas-an overview. Transactions of the Gulf Coast Association of Geological Societies. 40, 625-634.

Morton, R.A., Blum, M.D., White, W.A., 1996. Valley fills of incised coastal plain rivers, southeastern Texas. Transactions of the Gulf Coast Association of Geological Societies. 46, 321-331.

Morton, R.A., Purcell, N.A., Peterson, R.L., 2001. Shallow stratigraphic evidence of subsidence and faulting induced by hydrocarbon production in coastal southeast Texas. U.S. Geological Survey Open File Report 01-274.

Moysey, S., Knight, R., Jol, H.M., 2006. Texture-based classification of ground-penetrating radar images. Geophysics. 71(6), K111-K118.

Neal, A., 2004. Ground-penetrating radar and its use in sedimentology: principles, problems and progress. Earth-Science Reviews. 66, 261-330.

Olhoeft, G.R., 2002. Applications and frustrations in using ground penetrating radar. IEEE AESS Systems Magazine. February, 12-20.

Olhoeft, G.R., 2006. Ground Penetrating Radar: ground probing radar, subsurface radar, georadar, earth sounding radar. URL: http\\www.g-p-r.com

Pelpola, C.P., Hickin, E.J., 2004. Long-term bed load transport rate based on aerial-photo and ground penetrating radar surveys of fan-delta growth, Coast Mountains, British Columbia. Geomorphology. 57, 169-181.

Phillips, J.D., 1987. Sediment budget stability in the Tar River basin, North Carolina. American Journal of Science. 287, 780-794.

Phillips, J.D., 1991. Fluvial sediment delivery to a coastal plain estuary in the Atlantic Drainage of the United States. Marine Geology. 98, 121-134.

Phillips, J.D., 2001. Sedimentation in bottomland hardwoods downstream of an east Texas dam. Environmental Geology. 40, 860-868.

Phillips, J.D., 2003. Sediment retention in stream corridors of the lower Trinity River basin, Texas. Report to the Texas Water Development Board, Austin. pp. 1-25.

Phillips, J.D., Slattery, M.C., Musselman, Z.A., 2004. Dam-to-delta sediment inputs and storage in the lower Trinity River, Texas. Geomorphology. 62, 17-34.

Phillips, J.D., Slattery, M.C., Musselman, Z.A., 2005. Channel adjustments of the lower Trinity River, Texas, downstream of Livingston Dam. Earth Surface Processes and Landforms. 30, 1419-1439.

Phillips, J.D., Slattery, M.C., 2006. Sediment storage, sea level, and sediment delivery to the ocean by coastal plain rivers. Progress in Physical Geography. 30, 1-18.

Phillips, J.D., 2006. Trinity River delta accretion rates. Unpublished Report. Geography Department, University of Kentucky. 14 pp.

Phillips, J.D., Gomez, B., 2007. Controls on sediment export from the Waipaoa River basin, New Zealand. Basin Research. 19, 241-252.

Pufahl, P.K., James, N.P., Bone, Y., Lukasik, J.J., 2004. Pliocene sedimentation in a shallow, cool-water, estuarine gulf, Murray Basin, South Australia. Sedimentology 51, 997–1027.

Roberts, M.C., Niller, H.P., Helmstetter, N., 2003. Sedimentary architecture and radar facies of a fan delta, Cypress Creek, West Vancouver, British Columbia. In: Brisow, C.S., Jol, H.M. (Eds.), Ground Penetrating Radar in Sediments. Geological Society of London Special Publication. 211, 111-126.

Rodriguez, A.B., Anderson, J.B., Siringan, F.P., Taviani, M., 2004. Holocene evolution of the east Texas coast and inner continental shelf: along-strike variability in coastal retreat rates. Journal of Sedimentary Research. 74, 405-421.

Rodriguez, A.B., Anderson, J.B., Simms, A.R., 2005. Terrace inundation as an autocyclic mechanism for parasequence formation: Galveston estuary, Texas, U.S.A. Journal of Sedimentary Research. 75, 608-620.

Royse, C.F., 1970. An Introduction to Sediment Analysis. Arizona State University, Tempe, AZ. 180 pp.

Sass, O., 2007. Personal communication. Institut für Geographie, Universität Augsburg.

Sensors and Software, 2003. EKKO_View Enhanced and Ekko_View Deluxe: User's Guide. Sensors and Software, Ontario. 104 pp.

Sensors and Software, 2005. EKKO-for-DVL pulseEKKO 100: User's Guide. Sensors and Software, Ontario. 68 pp.

Slattery, M.C., Phillips, J.D., 2005. Relative importance of fluvial and nonfluvial sediment sources to Galveston Bay. Report to the Texas Water Development Board, Austin.

Smith, D.G., Jol, H.M., 1997. Radar structure of a Gilbrt-type delta, Peyto Lake, Banff National Park, Canada. Sediment. Geol. 113, 195-209.

Solis, R.S., Longley, W.L., Malstaff, G., 1994. Influence of inflow on sediment deposition in delta and bay systems. In: Longley, W.L. (Ed.), Freshwater Inflows to Texas Bays and Estuaries. Texas Water Development Board, Austin, 56-70.

Stork, S.V., Sneed, M., 2002. Houston-Galveston area from space—A new tool for mapping land subsidence. U.S. Geological Survey Fact Sheet 110-002, URL: http://water.usgs.gov/pubs/fs/fs-110-02/

Tercier, P., Knight, R., Jol, H., 2000. A comparison of the correlation structure in GPR images of deltaic and barrier-spit depositional environments. Geophysics. 65(4), 1142-1153.

Tisdall, A.L., 1951, Comparison of methods of determining apparent density of soils, Australian Journal of Agricultural Research, 2, 349-354.

Van Dam, R.L., Schlager, W., 2000. Identifying causes of ground-penetrating radar reflections using time-domain reflectometry and sedimentological analyses. Sedimentology. 47, 435-449.

Wellmeyer, J.L., Slattery, M.C., Phillips, J.D., 2005. Quantifying downstream impacts of impoundment on flow regime and channel planform, lower Trinity River, Texas. Geomorphology. 69, 1-13.

White, W.A., Calnan, T.C., 1991. Submergence of vegetated wetlands in fluvial-deltaic area, Texas Gulf coast. Coastal Depositional Systems of the Gulf of Mexico. 12th Annual Research Conference. Society of Economic Paleontologists and Mineralogists, Gulf Coast Section, Tulsa, OK, 278-279.

White, W.A., Morton, R.A., Holmes, C.W., 2002. A comparison of factors controlling sedimentation rates and wetland loss in fluvial-deltaic systems, Texas Gulf coast. Geomorphology. 44, 47-66.

VITA

EDUCATION

University of Nebraska at Omaha, Omaha, NE, May 2003
Bachelor of Science, Geology GPA: 3.98, Overall GPA: 3.86

Texas Christian University, Ft. Worth, TX, Anticipated May 2008
Master of Science, Environmental Science GPA: 4.0

PROFESSIONAL EXPERIENCE

Feb. 07-Present — **XTO Energy** Fort Worth, TX
Geology Intern
- Correlatation and analysis of well logs
- Geologic mapping and interpretation
- Pick formation tops and coal seams to perforate
- Data compilation and research

July 03-April 05 — **URS Corporation** Omaha, NE
Geologist/Environmental Scientist

May 03-July 03 — **Terracon** Omaha, NE

May 99-Aug. 99 — *Environmental Scientist/Intern*
- Contour mapping and cross-section development
- Subsurface Investigations and Lithologic Logging
- Responsible for authoring health and safety plans, phase II reports, and field sampling plans
- On-site Management of Hollow Stem Auger (HSA) and Direct Push Technology (DPT) Crews
- Sediment, Surface Soil, and Subsurface Soil Sampling
- Surface Water and Groundwater Sampling
- Monitoring Well and Piezometer Installation and Abandonment

COMPUTER SKILLS

Petra, ArcGIS, Surfer, gINT, Microsoft Office, Visual Basic, SPSS, SAS, Minitab, Canvas, Internet

RELEVANT COURSES

- Petroleum Geology, Well Logging, and Seismic Stratigraphy
- Sedimentology, Stratigraphy, and Structural Geology
- Mineralogy, Petrology, and Geochemistry
- Computer Based Sub-Surface Geologic Mapping, Geographic Information Systems, and Field Based Geologic Mapping
- Computer Literacy with Programming and Statistical Methods

HONORS

- Dean's List: Fall 96-Fall 98, Spring 00, Fall 02; Chancellor's List: Fall 01
- Outstanding Undergraduate Award in Geology 03
- Yatkola-Edwards Research Grant: 02, Goodrich Scholarship 96
- Nebraska Gem and Mineral Club Scholarship 02

RESEARCH

- Multiple glacial tills in an exposure along the lower Elkhorn River, Nebraska. GSA Abstracts with Programs (2003) vol. 35, no. 2, p. 58.
- An assessment of Ground Penetrating Radar as a technique in quantifying sediment accumulation in the Trinity River delta, TX.

ABSTRACT

AN ASSESSMENT OF GROUND PENETRATING RADAR AS A TECHNIQUE IN QUANTIFYING SEDIMENT ACCUMULATION ON THE TRINITY RIVER DELTA, TX

By Lee Michael Todd, M.S., 2008
Department of Environmental Science
Texas Christian University

Thesis Advisor: Michael Slattery
Professor of Environmental Science and Chair of the Department

This thesis uses Ground Penetrating Radar (GPR) and traditional coring methods to quantify Holocene sedimentation rates in the Trinity River Delta, Texas. Results showed that, while GPR is useful in determining subsurface stratigraphy in coarse-grained environments such as sand bars, it is not useful for subsurface investigations in marshes, where high clay and water content of the sediments attenuate the GPR signal. Radiocarbon dating of shell fragments recovered from sediment cores (292-536cm) ranged from 2.8 to 3.2 Ka. Mean sediment accumulation rates varied between 1.2 and 1.8 mm yr^{-1} for two areas of the delta, consistent with previous research. At these rates, modern sediment input from the Trinity River is inadequate to account for sediment accretion in the delta. Therefore, other non-fluvial sediment sources must be contributing to the accretion of sediment within the delta.